Novel Approaches for Investigating the Soldier Survivability Tradespace

Matthew Mavor

Thesis submitted to the University of Ottawa
in partial Fulfillment of the requirements for the
Doctorate of Philosophy in Human Kinetics

School of Human Kinetics
Faculty of Health Sciences
University of Ottawa

Table of Contents

Dedication

I'd like to dedicate this dissertation to all of those I've lost since I've started my graduate studies: Mom, Dad, Grandma and Grandpa Mavor, Grandma Colbert, Great Uncle Peter, Great Aunt Faythe, and my family dog Kassie.

Each one of you impacted my life beyond measure and helped shape me into the person I am today. I will continue working hard and keep making you proud. Thank you for everything.

Acknowledgements

I may be the author of this dissertation, but this work would not have been possible without the support of several amazing people.

I first would like to acknowledge my supervisor Dr. Ryan Graham who has mentored me for the better part of a decade and has helped me realize my full potential by seeing something in me that I didn't. Words cannot express how grateful I am for all you have done for me. Thank you.

My Defence Research and Development Canada colleagues helped make my second and third papers possible. This was done by supporting me during my month-long stay at DRDC Toronto during the summer of 2019 and providing excellent feedback and guidance through the editing and study design process. Without your help, these studies would not have been possible.

I would like to express my gratitude towards thesis committee and all coauthors for their time and support throughout my PhD journey to make this dissertation possible.

I started my tenure at uOttawa as the sole graduate student in the Spine and Movement Biomechanics lab. That quickly changed, which gave me the opportunity to work and become friends with some amazingly talented graduate students, collectively known as RDT (if you know, you know): Alexandre, Eric, Gwyneth, Isabel, Kristen, Mina, Mohammad, Reza, Tianna, Victor, Wantuir Jr., and Xiong. I will forever remember our lunchtime Euchre and Crib games, conference/general outings, office shenanigans, and con-ver-saaaations.

Finally, I would like to thank my family for their support. Specifically, my partner Samantha has always been there to support me through the tough times and celebrate the good, while my fur children, Seeker and Kira, bring much-needed joy to my life. I love you all.

Co-Authorship

This dissertation includes two published, and one un-published manuscript. The authorship is as follows:

Chapter 3: Mavor, M.P., Ross, G.B., Clouthier, A.L., Karakolis, T., Graham, R.B., 2020. Validation of an IMU suit for military-based tasks. Sensors 20, 1–14. https://doi.org/10.3390/s20154280

Chapter 4: Mavor, M.P., Gruevski, K.M., Ross, G.B., Akhavanfar, M., Clouthier, A.L., Bossi, L.L.M., Karakolis, T., Graham, R.B., 2022. A data-driven framework for assessing soldier performance, health, and survivability. Appl. Ergon. 104, 103809. https://doi.org/10.1016/j.apergo.2022.103809

Chapter 5: Mavor, M.P., Chan, V.C., Gruevski, K.M., Bossi, L.L.M., Karakolis, T., Graham, R.B., In Prep. Assessing the Soldier Survivability Tradespace Using a Single IMU.

For each manuscript, M. P. Mavor completed the tasks of conceptualization and design of the research, acquisition of the data, analysis and interpretation of the data, writing the manuscripts, and critical revision of the manuscripts before publication.

Abstract

The overarching goal of this work was to develop novel data collection and analysis methods to better understand how soldier burden affects the soldier survivability tradespace (i.e., performance, musculoskeletal health, and susceptibility to enemy action). To achieve this goal, three studies were completed: 1) a mobile inertial measurement unit (IMU) suit was validated against an optical motion capture (OPT) system; 2) data from the IMU suit was used to develop a framework for morphing movement patterns to represent intermediary body-borne load masses and personal characteristics; and 3) a single IMU was used to develop a human activity recognition algorithm and calculate tradespace metrics.

In study one, a whole-body IMU suit (MVN Link, Xsens, Netherlands) was validated against an OPT system (Vantage V5, Vicon, United Kingdom) for military-based movements using the root mean squared error (RMSE) of joint angles and Pearson correlation coefficients of principal component (PC) scores. During a standard implementation (i.e., using different biomechanical models and not attempting to align them; V_{OPT} vs. X_{IMU}), average RMSE values across all tasks were less than 9° for the lower limbs but up to 40.5° for the upper limbs. When using the same biomechanical model and applying an alignment procedure (V_{OPT} vs. $V_{IMU\text{-}CAL}$), RMSE values decreased to an average of 2.5º and 17.5º for the lower and upper limbs, respectively. Of the 48 retained PCs, 38 (79%) had scores with a high or very high positive correlation ($\geq$ +0.70) between the OPT and IMU systems, 15 (31%) of which had scores with a very high correlation ($\geq$ +0.90). The average Pearson correlation coefficient was 0.81 (SD = 0.14). Given these results, the IMU system was deemed appropriate for collecting military-based movement patterns.

In study two, principal component analysis (PCA) and linear discriminant analysis (LDA) were used to generate whole-body morphable movement patterns to represent intermediary body-

borne loads and personal characteristics (sex, body mass, military experience). Reconstructed movements were used for animation, musculoskeletal modelling, exposure time calculations, and susceptibility calculations; all calculated values were comparable to previous research. This project displayed that a relatively small representative dataset can be used to simulate the change in whole-body movement patterns caused by many different body-borne loads and personal characteristics not originally collected. By implementing this framework, defence scientists can reduce the amount and complexity of data collections needed to better understand the impact on the survivability tradespace caused by all types of soldier burden.

Study three focused on developing a deployable method for calculating tradespace metrics in the field. Three deep neural network (DNN) architectures were trained to identify eleven class labels using data from a single IMU on the upper back. Data were collected during an indoor laboratory-based protocol and an outdoor simulated two-person section attack. The predictions made by the DNNs were processed through a two-step logical algorithm to apply real-world constraints and expand the predictions to 19 class labels. The deep convolutional long short-term neural network architecture outperformed the convolutional neural network and fully-connected neural network for all three approaches: indoor only, section attack only, and general. Movements were identified with a high degree of accuracy (> 87% for accuracy and weighted F1-score), and tradespace metrics were calculated within 0.17 seconds, 0.21 shots, and 1.25% susceptibility compared to the tradespace metrics calculated from the ground truth labels.

Overall, the data-driven methods developed throughout this dissertation can be used by defence scientists and military leaders to improve the understanding of the survivability tradespace, which has the potential to improve the quality of life of soldiers, making them more fit and ready to fight, thus increasing the likelihood of mission success.

List of Tables

List of Figures

List of Equations

Definition of Terms

3D	Three-dimensional
BTK	Biomechanical Toolkit
C3D	Coordinate three-dimensional
CAF	Canadian Armed Forces
CMC	Coefficient of Multiple Correlation
CNN	Convolutional Neural Network
CPU	Central Processing Unit
CSV	Comma Separated Variable
DeepConvLSTM	Deep Convolutional Long Short-term Neural Network
DNN	Deep Neural Network
DTW	Dynamic Time Warping
EMG	Electromyography
FC	Fully Connected Neural Network
FFO	Full Fighting Order
GPU	Graphics Processing Unit
GRF&M	Ground Reaction Force and Moment
GUI	Graphical User Interface
HAR	Human Activity Recognition
HD	High Definition
IMU	Inertial Measurement Unit
KTP	Kneel-to-prone
KTR	Kneel-to-run
LDA	Linear Discriminant Analysis
LDF	Linear Discriminant Function
LEAP	Load Effects Assessment Program
LFB	Lifting Full Body
LSTM	Long Short-term
NATO	North Atlantic Treaty Organization
OPT	Optical Motion Capture
PC	Principal Component
PCA	Principal Component Analysis
PCHIP	Piecewise Cubic Hermite Interpolating Polynomial
PTK	Prone-to-kneel
PTR	Prone-to-run
RAM	Random Access Memory
ReLU	Rectified Linear Unit
RMSE	Root Mean Squared Error
RMSProp	Root Mean Squared Propagation
RNN	Recurrent Neural Network
ROM	Range of Motion
RTK	Run-to-kneel
RTP	Run-to-prone

SD	Standard Deviation
SGD	Stochastic Gradient Descent
STR	Stand-to-run
$\mathbf{V_{IMU}}$	Visual 3D model driven by the IMU system
$\mathbf{V_{OPT}}$	Visual 3D model driven by the OPT system
$\mathbf{V_{IMU\text{-}CAL}}$	Visual 3D model driven by the IMU system aligned to the OPT coordinate system
$\mathbf{X_{IMU}}$	Xsens model driven by the IMU system

Chapter 1: Introduction

Soldier burden comes from the cumulative effect of internal and external stressors on the dismounted soldier that are oppressive, difficult to bear, and may elicit a reduction in the performance of military tasks (Armstrong and Bossi, 2021). There are four main categories where soldier burden can arise: the environment (i.e., weather, terrain), metabolic demands (i.e., heat/cold stress, fatigue), equipment properties (i.e., mass, mass distribution, coverage, bulk, stiffness, breathability, and thermal resistance), and psychological stressors (Bossi et al., 2020). However, doctrine guidelines across many North Atlantic Treaty Organization (NATO) members and much of the previous literature focus on the absolute mass of the equipment being carried relative to body mass (Drain et al., 2012; Oudenhuijzen et al., 2021). To keep soldiers safe while being effective war fighters, doctrine guidelines set the maximum load to be carried at 30% of body mass during an attack and 45% during an approach (Drain et al., 2012; Oudenhuijzen et al., 2021). However, there is a large disconnect between doctrine and the decisions being made on the battlefield, where military leaders are tasking soldiers with ~65% of body mass regardless of duration, threat, and environmental conditions. This is because the essential equipment being carried are quite heavy, comprising of protection, weapons, communications, sustainment, sensor equipment, and combat supplies specific to a mission's objective (Bossi et al., 2020; Oudenhuijzen et al., 2021).

The essential equipment being tasked to the soldiers are designed to protect soldiers from enemy action, complete specific mission objectives, and sustain soldiers on the battlefield. It is important that military leaders carefully consider the trade-offs between the benefits of additional equipment and the harms they do to the human body (Bossi et al., 2020). These considerations encompass the soldier survivability tradespace, which specifically evaluates soldier performance

(i.e., exposure time, movement velocity), musculoskeletal health (i.e., joint loading, posture), and survivability (i.e., likelihood of being hit by enemy action, likelihood of experiencing a traumatic event; Bossi et al., 2020).

It is well documented that an increase in body-borne load will result in a decrease in all tradespace metrics: performance (Billing et al., 2015; Hunt et al., 2016; Laing-Treloar and Billing, 2011), musculoskeletal health (Attwells et al., 2006; Brown et al., 2014a; Sturdy et al., 2021), and susceptibility (Billing et al., 2015; Hunt et al., 2016). Personal characteristics such as sex (Harper et al., 1997; Laing-Treloar and Billing, 2011), body composition (Lyons et al., 2005), stature (Martin and Nelson, 1986), and fitness (Billing et al., 2015; Hunt et al., 2016) can exacerbate the negative effects body-borne loads have on the survivability tradespace. Although these phenomena are quite clear, much of this work focused on male soldiers walking/running, representing only a small portion of the many tasks dismounted soldiers perform and demographics present in the soldier population. Therefore, there is much work to be done in the field of defence science to fully understand how all aspects of soldier burden affect the survivability tradespace for all movement patterns across many demographics. However, to feasibly increase our understanding of the survivability tradespace, novel data collection and analysis approaches are needed.

One novel data collection technique that can be applied to defence science is the use of inertial measurement units (IMUs), an emerging technology with growing acceptance in the scientific community for collecting human movement patterns. IMUs are ideal for military movements as they can be worn under operational clothing, are highly mobile (i.e., can be used in the field in many environments), and, when linked to a biomechanical model, can provide quality movement data comparable to gold-standard optical motion capture systems (Robert-Lachaine et al., 2017a; Schepers et al., 2018; Zhang et al., 2013). Although there are several perceived benefits

of IMUs for defence science research, previous validation studies do not account for the rapid movements and changes in height (i.e., running to prone) that soldiers perform. Thus, a validation study must be performed before an IMU system can be used to analyze soldiering movements.

While IMUs may be the answer to data acquisition, recruiting and collecting data on a diverse soldier population who perform all possible movements under infinite burden combinations is impractical from both a time and monetary perspective. We can address these limitations by applying novel data analysis techniques that can simulate intermediary experimental conditions from a relatively small but representative data set. Previous visual perception research outlines methods using principal component analysis and linear discriminant analysis to incrementally morph a movement pattern as more male/female (Troje, 2002), depressed/never-depressed (Michalak et al., 2009), and sad/happy (Michalak et al., 2009). Additionally, these same methods have been used in sports research to classify novice versus professional athletes (Ross et al., 2018). Using these published methods, whole-body operationally-relevant morphable movement patterns that incrementally change their behaviours based on changes to any aspect of soldier burden or personal characteristics could be developed. Such a methodology would simplify future data collections since intermediary experimental conditions could be simulated rather than collected. Interactions between soldier burden and personal characteristics could also be easier to identify, leading to better decisions about equipment tasking among soldiers and armour procurement.

Although the above methodology can accelerate our understanding of the survivability tradespace, it relies on deliberate data collection sessions and would use a non-deployable data collection system. Therefore, a novel data collection and analysis approach that is deployable is needed. One such approach is to use a human activity recognition (HAR) algorithm that identifies

operational movement patterns using data collected by a single IMU. In a military context, HAR has been applied to identify loaded marching, walking, running, jumping, and manual materials handling tasks with average accuracies across studies of 87.5% to 98.5% (Clements et al., 2013; Papadakis et al., 2020; Wyss and Mäder, 2010). However, these movements are a small subset of the movements performed by soldiers. Moreover, these studies were either performed before the development of or did not use the current gold standard architecture in HAR research: the deep convolutional long short-term memory neural network (Ordóñez and Roggen, 2016). A HAR algorithm based on a single IMU that identifies many operationally-relevant movements would benefit our understanding of the survivability tradespace. This method would enable field-based data collection protocols by using it as a preprocessing tool to supplement other technologies (e.g., identify movements that led up to an increase in heart rate or skin temperature), using it to directly calculate performance and susceptibility metrics, and understand the performance differences within a platoon during drills, among other applications.

The discussed data collection and analysis techniques have been successful applied to many fields of research but have either not at all been used nor not directly applied to the survivability tradespace. Within this dissertation, I present three studies that aim to develop the data collection and analysis tools defence scientists need to continue the important work of reducing the burden on dismounted soldiers. Study one validates a whole-body IMU suit for eight operationally-relevant movement patterns for the dismounted soldier against a gold-standard optical motion capture system. Study two uses the validated IMU suit to develop a framework to morph movement patterns to calculate changes to exposure time, velocity, joint loading, number of enemy shots fired, and susceptibility to enemy action caused by incremental changes to body-borne load magnitude, sex, body mass, and military experience. Study three develops a HAR

algorithm using data from a single IMU located on the upper back to identify 19 class labels from movements performed indoors and outdoors; the predictions were used to calculate tradespace metrics: exposure time, the number of shots fired, and susceptibility to enemy action. I hope that these novel data collection methods and analysis techniques will enable data-driven decisions that will influence doctrine/behaviours when tasking essential equipment to individual soldiers. This, in turn, will help reduce the risk of soldiers developing musculoskeletal injuries caused by overloading (Roy et al., 2013, 2012), reduce traumatic events by reducing susceptibility to enemy action (Billing et al., 2015; Hunt et al., 2016; Laing-Treloar and Billing, 2011), and optimize soldier performance.

Chapter 2: Literature Review

2.1 Soldier Burden

Military doctrine across many North Atlantic Treaty Organization (NATO) nations advises that the maximum body-borne load to carry for an approach/march and fighting is 45% and 30% of body mass, respectively (Drain et al., 2012; Oudenhuijzen et al., 2021). These percentages were selected to ensure that soldiers can perform their operational duties without undue fatigue or injury. However, epidemiological evidence suggests that carrying over 25% of one's body mass puts one at risk for knee, shoulder, and back injuries (Roy, 2011). A large body of literature supports that increasing body-borne loads leads to several negative biomechanical, physiological, and cognitive effects (Sanderson et al., 2021). Although, the reality is that despite doctrine and the overwhelming evidence, soldiers are being tasked with carrying body-borne loads of 55% to 85% of an average soldier's body mass (Oudenhuijzen et al., 2021).

2.1.1 Characterizing Body-Borne Loads

Soldiers are expected to carry a diverse range of equipment summarized by seven main categories: protection, weapon systems, sustainment, enhanced vision, subsistence, C4I systems (communication), and miscellaneous (Oudenhuijzen et al., 2021). Protection is the heaviest category, representing 33% of the body-borne load, including non-ballistic (i.e., environmental, hearing, solar, and insect protection) and ballistic protection (i.e., hard and soft armour and protective eyewear and helmet; Oudenhuijzen et al., 2021). The second heaviest category is weapon systems, which account for 30% of the body-borne load and incorporates the weapons themselves (i.e., small arms, anti-tank weapons, slings, ancillaries, etc.), ammunition (i.e., spare ammunition not in the weapon, pyrotechnics, grenades, etc.), and weapon-mounted sights. Subsistence includes both the non-powered items that meets a soldier's basic needs for survival

(i.e., food, water, utensils, water carriers, etc.) and powered items to maintain electronic equipment (i.e., spare batteries, power generators, fuel, etc.); this category represents 14% of the body-borne load (Oudenhuijzen et al., 2021). The sustainment category is sub-categorized into load carriage equipment (i.e., backpacks, load carriage vests, pouches, etc.) and overnight sustainment (i.e., any part of the sleeping system, toiletries, shelter and its associative lighting/heating, etc.); sustainment represents 10% of the body-borne load (Oudenhuijzen et al., 2021). C4I systems are the communication equipment used by soldiers (i.e., radio, headsets, displays, GPS, maps, etc.), which represent 6% of the body-borne load (Oudenhuijzen et al., 2021). Miscellaneous is a catch-all category that represents 5% of the body-borne load, which incorporates mission-specific equipment (i.e., breaching kit, ladders, axes, barrier materials, etc.), medical equipment (i.e., first aid kits, medicine, medevac equipment, etc.), and personal equipment (i.e., sewing kit, reading material, wallet, etc.; Oudenhuijzen et al., 2021). The lightest category is enhanced vision, representing 2% of the body-borne load, including head-mounted gear such as night-vision goggles and hand-held gear such as binoculars, glowsticks, flares, and more. (Oudenhuijzen et al., 2021).

Intuitively, a soldier would be tasked to carry equipment that is representative of the combative environment such that performance is optimized while maintaining soldier comfort and accomplishing specific objectives. However, in a recent NATO report, Oudenhuijzen et al. (2021) had five nations participate in tasking the equipment for soldiers for three hypothetical combat scenarios and found that despite changes to mission duration, enemy threat, and environmental conditions, the mass of the body-borne load was relatively the same; the average standard deviation within nations across scenarios was only 3.9 kg. The tasked loads were also very heavy, with an average of 54 kg (68% body mass) or more than twice the doctrinally recommended fighting load and 1.5 times the approach load. An explanatory reason for the consistently high body-borne loads

despite changes to combat scenarios is that a large focus of importance is placed on two main groups that comprised 63% of all the load carried: protection (33%; 18 kg) and weapons (30%; 16 kg).

Unfortunately, the focus that military leaders place on weapons and protection is inadvertently burdening the soldier and negatively affecting the survivability tradespace, nullifying many potential benefits. An alternative approach to keeping soldiers safe is the layered integrated survivability or "onion" model: 1) don't be there, 2) don't be seen, 3) don't be targeted, 4) don't be hit, and 5) if hit, don't be penetrated (Bossi et al., 2014; Guzie, 2004). When the focus is to give soldiers more protection (i.e., focusing on item five), it inadvertently impacts the more superficial layers through the combination of negative biomechanical, physiological, and cognitive changes that reduce overall performance, making soldiers more likely to be seen, targeted, and hit, ultimately leading to a greater potential for a traumatic injury.

2.1.2 Biomechanical and Physiological Responses

It is unanimously accepted that carrying body-borne loads cause a variety of negative biomechanical and physiological adaptations. The body of literature in these areas primarily focuses their experimental design on studying changes to gait/effort while walking when exposed to a change in the mass of the body-borne load. This focus is likely due to the relative ease of collecting gait data combined with human dependence on walking/running as their primary mode of locomotion. Unfortunately, little is known about how many other operationally-relevant movement patterns are negatively affected or how other equipment characteristics such as bulk and stiffness affect a soldier's biomechanical and physiological responses to body-borne load. However, this literature gap is being addressed by the Dutch Ministry of Defence by integrating

modular body-borne setups in their experimental design to assess bulk, stiffness, and mass (Gijsbertse et al., 2021).

Previous literature has identified many negative biomechanical changes to gait in response to heavy body-borne loads. As the mass of the body-borne load increases, so do ground reaction forces during heel-strike and toe-off (Birrell et al., 2007; Lidstone et al., 2017), forces at the L_4-L_5 intervertebral joint and hip (Sturdy et al., 2021), and flexion moments on the knee, hip, and trunk (Brown et al., 2014b). To accommodate these forces, soldiers adapt their kinematics by increasing trunk (Attwells et al., 2006; Brown et al., 2014b), hip (Attwells et al., 2006; Wang et al., 2013), and knee flexion angles (Attwells et al., 2006; Wang et al., 2013), as well as increasing pelvis anterior tilt (Birrell and Haslam, 2009; Wang et al., 2013) and pelvic rotation (Birrell and Haslam, 2009). Muscle-specific responses have also been shown where the gluteus maximus displays an increase in activation with a decreased contractile velocity, whereas the vastus lateralis increases muscle activation and contraction velocity when performing an agility run with jumps (Kessels et al., 2021). Spatiotemporal changes to gait have also been found where increases in body-borne load cause individuals to shorten their stride length, increase their stride frequency, increase the variability of their stride width, and increase the amount of time in double support (Attwells et al., 2006; Birrell and Haslam, 2009). When navigating obstacles, minimum foot clearance increases, and trail foot variability decreases, suggesting a guarding effect to avoid tripping (Brown et al., 2016). Much of the negative adaptations seen in gait also translate to cutting maneuvers (i.e., sudden change of direction while running), where an increase in stance time, hip flexion and adduction moments, knee flexion moments, hip flexion and adduction angles, and knee flexion angles have been observed as the body-borne load increases (Brown et al., 2014a). Drop landing (i.e., stepping off an elevated platform) is also negatively affected by increased ground reaction

forces, knee flexion moments, and hip flexion moments (Seymore et al., 2019). The highlighted biomechanical changes can cause a variety of musculoskeletal injuries and skin disorders, which will lower a soldier's overall quality of life and operational readiness (Knapik et al., 2004).

As the body-borne load carried increases, so does physiological demand. Heart rate, minute ventilation, oxygen uptake, and energy expenditure have significantly increased in response to body-borne loads (Lidstone et al., 2017; Majumdar et al., 1997). Adding armour also impairs heat dissipation where core temperature, skin temperature, and heart rate are significantly higher than wearing no armour (Pyke et al., 2015). Breathing mechanics are also negatively affected by body-borne loads. Pulmonary function is affected by both the compression of the armour (Armstrong and Gay, 2016) and the mass of backpack loads (Dominelli et al., 2012), eliciting a reduction in forced vital capacity, increased breathing power requirement, and a decrease in expiratory lung volume (Armstrong and Gay, 2016; Dominelli et al., 2012). These physiological responses to body-borne load can contribute to early-onset fatigue (Beekley et al., 2007; Phillips et al., 2016; Wang et al., 2013), which further degrades the biomechanical changes presented above, putting soldiers at a higher risk for injury.

It is important to note that much of the literature presented above-studied loads at or below 40 kg (interquartile 3), representing 53% of the participants' body mass. This is approximately 13 kg less than what Oudenhuijzen and colleagues (2021) found when interviewing international military leaders about what equipment they would task soldiers for three hypothetical combat scenarios. Of the presented work, only two studied loads representative of the Oudenhuijzen et al. (2021)'s findings: Attwells et al. (2006), who studied biomechanical changes up to 50 kg (66% of body mass), and Beekley et al. (2007) who studied loads up to 70% lean body mass, or ~48 kg.

Thus, given the discrepancy between the loads studied versus tasked, the biomechanical and physiological changes are expected to be more pronounced in the real world than reported.

2.1.3 Impact on Performance

The presented biomechanical and physiological responses to an increase in body-borne load affect soldier performance. It has been shown that during simulated break contact (i.e., five 30-metre prone-to-run tasks every 44 seconds) and a fire and movement tasks (i.e., 16 six-metre kneel-to-run tasks every 20 seconds), exposure time (i.e., time exposed to enemy fire) increases by 0.8% and 1.1%, respectively, per kilogram of body-borne load (Billing et al., 2015; Hunt et al., 2016). Laing-Treloar and Billing (2011) identified a 30% increase (+2.0 seconds) in exposure time when completing a break contact simulation when carrying a 21.6 kg body-borne load than unloaded and unarmed. Billing et al. (2015) found that soldiers are exposed for 14% longer (+1.1 seconds) during a break contact simulation and exposed for 18% longer (+0.8 seconds) during a fire and movement task when carrying a 30 kg (37% average body mass) compared to a 9.8 kg (12% average body mass) body-borne load.

A semi-standardized obstacle course used by many allied nations is the Loads Effects Assessment Program (LEAP), developed by Human Systems Inc. (Canada) in partnership with the United States Marines. The Canadian LEAP course consists of ten obstacles: hatch and tunnel, sprint, stairs and ladder, agility run, casualty drag, window vault, bounding rushes, balance beam, crawls, and wall vault, with some variability between nations (Gruevski et al., 2020). Increasing the mass of body-borne loads increase the time to complete the entire LEAP course (Bossi et al., 2016; Gijsbertse et al., 2021; Karakolis et al., 2017; Kessels et al., 2021; Pandorf et al., 2002; Vitali et al., 2019). However, on an obstacle-by-obstacle basis, some are more impacted than others. Vitali et al. (2019) found significant decreases in performance metrics for all obstacles except for

an additional manual material handling task and the casualty drag, which had mixed results. Gijsbertse et al. (2021) assessed how bulk, stiffness, and mass effect LEAP performance. Body-borne load increased overall completion time by 1.5%/kg, and average completion time for each obstacle increased by 1.8%/kg, but observations as high as 4.5%/kg were reported for the balance beam task (Gijsbertse et al., 2021). Increasing bulkiness and stiffness with a minimal increase in body-borne load (~ 1 kg) significantly increased the completion time for the entire LEAP course, with the most affected obstacle again being the balance beam, followed by the hatch and tunnel and wall climbing obstacles (Gijsbertse et al., 2021). When bulk, stiffness, and load were combined (~ 10 kg), overall LEAP completion time increased by ~30%; comparatively, a 10 kg load increased completion time by ~13 %, and a 30 kg load increased completion time by ~51% (Gijsbertse et al., 2021). These results highlight the importance of considering other body-borne load characteristics beyond load when trying to maintain soldier performance. Body-borne load also affects performance during low-intensity long-duration movements. Over a 10-kilometre march, Harper et al. (1997) found that increasing the body-borne load from 18 kg to 36 kg resulted in a completion time increase of 12.5 minutes (99.1 vs. 121.6 minutes). Pandorf et al. (2002) found that when completing a 3.2 km run, completion time increased by 19% (5 minutes) when carrying a 27 kg body-borne load and increased by 44% (11 minutes) when carrying a 41 kg load compared to a 14 kg body-borne load.

It is clear that soldier performance during long and short-duration movements is negatively affected by an increase in body-borne load, and there is emerging evidence for other equipment characteristics such as bulk and stiffness (Gijsbertse et al., 2021). While military doctrine aims to reduce these negative effects, the suggested mass is often close to what is incorporated into experimental design, which produced the results discussed above. However, the way doctrine

approaches body-borne loads is to focus on the mass of the load in the context of percent body mass. Unfortunately, this is an oversimplified view of a soldier's capacity to carry body-borne loads since many personal characteristics can impact one's ability to accommodate heavy body-borne loads that are not considered.

2.1.4 Personal Characteristics

Modern militaries around the globe are focusing on diversifying their armed forces. For example, the Canadian Armed Forces want an inclusion rate of 25% women across all service members by 2026; currently, 16% of service members are women (Government of Canada, 2022). Although diversity is an essential part of the modern military, it is essential to acknowledge and account for the modifiable and non-modifiable personal characteristics of a large and diverse population. Sammito et al. (2021) performed a systematic review that identified 57 risk factors that contribute to musculoskeletal injury risk in the military. Of the 15 strongly related risk factors that contribute to musculoskeletal injury, four are modifiable personal characteristics (i.e., body fat, body mass, physical fitness, and smoking), and three are non-modifiable (i.e., previous injury, race/ethnicity, sex; Sammito et al., 2021).

Improving modifiable personal characteristics is likely to have the greatest impact on the survivability tradespace. Low physical fitness is often combined with higher body fat levels and possibly other poor behaviours (e.g., smoking). Lyons et al. (2005) found that the ratio between lean body mass and dead mass (i.e., body fat and carried body-borne load) and ventilatory capacity (VO_2) are strong predictors of metabolic demand. From a physiological perspective, those with less fat mass can accommodate heavier body-borne loads (Lyons et al., 2005). However, exercise interventions should focus not only on lowering body fat, but improving lower limb strength. During a fire and movement (i.e., 16 six-metre bounds) task, lower limb power in the form of

vertical jumps (Billing et al., 2015), standing broad jump (Stein et al., 2022), and critical velocity (Hunt et al., 2016; Stein et al., 2022) are predictors for higher exposure times and thus susceptibility to enemy action. When Billing et al. (2015) separated their population into "fast" and "slow" groups, they reported that the slow group was almost twice as susceptible as the fast group per additional kilogram of body-borne load (slow: 1.40 %/kg; fast: 0.78 %/kg). When analyzed further, Hunt et al. (2016) reported that the most critical portion of the break contact simulation was the initial acceleration from kneeling and peak velocity. Therefore, exercise interventions targeting lower limb power can profoundly impact the survivability tradespace. A 10-week training program focused on load carriage capacity has been shown to elicit positive changes to general fitness measures (i.e., pushups, situps, and estimated VO_2), maximal squat jump force output (Wills et al., 2019), and lower limb kinematics and kinetics during a 5 km march (Wills et al., 2021b). These observed changes could help reduce the risk of musculoskeletal injury during extended marches (Wills et al., 2021b) and may be transferable to an increase in performance and reduced susceptibility to enemy action during tactical movements.

It is important to note that the results from the above literature are based on male participants; however, several sex-based differences have been reported. During a 10 km loaded march, Harper et al. (1997) found that when carrying an 18 kg, 27 kg, and 36 kg load, males consistently had completion times ~79% of that of females, which represents a ~20-minute difference at 18 kg and a ~30-minute difference when carrying 36 kg. For tactical movements, Laing-Treloar and Billing (2011) found that females were more affected by heavier body-borne loads compared to males when completing a break contact simulation. Males increased their exposure time by 1.7 seconds (1.33%/kg; 29%) while females increased their exposure time by 2.5 seconds (1.63%/kg; 36%) when carrying 21.6 kg versus unloaded and unarmed (Laing-Treloar

and Billing, 2011). To improve load carriage capacity in women, Wills et al. (2021a) implemented the same 10-week training program as Wills et al. (2019); while beneficial adaptations to load carriage were observed in both sexes, the specific modes of change were different. Post-training, when completing a 5 km 23 kg loaded march, males tended to adopt their knee and ankle kinematics/kinetics to favour a more ankle-driven propulsion strategy, while females adopted their hip and knee kinematics/kinetics to favour a more hip-driven strategy (Wills et al., 2021a).

Given that both modifiable and non-modifiable personal characteristics, equipment properties and environmental conditions all can alter one's response to a body-borne load, it is likely that more complex metrics are needed to create guidelines for carrying body-borne loads. Targeted data collections are needed to increase our understanding of how these factors interact, ideally, in the environments where the movements are performed to increase generalizability. To properly collect these data, novel data collection methods will need to be implemented.

2.2 Novel Data Collection Approach

2.2.1 Data Collection Challenges

Traditionally, biomechanical analyses are done by tracking human movement patterns through placing passive/active markers on anatomical landmarks, which are tracked by an optical motion capture (OPT) system and then associated with a musculoskeletal model to understand what impact an experimental condition had on the body (Robertson et al., 2014). Of course, additional equipment can be used to collect data synchronously with the OPT system to gain more information (e.g., force plates, electromyography). To avoid marker artefacts, participants are asked to bare skin or wear specialized clothing that is skin tight, so reflective markers can be taped/fastened to the body while avoiding skin and clothing artefacts (Benoit et al., 2015;

Robertson et al., 2014). Further, marker trajectories can only be reliably collected if they are fully visible and within the calibrated volume (Robertson et al., 2014).

Given the limitations of the OPT system, it becomes difficult to collect movement patterns of individuals wearing operational clothing. If markers are placed on the torso, the researcher will be collecting the movement patterns of the equipment itself rather than the human body underneath. Occlusions also become a serious concern when wearing bulky equipment. For example, if carrying a backpack, depending on the size and shape, it may cover the sacrum entirely and make it impossible to place reflective markers on the back. These limitations may be a driving factor as to why most of our knowledge on body-borne loads revolve around lower limb kinematics during walking/running tasks since researchers can ask participants to wear tight shorts and place markers directly on the skin (e.g., Brown et al., 2014b, 2014a; Ramsay et al., 2016) without much interference from the trunk-worn loads. That is not to say the literature does not provide an understanding of trunk kinematics/kinetics. Two-dimensional analyses have been done to show trunk flexion increases with body-borne load (Attwells et al., 2006; Martin and Nelson, 1986), and more recently, three-dimensional musculoskeletal modelling has been applied to individuals carrying backpacks (Sturdy et al., 2021). However, the trunk is typically treated as a rigid body by placing markers on the sternum, acromions, and C7 spinal process (Attwells et al., 2006; Sturdy et al., 2021). Further, much of our knowledge is limited to the OPT system's small capture volumes, with most studies performed on treadmills (e.g., Lidstone et al., 2017; Wang et al., 2013) or over distances of 10 metres or less (e.g., Attwells et al., 2006; Brown et al., 2014b; Liew et al., 2016a; Sturdy et al., 2021).

2.2.2 Inertial Measurement Units

Although OPT data collections have been instrumental in defining what occurs in the human body when carrying body-borne loads, the inherent limitations in the experimental design make it difficult to generalize what was observed in the laboratory to the field. It is also challenging to apply the experimental setup to other operationally-relevant movements that will inherently occlude markers (e.g., taking cover, kneeling, prone, crawling, etc.) or feasibly assess workplace tasks (e.g., marksmanship, ladder climbing, tunnel navigation, etc.). Therefore, novel data collection methods are needed to further our understanding of how body-borne load characteristics affect soldiers beyond gait.

A novel method of motion capture, with growing acceptance in the research community, is to use wearable inertial measurement units (IMUs) to capture body kinematics. IMUs are small portable devices with an accelerometer, gyroscope, and magnetometer, which measure linear acceleration, angular velocity, and the earth's magnetic field. To make sense of these data streams in a biomechanics context, IMU data can be fused to update the sensor's orientation (e.g., Madgwick, Kalman, complementary filters), which is then oriented to a participant's segments (i.e., feet, shanks, thighs etc.), allowing the calculation of joint kinematics (Seel et al., 2012) that are comparable to OPT systems (Mavor et al., 2020; Robert-Lachaine et al., 2017a; Schepers et al., 2018).

Similar to OPT systems, IMUs are taped directly on the skin or fastened to specialized clothing. However, unlike OPT systems, IMUs are not limited by line-of-sight. Rather, data are streamed through Bluetooth or Wi-FI or are stored onboard to be downloaded later (Schepers et al., 2018). Therefore, any clothing can cover the IMU sensor when collecting whole-body movement data as long as it does not interfere with the sensor's movement or data stream signal,

if applicable. Additionally, IMUs are not limited by their environment (except magnetic disturbances), allowing for outdoor data collection over long distances and differential terrain, which is not possible with OPT systems. These advantages over an OPT system make IMU technology an excellent candidate for collecting whole-body soldier movement patterns.

One commercially available whole-body IMU system is the Xsens MVN BIOMECH Link (Xsens, Netherlands). The Xsens IMU system comprises of 17 sensors placed over the body on key segments and are fused with a biomechanical model to calculate joint and segment kinematics (Roetenberg et al., 2013a). The Xsens IMU system collects at a frequency of 240 Hz, is marketed as being fully resistant to magnetic interference, and has been validated against a gold standard OPT system for overground walking (Schepers et al., 2018), running (Schepers et al., 2018; Zhang et al., 2013), and stair ascent/descent (Zhang et al., 2013). Schepers et al. (2018) reported an RMSE in joint angles of less than 5° in the flexion/extension axis of the hip, knee, and ankle and an RMSE of less than 8° in the other two off-axes when OPT and IMU data were processed using the gait 2392 OpenSim model (Delp et al., 2007). Zhang et al. (2013) reported a coefficient of multiple correlation (CMC) of greater than 0.96 for the flexion/extension axis of the ankle, knee, and hip and a CMC ranging from 0.5 – 0.85 in the other two off-axes. Based on these findings, it appears that the Xsens IMU system is very accurate in the flexion/extension axis for lower limb joint angles but has a poorer performance in the ab/adduction and rotation axes.

An alternative to a whole-body IMU suit is using a single IMU. While it is not possible to collect whole-body kinematic data, as it will not be coupled to a biomechanical model, researchers have used the data from a single IMU to answer several research questions. In a military context, a single IMU was used to identify changes in exposure time and susceptibility caused by body-borne loads and personal characteristics (Billing et al., 2015; Hunt et al., 2016). Military

researchers have also applied pattern classification and machine learning to identify loaded vs unloaded walking (Clements et al., 2013) and classify operationally-relevant movement patterns (Clements et al., 2012; Papadakis et al., 2020; Wyss and Mäder, 2010). Machine learning for human activity recognition is discussed more below.

Given the early promise of IMU technology, it may be desirable to collect whole-body IMU data to understand the musculoskeletal health portion of the survivability tradespace and use a single IMU for the performance and susceptibility portion. In this way, detailed data collection procedures that analyze joint kinematics and kinetics could categorize the whole-body IMU system, while a single IMU is a deployable technology to collect meaningful information in the field. While this appears to be an excellent approach, the reality of collecting and analyzing a representative number of movements from a diverse population wearing a vast selection of equipment properties (i.e., mass, bulk, stiffness, etc.), in diverse environments, and under an array of psychological stressors makes fully understanding how soldier burden affects the survivability tradespace infeasible both from a time and monetary perspective unless novel analytical methods are used.

2.3 Novel Data Analysis Approach

2.3.1 Machine Learning

Machine learning algorithms are powerful data analysis tools that has been embraced by researchers in almost every field of research. Machine learning is an umbrella term for many different algorithms executed on a computer that can learn and adapt without explicit instructions by discovering patterns within a dataset (Machine Learning, 2020). The method in which the algorithms learn is unique to each algorithm. However, the typical workflow is to present the algorithm with a set of training data consisting of features (i.e., important aspects of the data that

are chosen by the researcher or are derived by the algorithm), test the algorithm's ability to classify or predict data it has not seen before, and then implement the algorithm in the context of the real-world problem it has been designed for (Duda et al., 2001). Of interest for this dissertation are the algorithms that classify data to separate two or more data classes (i.e., categories or groups), which can then be used to classify new unseen data (Duda et al., 2001).

Data obtained from human movement patterns are in the highly dimensional time-series domain. This is not ideal for machine learning algorithms as each data point would be viewed as a feature, which results in an exponential increase in the number of trials/participants needed to get a reasonable classification rate (Bengio et al., 2005). Since one of the challenges to studying soldier burden is recruiting a large and generalizable soldier population, the data's dimensionality and thus the number of features need to be reduced.

2.3.2 Feature Extraction

Principal component analysis (PCA) and convolutional neural networks (CNNs) are two algorithms that have been successfully applied to human movement data to extract key features prior to classification. PCA is a data reduction method that identifies the greatest modes of variance within a given signal for an entire dataset, which are deemed principal components (PC; Troje, 2002). In short, the covariance matrix of a dataset is orthogonally decomposed to obtain the eigenvalues and eigenvectors. Then, the decomposed matrix is projected onto each eigenvector (PC), and the new coordinate in the eigenvector space is termed the principal component score (PC score) of that data point for that PC (Robertson et al., 2014). These PC scores are then used as input for machine learning algorithms. Meanwhile, CNNs extract features by convolving, or filtering, over a windowed portion of a time-series signal (Clouthier et al., 2020; Ordóñez and Roggen, 2016). Depending on how well the windowed signal matches a corresponding filter, a

value between zero and one is placed in a feature map matrix (Clouthier et al., 2020; Ordóñez and Roggen, 2016; Ronneberger et al., 2015). Once the feature map is created, a method called pooling (e.g., maximum, mean) will reduce the feature map to identify the maximum value within a specified window, for example (Ronneberger et al., 2015). The final feature space is reshaped into a vector and used as input for a machine learning algorithm for classification (Clouthier et al., 2020; Ordóñez and Roggen, 2016; Ronneberger et al., 2015). This dissertation will focus on two machine learning algorithms: linear discriminate analysis (LDA) and long short-term memory neural networks (LSTM).

2.3.3 Linear Discriminant Analysis

LDA is a classification algorithm that uses discrete data as input (e.g., PC scores). LDA can classify multiple groups, but this dissertation will focus on binary classification. Using the assumption of equal variance between classes, a linear decision boundary is calculated. This decision boundary is termed the linear discriminant function (LDF) and is located orthogonal to the mean difference between classes multiplied by the inverse of the covariance matrix (Duda et al., 2001). The location of the LDF along this vector is determined through training (Duda et al., 2001). When applying PCA and LDA to movement data, the LDF can be transformed back into the mover space (i.e., the collected data) to describe how the two classes move differently (Troje, 2002). Importantly, an average movement pattern can be morphed by scaling the LDF:

$$MorphedMovement = \bar{x} + LDF * \alpha \quad \text{(Eq. 2.1)}$$

where $\bar{x}$ represents the mean movement pattern across both classes, LDF represents the linear discriminant function that describes the decision boundary between class labels, and α represents the scaling factor. Using Equation 2.1, movements can be altered to behave more like one class label than another by altering the α value (Troje, 2002). These methods have been successfully

applied to sports research to classify novice versus elite athletes (Ross et al., 2018) and to visual perception research, where gait movement patterns were iteratively expressed to behave as individuals who are more male/female (Troje, 2002), depressed/never-depressed (Michalak et al., 2009), and sad/happy (Michalak et al., 2009).

In a military context, the PCA/LDA method could be used to represent movement patterns under a spectrum of intermediary body-borne load characteristics (e.g., mass, bulk, stiffness), a variety of modifiable and non-modifiable personal characteristics (e.g., sex, military experience), environments (e.g., terrain, temperature), and psychological stressors that were never collected or cannot be collected. With this approach, it would become feasible to collect a representative dataset to understand the intermediary conditions and interactions between conditions by adding multiple LDFs together (Troje, 2008). Understanding what happens to tradespace metrics as soldier burden incrementally increases would make it possible to create decision tools that take into account aspects of the soldier system to keep soldiers safe without sacrificing musculoskeletal health, performance, and increasing susceptibility to enemy action.

2.3.4 Long Short-term Memory Neural Network

LSTM is a neural network architecture that is part of the recurrent neural network (RNN) family. RNNs can be thought of as a for loop, where a window of data are input for each iteration, and the output knowledge is transferred to the next node along with the new window of data (Du et al., 2021). Deep neural networks using the LSTM architecture have been successful at human activity recognition (HAR) and have been applied to gestures and activities of daily living (Lawal and Bano, 2020; Ordóñez and Roggen, 2016) and on non-sport specific movements (Clouthier et al., 2020). LSTM architectures overcome simple RNNs' limitation of short-term memory loss (Semeniuta et al., 2016) by regulating what information is the most important to pass on and what

information to forget (Ordóñez and Roggen, 2016). These decisions are regulated through gates that host sigmoid and tan functions, which scale the data between 0 and 1 and -1 and 1, respectively. These gates inform the cell state, which is the long-term memory of the LSTM networks and the hidden state, which is the short-term memory (Ordóñez and Roggen, 2016). Data included in the long and short-term memory are passed along to the next node along with the next chronological datapoint (Lawal and Bano, 2020; Ordóñez and Roggen, 2016). This is repeated until all data are included.

As discussed, features need to be extracted from time-series data when using machine learning algorithms. When using an LSTM architecture, CNNs are typically used to extract features of windowed sections of input data (e.g., Clouthier et al., 2020; Lawal and Bano, 2020; Ordóñez and Roggen, 2016). For example, the deep neural network DeepConvLSTM uses four convolutional layers, two LSTM layers, and a softmax layer (Ordóñez and Roggen, 2016). Features of windowed input data are extracted using the convolutional layers and fed into the LSTM layers for classification (Ordóñez and Roggen, 2016). Class scores are output from the LSTM layers into a softmax layer which translates these scores into probabilities (Ordóñez and Roggen, 2016).

2.3.5 Human Activity Recognition

The current gold standard for human activity recognition (HAR) is the DeepConvLSTM architecture (Ordóñez and Roggen, 2016). This architecture was developed using data from multiple IMUs/accelerometers and achieved superior performance at recognizing gestures and activities of daily living compared to other machine learning methods (Ordóñez and Roggen, 2016). Using a variety of HAR methods, researchers have been able to identify many activities of daily living (Ankita et al., 2021; Ordóñez and Roggen, 2016; Russell et al., 2021), non-specific

sporting movements (Clouthier et al., 2020), workplace postures (Abobakr et al., 2019) and tasks (Bangaru et al., 2021), and military activities (Clements et al., 2012; Papadakis et al., 2020; Wyss and Mäder, 2010), among many others. Using the knowledge obtained from the HAR algorithms, researchers have been able to perform workplace ergonomic assessments (Abobakr et al., 2019; Antwi-Afari et al., 2020) and at-home monitoring of activities of daily living (Lockhart et al., 2013).

Previous HAR literature with a military focus has been able to identify walking, running, (Clements et al., 2012; Papadakis et al., 2020; Wyss and Mäder, 2010), jumping (Papadakis et al., 2020), loaded marching, lifting and carrying loads, and digging (Wyss and Mäder, 2010). Across this work, the authors were able to obtain high accuracies (87.5% to 98.5%) when identifying movement patterns using a uniaxial accelerometer + heart rate monitor (Wyss and Mäder, 2010), triaxial accelerometer + GPS (Clements et al., 2012), and an IMU (Papadakis et al., 2020). Researchers have also been able to identify a change in body-borne load using a single triaxial accelerometer (Clements et al., 2013; Williamson et al., 2015). The above work used a variety of pattern classification and machine learning approaches to correctly recognize military movement patterns. Given the success of the DeepConvLSTM architecture for HAR, it may be possible to obtain similar levels of accuracy across a diverse set of military movements using a single IMU.

2.4 Research Questions and Hypotheses

2.4.1 Study 1

IMU-based motion capture methods appear to be ideal for understanding biomechanical variables in a military context since they are portable and can be worn under operational clothing. However, there are no validation studies for military-based movements beyond walking and running. Therefore, study one was designed to answer the following two research questions: 1) “is

the Xsens MVN Link IMU suit valid for capturing whole-body kinematics of eight military-based movement patterns that include prone and kneeling postures?" and 2) "is the observed error due to technology or biomechanical model differences?". It was hypothesized that 1) there would be good agreement between the kinematics and marker trajectories captured through IMU suit and a motion capture system as assessed through root mean squared error of joint angles and Pearson correlations of PC scores and 2) the majority of the error would be caused by model differences, which can be mitigated by using a common biomechanical model.

2.4.2 Study 2

Recruiting and collecting motion capture on a diverse population under a variety of soldier burdens is impractical from a time and monetary prospective; however, it is essential for understanding all aspects of the survivability tradespace. Study two asked the research question "can a data-driven framework be developed to simulate intermediary body-borne and personal characteristics not originally collected?" It was hypothesized that it would be possible to use PCA and LDA to create quality morphable movement patterns of intermediary movers and produce similar performance, musculoskeletal health, and susceptibility metrics as previous literature.

2.4.3 Study 3

Although a whole-body IMU suit can provide a tremendous amount of biomechanical information and drive many essential research questions, it is not practical for widespread usage due to the cost, complexity, and fragility. An alternative approach is to use a single IMU to inform a human activity recognition algorithm designed to identify military-based movements. Thus, study three aimed to answer the research question: "Can a deep neural network be trained to identify eleven movement types using data from a single IMU located on the upper back?" It was

hypothesized that a deep neural network could be trained to predict movement patterns with an accuracy of 85% or more using a single IMU.

Chapter 3: Validation of an IMU Suit for Military-Based Tasks

Sensors 2021, 20, 1–14. https://doi.org/10.3390/s20154280

3.1 Abstract:

Investigating the effects of load carriage on military soldiers using optical motion capture is challenging. However, inertial measurement units (IMUs) provide a promising alternative. Our purpose was to compare optical motion capture with an Xsens IMU system in terms of movement reconstruction using principal component analysis (PCA) using correlation coefficients and joint kinematics using root mean squared error (RMSE). Eighteen civilians performed military-type movements while their motion was recorded using both optical and IMU-based systems. Tasks included walking, running, and transitioning between running, kneeling, and prone positions. PCA was applied to both the optical and virtual IMU markers, and the correlations between the principal component (PC) scores were assessed. Full-body joint angles were calculated and compared using RMSE between optical markers, IMU data, and virtual markers generated from IMU data with and without coordinate system alignment. There was good agreement in movement reconstruction using PCA; the average correlation coefficient was 0.81 ±0.14. RMSE values between the optical markers and IMU data for flexion-extension were less than 9°, and 15° for the lower and upper limbs, respectively, across all tasks. The underlying biomechanical model and associated coordinate systems appear to influence RMSE values the most. The IMU system appears appropriate for capturing and reconstructing full-body motion variability for military-based movements.

3.2 Introduction

Load carriage is an important component of typical occupational activities for military soldiers. When on the battlefield and during training, soldiers wear bulky clothing, stiff armour, and carry heavy backpacks. The items a soldier carries are lifesaving and operationally-relevant. However, they may also lead to musculoskeletal injuries over time (Andersen et al., 2016; Orr et al., 2015; Roy, 2011) and impair overall performance (e.g., movement speed and exposure time) (Billing et al., 2015; Hunt et al., 2016). To better understand the demands placed on the body by typical military loads, researchers have studied the effects of load carriage on joint kinematics using optical motion capture. Operationally-relevant loads increase trunk flexion, lower limb flexion range of motion (ROM), and walking speed during gait (Attwells et al., 2006; Majumdar et al., 2010). However, optical motion capture is generally confined to use in a laboratory setting and measuring motion in a more natural working environment is not typically feasible. Furthermore, optical motion capture requires line of sight between the cameras and body-mounted markers, which makes it challenging to study the effects of wearing military equipment as the markers must not be covered.

Inertial measurement units (IMUs) are becoming increasingly popular as a method of measuring human movement that overcomes some of the barriers of optical motion capture. IMUs are small devices that contain sensors to make inertia-based measurements of motion. These may consist of an accelerometer, gyroscope, and magnetometer that measure linear acceleration, angular velocity, and variations in the magnetic field, respectively. A range of kinematic and kinetic variables, including joint angles can be calculated by fusing data from these sensors and incorporating constraints from a biomechanical model (Lin and Kulić, 2012; Roetenberg et al., 2013b). IMUs can be placed directly on the skin, can be covered with clothing, and are highly

transportable, which directly addresses the aforementioned limitations of optical systems. These benefits of IMU technology allow researchers to study individuals in their natural environment, while wearing the appropriate clothing and equipment needed to perform a given task.

Growing interest in the potential of IMUs has led to a number of validation studies that aim to assess the accuracy of joint kinematics calculated using these wearable sensors. Typically, accuracy has been quantified by comparing joint angles calculated using IMU systems to optical motion capture through root mean squared error (RMSE) (Adamowicz et al., 2019; Karatsidis et al., 2019), correlation coefficients (Ferrari et al., 2010; Morrow et al., 2017), and/or Bland-Altman limits of agreement (Robert-Lachaine et al., 2017a; Teufl et al., 2019). Efforts have largely been focused on IMU system validation for lower limb angles during gait (Laudanski et al., 2013; Robert-Lachaine et al., 2020; Zügner et al., 2019). However, other activities, including stair climbing, kicking, materials handling, and skiing (Robert-Lachaine et al., 2017a; Supej, 2010; Zhang et al., 2013) and upper body angles (Chapman et al., 2019; Cutti et al., 2008) have been examined as well. Lower limb sagittal plane angles have been found to have relatively low RMSE ranging from 2–11° (Ohtaki, Y, Sagawa, K, Inooka, 2001; Schepers et al., 2018; Seel et al., 2014; Weygers et al., 2020) and good correlation coefficients from 0.9–1.0 (Al-Amri et al., 2018; Ferrari et al., 2010; Karatsidis et al., 2019) with optically-derived angles. Errors tend to be greater and correlations worse for frontal and axial plane angles (Ferrari et al., 2010; Schepers et al., 2018; Zhang et al., 2013). Studies reporting full-body angles have demonstrated larger errors for upper body angles, compared to lower limb angles (Robert-Lachaine et al., 2017a, 2017b). These previous IMU system validation studies were aimed at investigating movements that target the lower limbs and manual materials handling tasks where there was little translation by the participant. These are not representative of the prone positions or rapid changes in height that are

typically performed by soldiers. As a result, the validity of using an IMU system to measure military-based movements remains unclear.

Our larger, overarching goal is to generate morphable models of movement using principal component analysis (PCA) and linear discriminant analysis. That is, we intend to incrementally alter and represent military movement patterns between two body-borne load conditions without actually collecting an intermediate load. This will allow us to simulate a spectrum of body-borne load conditions that are infeasible to collect. Before this can be accomplished, we must establish an accurate method of measuring full-body movement during typical military activities in the field while wearing operationally-relevant loads. The purpose of this investigation was to compare an IMU system (MVN BIOMECH Link, Xsens, Enschede, Netherlands) with an optical (OPT) motion capture system (Vantage V5, Vicon, Oxford, UK) for a variety of operationally-relevant military movements. To be comparable to previous research, we compared the RMSE of the joint angles calculated using the IMU system to the OPT system. We calculated joint angles using the IMU data in multiple ways to determine the differences between systems that could be expected in practice, and to examine any difference due to the biomechanical models used by each system and the technology itself. We also examined the agreement of the systems in terms of full-body movement variability as captured using PCA as this pattern recognition technique will be used in the future to generate morphable models of movement.

3.3 Materials and Methods

3.3.1 Participants

Ten male and 10 female civilian participants were recruited for this study. However, due to technical difficulties caused by both systems, which made the data unusable, only nine males and nine females were analyzed. Mean age, height, and mass of all participants were 23.7 years

(standard deviation (SD) = 3.44), 175 cm (SD = 7.93), and 71.9 kg (SD = 13.2), respectively; all participants' demographics are reported in Table 3.1. All participants read and signed the participant information letter, which was approved by the University of Ottawa ethics board (approval number H-06-18-721), before data collection began.

Table 3.1. Participant demographics.

	Number of Participants	Age (years)	Height (cm)	Mass (kg)
		Mean (SD; Range)	Mean (SD; Range)	Mean (SD; Range)
All	20	23.7 (3.44; 13.0)	175 (7.93; 30.3)	71.9 (13.2; 42.2)
Female	10	22.3 (2.26; 4.00)	171 (9.23; 26.2)	63.5 (6.80; 11.3)
Male	10	25.1 (3.93; 13.0)	179 (3.91; 11.7)	80.3 (12.8; 36.3)

Note: SD = Standard deviation. Range = maximum value minus the minimum value.

3.3.2 Participant Preparation and Equipment

Participants were asked to change into athletic shorts and a Lycra® T-shirt that is specifically designed for the Xsens system. The T-shirt has Velcro® locations on the shoulders to place sensors, zippers on the back to contain wires, and pockets in the back to host the battery and onboard computer.

Participants were first outfitted with 17 IMU sensors, which were placed on the back of the head, sacrum, sternum, and bilaterally on the upper arms, forearms, hands, shoulders, thighs, shanks, and feet. The pelvis, upper limb, and lower limb sensors were affixed to the skin using neoprene bands, specialty gloves were used for the hand sensors, an elastic headband was used for the head sensor, the trunk sensors (sternum and shoulders) were placed in the T-shirt described above, and the feet sensors were placed inside participants' shoes using a neoprene insert.

A cluster-based optical marker set was then placed atop the IMU system. Passive four-marker clusters were affixed to the body with Velcro® atop the IMU system's neoprene bands to be in a similar locality as the IMU system for each segment. The four-marker cluster placed

approximately over the T_{10}–T_{12} vertebrae was placed using a neoprene band that wrapped around the abdomen and over the IMU system's battery pack and onboard computer; the cluster was placed between the hardware. A three-marker cluster was taped onto the dorsal aspect of the toe bed of the participants' shoes and four individual markers were taped onto the headband. Individual markers were also taped to specific anatomical landmarks (bilaterally on the medial and lateral malleoli, medial and lateral condyles of the humerus and femur, greater trochanter of the femur, radial and ulnar styloid processes, PSIS, ASIS, iliac crests, acromions, and dorsum of the hands and on C7) so a whole-body biomechanical model could be created.

Participants' kinematic data were captured simultaneously from both the IMU (MVN BIOMECH, Xsens, Enschede, Netherlands) and OPT (Vantage 5, Vicon, Oxford, UK) motion capture systems at 240 Hz. A common event of hand clapping/floor smacking was used to synchronize both motion capture systems. A visual representation of the participant setup is displayed in Figure 3.1.

Figure 3.1 Participant setup. A cluster-based optical marker set was worn on top of the Xsens IMU suit.

3.3.3 Movement Protocol

Participants were asked to perform eight operationally-relevant military movements: running, walking, kneel-to-prone (KTP), prone-to-kneel (PTK), kneel-to-run (KTR), prone-to-run (PTR), run-to-kneel (RTK), and run-to-prone (RTP). All tasks were performed three times in a straight line with the exception of walking, where participants were asked to walk in a criss-cross pattern measuring 3.5 m x 2 m twice (i.e., two repetitions of walking forward 3.5 m, turning 135° clockwise to walk on a diagonal 4 m, turning 135° counter clockwise to walk forward 3.5 m, and turning 135° counter clockwise to walk on a 4 m diagonal to return to the start position).

Due to the limited field of view of the OPT system, participants started ~3.5 m outside of the capture volume for the RTK and RTP movements and were instructed to transition into kneeling or prone in the middle of the capture volume. Conversely, during the KTR and PTR movements, participants started in the middle of the capture volume and were instructed to run ~3.5 m outside the capture volume. For the running movement, participants started ~3.5 m outside the capture volume and were instructed to run through the capture volume, beginning their deceleration ~3 m past the capture volume. For movements that began outside the capture volume, participants performed the hand clap in the middle of the OPT capture volume, jogged to the start position, performed the movement, and then hand clapped/floor smacked at the end of the movement. For those movements ending outside of the OPT capture volume, participants completed the movement then jogged back to the middle of the capture volume to perform a hand clap.

3.3.4 Data Processing

Three-dimensional (3D) time series marker trajectories from all trials and repetitions were exported from the OPT motion capture system to coordinate 3D file format (C3D). Prior to

exporting, OPT marker trajectories were gap filled and filtered using a 4th order Butterworth filter in Nexus 2.5 (Vicon, Oxford, UK). MVN Analyze (Xsens, Enschede, Netherlands) provides 64 3D time series marker trajectories of virtual markers for the IMU data that are generated based on the pose of each segment and their underlying biomechanical model. These were exported in C3D format as well. For PCA, only those markers that were similar between systems (N = 30; Appendix B Table B1) were imported into Matlab (2018b The MathWorks, Natick, MA, USA). For the joint angle RMSE analysis, C3D data from both systems (Appendix B Table B2) were imported into Visual3D (C-motion, Germantown, MD, USA) to calculate joint angles using the Visual3D six degrees of freedom pose computation algorithm (Figure 3.2), which were subsequently imported into Matlab for further analysis (V_{OPT} and V_{IMU}). Joint angles were calculated a second time from the Visual3D IMU data after applying a method to better align the segment anatomical coordinate systems to those in the optical data model ($V_{IMU\text{-}CAL}$). In this procedure, for each body segment the angular velocities of adjacent segments were calculated with respect to that body segment for both V_{OPT} and V_{IMU} models throughout all motion trials. This was used to calculate a transformation matrix between the anatomical coordinate systems of the two models for each body segment. The transformation matrix was applied to the coordinate systems in the V_{IMU} model to calculate $V_{IMU\text{-}CAL}$ (de Vries et al., 2009). This enabled a closer comparison of the two measurement technologies by mitigating error due to coordinate system alignment (Robert-Lachaine et al., 2017a). Joint angles were also calculated directly from the IMU data in the MVN Analyze software and imported into Matlab for comparison (X_{IMU}). All data were synchronized using the peak acceleration of the hand markers (OPT)/hand segments (X_{IMU}) during the hand clap/floor smack events.

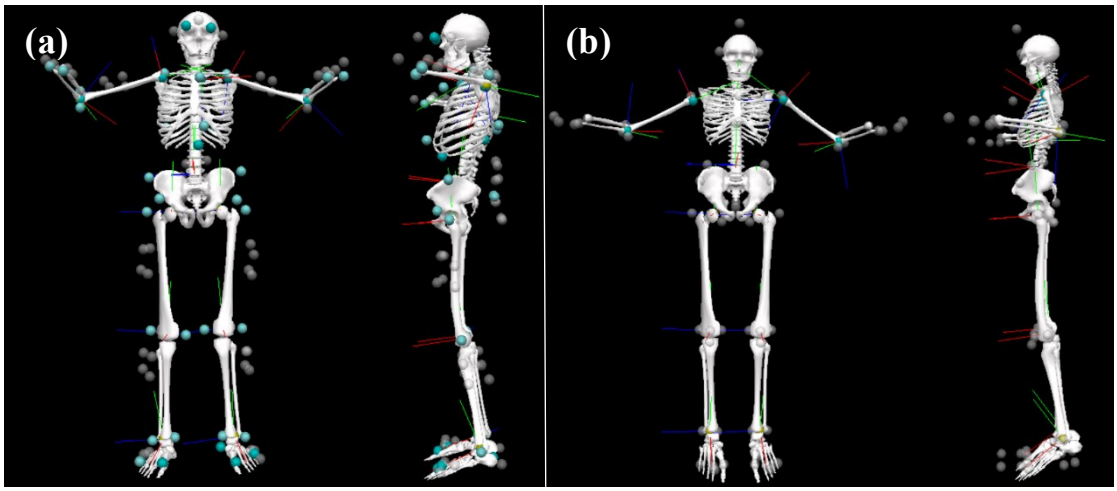

Figure 3.2. Example Visual3D model for a representative participant. Visual3D's 6 degree-of-freedom model was used for all joint angle calculations. (**a**) Model built from OPT data (V_{OPT}). (**b**) Model built with IMU data (V_{IMU}). Tracking markers used can be found in Appendix B Table B2.

3.3.4.1 Principal Component Analysis

For both systems, 3D marker trajectories were synchronized then cropped. For the walk and run trials, each gait cycle was cropped based on heel strike, while the remaining movement trials were cropped based on visually-identified start and end points. All trials were then normalized to 101 data samples using a piecewise cubic Hermite interpolating polynomial (PCHIP). These data were reshaped from the original 101 × 90 matrix (101 data points × (30 markers * 3 axes)) to a 1 × 9090 vector. For each movement type, the newly shaped vectors were horizontally concatenated to create a N × 9090 matrix, where the first $\frac{N}{2}$ rows were OPT data and the last $\frac{N}{2}$ rows were IMU data. PCA was applied to each N × 9090 matrix.

PCA was applied separately for each movement based on the way the participants performed the movement. The KTP, PTK, PTR, KTR, RTP, RTK, and Run tasks were separated as left or right movers. For example, for the KTP task, the participants who kneeled with their left leg were considered left movers versus participants who kneeled with their right leg were right movers, and, therefore, were analyzed through PCA separately. This right versus left kneeling criteria was used for the prone transitional tasks as well, as a kneel is a functional movement in

the transition into and out of prone. Run was separated based on either a left or a right gait cycle. Additionally, for the walking task, gait cycles were separated by left and right sides as well as the four directions that made up the crisscross pattern (i.e., left gait and right cycles were analyzed separately for the initial forward progression, both diagonals, and the second forward progression for a total of 8 PCA models). Movements were analyzed separately based on left and right sides because PCA identifies the greatest modes of variance within a dataset. Therefore, if both left and right movers were included in the same analysis, PCA would identify left versus right as the greatest difference, rather than the variance within the time series marker trajectories, which is of much greater interest.

For each movement type, the number of principal components (PCs) retained was the minimum amount to describe >90% of the variance within the marker trajectories. The PC scores for each retained PC were compared between the OPT and IMU systems using Pearson correlations; Spearman rank correlations were used for those data that violated parametric assumptions. Correlation coefficients from left and right sides as well as each walking direction were averaged together to represent one correlation coefficient for each retained PC for each movement. Correlation coefficients were interpreted as negligible (0.00 to ± 0.30), low (± 0.30 to ± 0.50), moderate (± 0.50 to ± 0.70), high (± 0.70 to ± 0.90), and very high (± 0.90 to ± 1.00); direction of the correlation was interpreted as either positive or negative. Variance explained by each PC from left and right sides were averaged as well.

3.3.4.2 Root Mean Squared Error

Joint angles calculated through Visual3D and MVN Analyze were imported into Matlab 2018b where a bias for each joint angle was removed by subtracting the joint angles from a standing calibration trial that was shared by both systems. Data were synchronized then cropped

and normalized to 101 data samples using PCHIP, as described above. Following normalization, the value of the first frame was subtracted throughout the entire joint angle so that all systems began at 0°. To ensure synchronization, flexion-extension data were compared using cross-correlation for all joints between V_{OPT} and V_{IMU}, V_{OPT} and $V_{IMU\text{-}CAL}$, and V_{OPT} and X_{IMU}. Those trials that had an optimal lag greater than 10 frames or less than −10 frames were excluded. For each joint, RMSE was calculated four times: (1) OPT calculated though Visual3D and IMU calculated through MVN Analyze (V_{OPT} vs. X_{IMU}), (2) both systems calculated through Visual3D (V_{OPT} vs. V_{IMU}), (3) both systems calculated through Visual3D with the segment coordinate systems alignment procedure for the IMU data (V_{OPT} vs. $V_{IMU\text{-}CAL}$), and (4) IMU data calculated by both MVN Analyze and Visual3D with coordinate system alignment (X_{IMU} vs. $V_{IMU\text{-}CAL}$) for each movement trial. V_{OPT} versus X_{IMU} was included to assess the overall difference between systems. V_{OPT} vs. V_{IMU} compares differences between the systems when the IMU joint angles are calculated in a way that is more similar to the method used for the OPT data while not requiring any information from the OPT system. V_{OPT} vs. $V_{IMU\text{-}CAL}$ was included to examine the difference due to technology while mitigating errors arising from differences in segment coordinate system alignment. X_{IMU} vs. $V_{IMU\text{-}CAL}$ was included to examine differences arising between models while controlling for segment coordinate system alignment between MVN Analyze and Visual 3D with no effect of technology.

3.4 Results

3.4.1 Principal Component Analysis

Between 4 and 9 PCs were retained for each movement to explain >90% of the variance for a total of 48 PCs across all movement types. Of the 48 retained PCs, 38 (79%) had scores with a high or very high positive correlation ($\geq$ +0.70) between the OPT and IMU systems, 15 (31%)

of which had scores with a very high correlation ($\geq$ +0.90). All correlation coefficients can be found in Table 3.2. A visual representation of the average movers obtained by the IMU and OPT systems are in Figure 3.3.

Table 3.2. Retained principal component (PC) correlation coefficients. Explained variance is in parentheses (%).

Task	PC1 (%)	PC2 (%)	PC3 (%)	PC4 (%)	PC5 (%)	PC6 (%)	PC7 (%)	PC8 (%)	PC9 (%)
RTK	0.948 (75.5)	0.770 (10.1)	0.744 (4.24)	0.939 (3.46)	-	-	-	-	-
RTP	0.937 (71.5)	0.701 (13.7)	0.810 (5.72)	0.988 (3.28)	-	-	-	-	-
KTR	0.903 (50.2)	0.702 (13.6)	0.792 (9.27)	0.970 (6.78)	0.923 (4.45)	0.849 (3.13)	0.586 (2.59)	0.612 (2.13)	0.744 (1.92)
PTR	0.829 (39.7)	0.774 (27.6)	0.678 (11.6)	0.865 (4.54)	0.882 (3.21)	0.735 (2.74)	0.887 (2.85)	-	-
KTP	0.963 (48.7)	0.961 (17.6)	0.936 (10.9)	0.884 (5.10)	0.509 (4.14)	0.702 (2.84)	0.923 (2.05)	-	-
PTK	0.867 (48.7)	0.931 (27.0)	0.962 (7.80)	0.643 (4.54)	0.710 (2.97)	0.954 (2.30)	0.848 (1.83)	-	-
Run	0.541 (61.3)	0.616 (27.3)	0.874 (2.97)	0.864 (2.58)	-	-	-	-	-
Walk	0.819 (60.0)	0.485 (22.8)	0.924 (13.7)	0.867 (6.69)	0.635 (3.95)	0.644 (1.60)	-	-	-

Note: RTK = run-to-kneel; RTP = run-to-prone; KTR = kneel-to-run; PTR = prone-to-run; KTP = kneel-to-prone; PTK = prone-to-kneel.

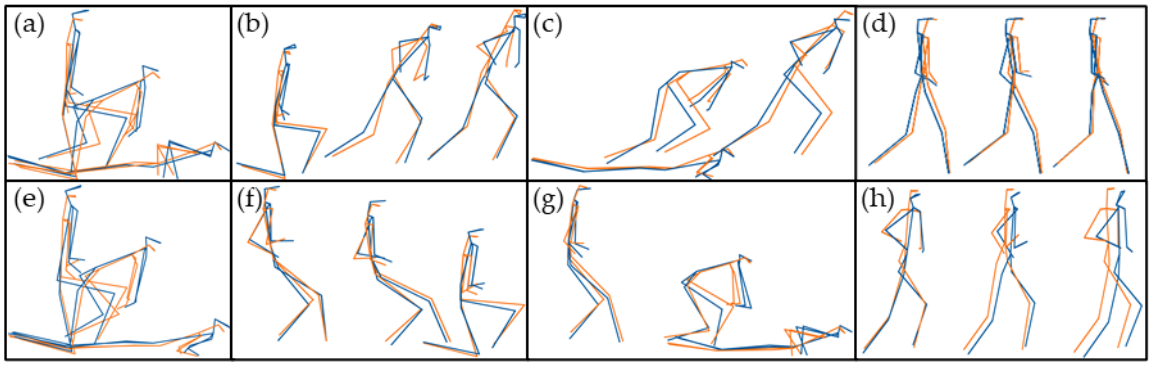

Figure 3.3. Military Movements. Blue represents an average OPT mover; orange represents average IMU mover (**a**) Kneel-to-prone (KTP); (**b**) Kneel-to-run (KTR); (**c**) Prone-to-run (PTR); (**d**) Walking; (**e**) Prone-to-kneel (PTK); (**f**) Run-to-kneel (RTK); (**g**) Run-to-prone (RTP); (**h**) Running.

3.4.2 Root Mean Squared Error

The magnitude of differences between kinematics calculated using the four methods varied depending on the type of movement performed (Figure 3.4). RMSE was lowest for walking trials, with RMSE values less than 5° for all axes and joints for OPT compared to IMU data processed in Visual3D, with and without the additional coordinate system alignment procedure (V_{OPT} vs. V_{IMU} and V_{OPT} vs. $V_{IMU\text{-}CAL}$). RMSE was less than 5° for all axes and joints for V_{OPT} vs. X_{IMU} with the exception of the left elbow axial rotation, which was less than 10°. Errors were greater for the other tasks, which involved faster movements and larger ranges of motion.

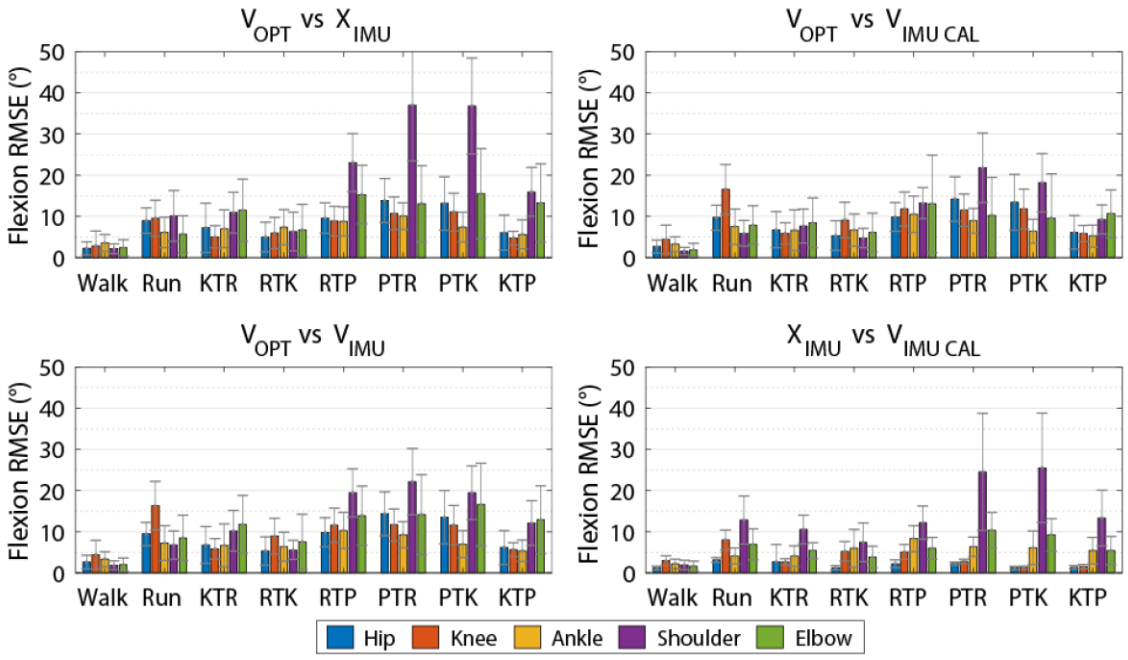

Figure 3.4. Joint flexion/extension angle RMSE values for each task for joint angles calculated from optical data using Visual3D (V_{OPT}), IMU data using Visual3D (V_{IMU}), IMU data using Visual3D with calibration to align anatomical coordinate systems with optical model ($V_{IMU\text{-}CAL}$), and IMU data using MVN Analyze (X_{IMU}). Presented data are averaged between left and right sides across all participants and repetitions for each trial. RTK = run-to-kneel; RTP = run-to-prone; KTR = kneel-to-run; PTR = prone-to-run; KTP = kneel-to-prone; PTK = prone-to-kneel.

Comparing OPT angles calculated in Visual3D with IMU angles calculated in MVN Analyze (V_{OPT} vs. X_{IMU}; Table 3.3) for all tasks, the mean RMSE across all joints was 10.2° (SD = 4.27) for flexion/extension, 9.30° (SD = 5.54) for ab/adduction, and 17.8° (SD = 15.7) for axial

rotation. RMSE values for this comparison were typically greater than the other comparisons. Axial rotation for the upper limb differed considerably between the two methods, with a mean RMSE of 35.6° (SD = 25.1).

Comparing both OPT and IMU joint angles calculated through Visual3D (V_{OPT} vs. V_{IMU}; Table 3.4) for all tasks, the mean RMSE across all joints was 9.61° (SD = 2.04) for flexion/extension, 7.28° (SD = 3.06) for ab/adduction, and 9.33° (SD = 4.84) for axial rotation. RMSE was less for lower limb joints than upper limb joints.

Table 3.3. Mean RMSE values V_{OPT} vs. X_{IMU}.

	Root Mean Squared Error (°)		
Joint	Flexion-Extension Mean (SD)	Ab/Adduction Mean (SD)	Axial Rotation Mean (SD)
Right Ankle	6.59 (1.76)	6.67 (1.37)	7.16 (2.58)
Left Ankle	7.34 (2.22)	6.11 (1.14)	5.90 (1.84)
Right Knee	7.52 (3.20)	4.73 (1.28)	6.44 (1.95)
Left Knee	7.15 (3.03)	4.97 (2.08)	7.62 (3.12)
Right Hip	8.07 (4.24)	3.95 (1.20)	3.87 (1.04)
Left Hip	8.38 (3.82)	4.07 (1.37)	4.22 (1.44)
Right Shoulder	19.1 (15.0)	15.2 (8.75)	31.0 (26.0)
Left Shoulder	16.5 (11.73)	15.6 (8.51)	31.9 (25.2)
Right Elbow	10.9 (5.30)	14.7 (7.00)	40.5 (27.6)
Left Elbow	10.1 (4.84)	17.1 (8.79)	39.2 (21.4)
Overall Mean	10.2 (4.27)	9.30 (5.54)	17.8 (15.7)

Note: Mean RMSE is calculated across all movement tasks. SD = standard deviation.

Table 3.4. Mean RMSE values V_{OPT} vs. V_{IMU}.

	Root Mean Squared Error (°)		
Joint	Flexion-Extension	Ab/Adduction	Axial Rotation
Right Ankle	6.50 (1.99)	6.21 (1.42)	6.21 (2.18)
Left Ankle	7.35 (2.37)	5.46 (0.83)	5.93 (1.74)
Right Knee	9.83 (4.51)	4.90 (1.29)	6.52 (1.84)
Left Knee	9.17 (3.63)	5.17 (2.13)	7.77 (2.99)
Right Hip	8.43 (4.29)	4.23 (1.14)	4.03 (1.04)
Left Hip	8.57 (3.89)	4.18 (1.35)	4.35 (1.43)
Right Shoulder	11.0 (6.46)	8.79 (3.16)	11.5 (6.62)
Left Shoulder	13.4 (8.44)	10.6 (3.52)	15.1 (10.9)
Right Elbow	10.6 (4.45)	11.8 (4.06)	16.7 (7.25)
Left Elbow	11.3 (5.36)	11.5 (3.85)	15.2 (6.72)
Overall Mean	9.61 (2.04)	7.28 (3.06)	9.33 (4.84)

Note: Mean RMSE is calculated across all movement tasks. SD = standard deviation.

For the V_{OPT} vs. $V_{IMU-CAL}$ comparison (Table 3.5), the mean RMSE across all joints for all tasks was 8.74° (SD = 1.25) for flexion/extension, 5.42° (SD = 1.52) for ab/adduction, and 7.18° (SD = 2.69) for axial rotation. The procedure to better align the anatomical coordinate systems in the IMU data with those of the OPT biomechanical model reduced the RMSE values compared to V_{OPT} vs. V_{IMU}, as expected.

Table 3.5. Mean RMSE values V_{OPT} vs. $V_{IMU\text{-}CAL}$.

	Root Mean Squared Error (°)		
Joint	Flexion-Extension	Ab/Adduction	Axial Rotation
Right Ankle	6.50 (2.09)	5.68 (1.35)	5.98 (2.13)
Left Ankle	7.23 (2.41)	5.34 (1.00)	5.90 (1.69)
Right Knee	9.91 (4.62)	4.89 (1.42)	5.38 (1.23)
Left Knee	9.30 (3.65)	4.57 (1.20)	6.07 (1.82)
Right Hip	8.36 (4.11)	3.72 (0.89)	3.97 (1.17)
Left Hip	8.64 (4.00)	4.09 (0.99)	4.06 (1.43)
Right Shoulder	9.86 (6.39)	4.67 (2.04)	8.64 (3.94)
Left Shoulder	10.6 (7.52)	5.21 (2.20)	11.0 (7.68)
Right Elbow	8.40 (3.77)	7.29 (3.46)	10.5 (3.83)
Left Elbow	8.60 (3.49)	8.73 (4.34)	10.3 (4.46)
Overall Mean	8.74 (1.25)	5.42 (1.52)	7.18 (2.69)

Note: Mean RMSE is calculated across all movement tasks. SD = standard deviation. .

Calculating joint angles from the IMU data in MVN Analyze versus Visual3D with the coordinate system alignment procedure (X_{IMU} vs. $V_{IMU\text{-}CAL}$; Table 3.6) resulted in mean RMSE across all joints for all tasks of 6.09° (SD = 4.31) for the flexion/extension axis, 7.45° (SD = 7.91) for ab/adduction, and 11.9° (SD = 13.2) for axial rotation. While errors in lower limb angles were generally relatively small, the different biomechanical models used to calculate the angles resulted in large difference in the upper limb joint angles, especially in the ab/adduction and axial rotation axes.

Table 3.6. Mean RMSE values X_{IMU} vs. $V_{IMU\text{-}CAL}$.

	Root Mean Squared Error (°)		
Joint	Flexion-Extension	Ab/Adduction	Axial Rotation
Right Ankle	4.44 (1.43)	4.03 (1.27)	4.17 (2.00)
Left Ankle	6.17 (2.40)	3.85 (1.43)	4.33 (1.86)
Right Knee	3.80 (2.49)	0.84 (0.28)	1.12 (0.52)
Left Knee	3.58 (2.03)	0.78 (0.23)	1.22 (0.59)
Right Hip	1.83 (0.72)	0.73 (0.23)	0.79 (0.23)
Left Hip	1.95 (0.87)	0.67 (0.16)	0.85 (0.27)
Right Shoulder	15.2 (10.1)	12.1 (6.10)	22.8 (22.4)
Left Shoulder	11.9 (5.97)	11.1 (5.58)	21.1 (16.4)
Right Elbow	5.36 (2.52)	19.7 (9.86)	29.7 (23.2)
Left Elbow	6.75 (3.10)	20.7 (9.87)	33.2 (20.0)
Overall Mean	6.09 (4.31)	7.45 (7.91)	11.9 (13.2)

Note: Mean RMSE is calculated across all movement tasks. SD = standard deviation.

Visual representations of the average waveforms across all movements for V_{IMU}, $V_{IMU\text{-}CAL}$, X_{IMU}, and V_{OPT} can be found in Figure 3.5.

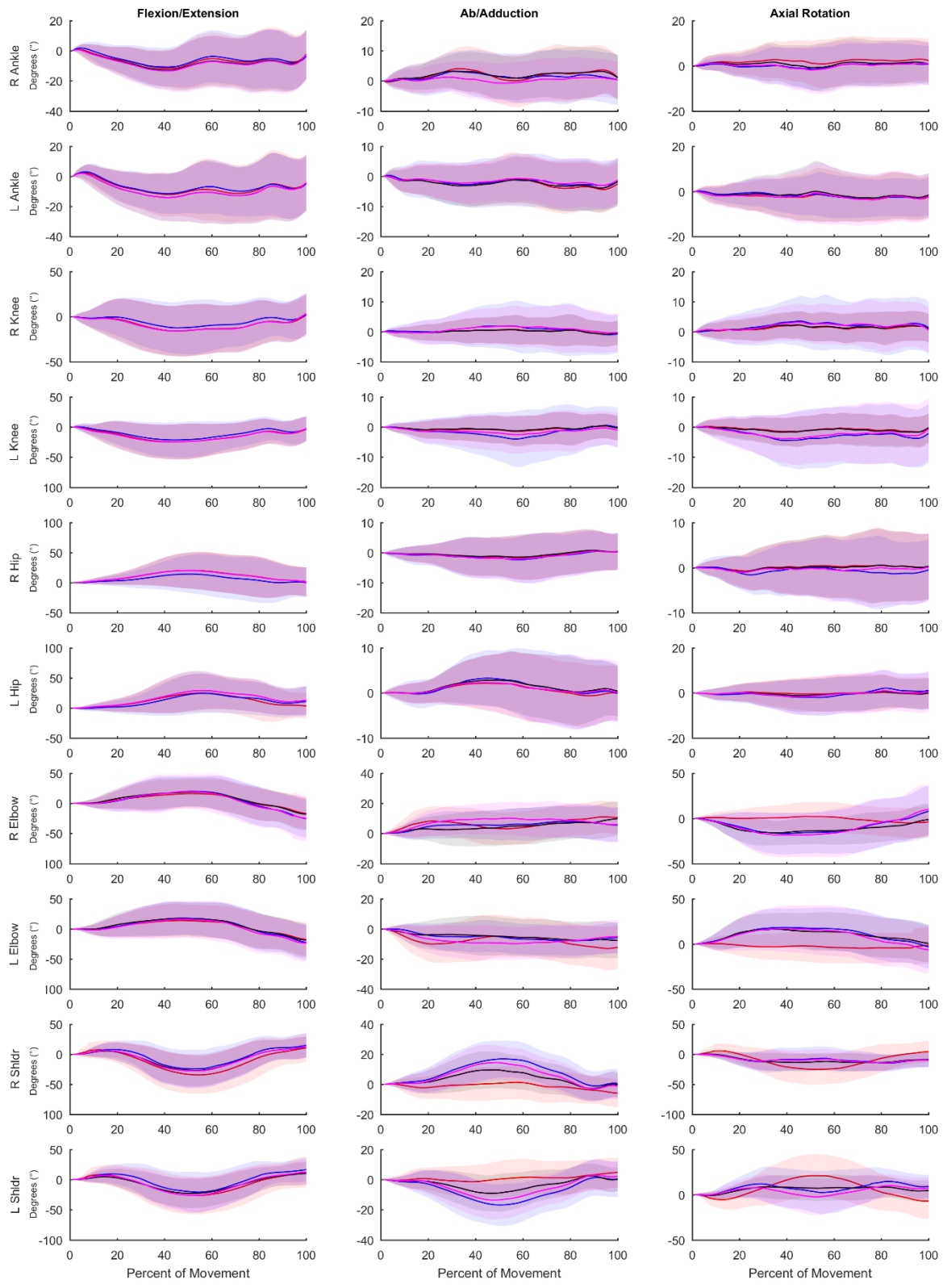

Figure 3.5. Average waveforms across all movements. Blue represents data captured through OPT (V_{OPT}); red represents data captured through IMU (X_{IMU}); **black** represents IMU data processed through Visual3D (V_{IMU}); magenta represents IMU data processed through Visual3D with the coordinate system alignment procedure ($V_{IMU\text{-}CAL}$). Shaded areas represent one standard deviation from the mean trajectory and are displayed in the same colour.

3.5 Discussion

The purpose of this investigation was to validate an IMU system against a gold standard OPT system for military-based movements using PCA and joint angle RMSE. Overall, the OPT and IMU systems produced PC scores that were highly positively correlated; the average correlation coefficient was 0.81 (SD = 0.14) across all 48 retained PCs (Table 3.2). This result instills confidence that both the OPT and IMU systems are reconstructing whole-body movement patterns similarly. Lower limb RMSEs for joint angles calculated using the IMU data for all methods compared to the OPT system were less than 10 degrees for all axes (Tables 3.3–3.6), while differences were greater between the systems for the shoulder and elbow angles. The angles measured using the OPT and IMU systems were most similar for walking trials, and RMSE tended to be greater for more rapid motions involving larger ranges of motion. RMSE was generally smaller for lower limb joint angles compared to upper limb angles.

Previous validation research of the Xsens IMU system against a gold standard OPT system during over ground walking (Karatsidis et al., 2019; Schepers et al., 2018; Zhang et al., 2013) and stair ascent (Zhang et al., 2013) reported lower limb joint angle RMSE values less than 5° (Schepers et al., 2018), 4° (Zhang et al., 2013), and 6° (Karatsidis et al., 2019) in the flexion axis and less than 8° (Schepers et al., 2018; Zhang et al., 2013) and 10° (Karatsidis et al., 2019) for the other axes. In the current study, for over ground walking, we observed joint angle RMSE values of less than 5° for the lower limbs across all axes when comparing V_{OPT} vs. X_{IMU}. Across all tasks studied, we observed V_{OPT} vs. X_{IMU} RMSE values of less than 8° for the lower limbs across all axes. Our results are also comparable to a study by Robert-Lachaine and colleagues (2017a), who reported RMSE values less than 8° for the lower limbs and shoulder axial rotation RMSE up to 40° during a manual materials handling task versus the 31.5° reported here. Robert-Lachaine et al.

(2017a) did report smaller differences for the knee (flexion RMSE 3.2° vs. 7.3° presented here) and elbow (axial rotation RMSE 12.2° vs. 39.9° presented here) compared to the present study. However, the higher RMSE values presented here may be attributed in part to the nature of the movements studied (i.e., material handling vs. rapid changes in height and large ranges of motion).

We used multiple methods in calculating joint angles from the IMU data to provide some insight into the sources of differences between the IMU and OPT systems. The V_{OPT} vs. X_{IMU} comparison is what would be expected during a typical analysis session, where overall differences are a result of coordinate system alignment, biomechanical model constraints, and the measurement technology used between the two systems. We found that the overall RMSEs between V_{OPT} vs. X_{IMU} were less than 9° for the lower limbs but up to 40.5° for the upper limbs. The V_{OPT} vs. V_{IMU} comparison was included to investigate the differences between the systems using a similar underlying biomechanical model for calculating joint angles, which resulted in an average reduction in RMSE values for the upper limb angles of 9.3° (21.6° vs. 12.3°) across all axes compared to the V_{OPT} vs. X_{IMU} comparison, while slightly increasing the error in the lower limb angles (< 2.5° for knee flexion and < 0.5° for all others). To further mitigate the error associated with coordinate system definition and focus on differences due to technology alone, we used an alignment procedure based on segment angular velocities (de Vries et al., 2009; Robert-Lachaine et al., 2017a). The V_{OPT} vs. $V_{IMU\text{-}CAL}$ comparison further reduced the RMSE between the OPT and IMU systems, especially in the upper limbs where RMSE values decreased on average by 13.0° (21.6° vs. 8.65°) across all axes compared to V_{OPT} vs. X_{IMU}. Robert-Lachaine et al. (2017a) used this method previously and found differences between OPT and IMU systems due to measurement technology alone to be less than 4° for most angles. While, we observed RMSEs of similar magnitude during walking, across all tasks, RMSEs were close to 10° for many of the

angles studied. Finally, we examined RMSE arising from model differences, while controlling for coordinate system alignment between systems (X_{IMU} vs. $V_{IMU-CAL}$). We observed that model differences contributed to a significant portion of the error, with RMSE values for the elbows up to 33.2°, while lower limb RMSE values were lower, indicating the lower limb model constraints and structure were more closely aligned between the two systems. However, model differences even when a coordinate system alignment procedure is applied made a large contribution to the overall error between the systems. Overall, the differences in the model and the constraints therein appear to influence RMSE values to a greater extent than the technology itself as whole-body ab/adduction and axial rotation, as well as upper limb flexion RMSE values were considerably lower in the V_{OPT} vs. $V_{IMU-CAL}$ (system error with coordinate system alignment) than in the X_{IMU} vs. $V_{IMU-CAL}$ comparison (model difference while controlling for coordinate system alignment).

Typical use of the Xsens system (V_{OPT} vs. X_{IMU}) results in differences in joint angles and time series marker trajectories compared to an OPT system. However, these differences are relatively low for the lower limbs (RMSE of less than 8° across all axes) and whole-body time series marker trajectories have similar modes of variance between systems (average correlation coefficient of 0.81 across the 48 retained PCs). Upper limb joint angle RMSE values are quite high (RMSE of 21.6° across all axes). However, if upper limb joint angles are of great interest, these values can be decreased by mitigating differences in biomechanical models with (V_{OPT} vs. $V_{IMU-CAL}$; RMSE of 8.7° across all axes) or without (V_{OPT} vs. V_{IMU}; RMSE of 12.3° across all axes) a coordinate alignment procedure. The coordinate system alignment procedure requires simultaneous collection of optical motion capture, which may negate some of the advantages of using an IMU system. However, the results of this comparison demonstrate that, particularly in the upper limbs, a large portion of the differences between the systems (V_{OPT} vs. X_{IMU}) is a result

of the biomechanical model, as opposed to differences in the actual measured position and orientation of body segments. Strictly looking at time series marker trajectories, PCA identified similar modes of variance between OPT data and virtual markers projected by the IMU system, with high or very high (≥ 0.70) PC score correlation coefficients in 38 of the 48 comparisons. This shows that time series marker trajectories can be reconstructed similarly between data derived from the Xsens IMU and the Vicon OPT systems. The RMSE values (average of 8.7° across all joints, axes, and tasks for V_{OPT} vs. V_{IMU}) provide an indication of the differences, compared to an OPT system that could be expected if the reconstructed markers are to be used for joint angle calculations. Whether this is acceptable will depend on the application. However, it indicates that joint angles similar to that of an OPT system can be calculated without the inherent line of sight and laboratory constrictions. The presented RMSE values in addition to the highly correlated PC score values show that the Xsens system is appropriate for our future purposes of creating morphable movement patterns. Users interested in other applications should be aware of the presented errors and make an informed decision if they are within an appropriate range for their intended purposes.

The present study has limitations. Although we have used the OPT system as a 'gold standard' for comparison, there are also errors associated with these systems. Therefore, the RMSEs we have calculated represent the observed differences between the two systems, as opposed to the difference between the IMU system and the 'true' movement. Due to the limited capture volume of the OPT system, for some movements participants were instructed to start/end their movement outside of the calibrated capture volume. Entering and exiting the calibrated space may cause higher sources of measurement error in the OPT system. Additionally, all OPT systems are limited by skin artefact, which would alter joint angle calculations, especially for more dynamic

movements. IMU systems, when collecting for long periods of time, experience positional drift. It was also noted that upper arm segments would become misaligned over time (i.e., when the participants touched their hands together one hand of the Xsens avatar would go through the other). Although, the Xsens avatar was realigned between movement trails, positional and segmental drift could contribute to lower correlation coefficients for some PCs and contribute to the higher RMSE values for the upper arm joints. Additionally, we realized some large anecdotal improvements with the Xsens tracking after discussing with their technology team who suggested: 1) a hand clap during the walking calibration process to improve upper limb tracking, and 2) to start and end all collections with the participant in standing. Unfortunately, this information was learned after this data collection ceased so it could not be implemented. However, we believe that these would improve the PC score correlation coefficients and reduce RMSE values in future work.

3.6 Conclusions

Overall, the IMU and OPT systems reconstructed the military-based movements in a similar fashion, represented by an average high positive correlation coefficient of 0.81 across the 48 retained PCs. RMSE values were the lowest in all axes for the lower limb joint angles and highest in the upper limb joint angles. The differences between the systems were due, in part, to the different biomechanical models used. While joint angles were most similar between the systems for over ground walking, the two technologies compared favourably for more dynamic movements as well. The IMU system compares well with the OPT system and appears appropriate for capturing and reconstructing full-body motion variability for military-based movements. Users interested in other applications should be aware of the presented errors and if they lie within an appropriate range for their intended purposes.

Conflicts of Interest: The authors declare no conflict of interest.

3.7 References

Adamowicz, L., Gurchiek, R.D., Ferri, J., Ursiny, A.T., Fiorentino, N., McGinnis, R.S., 2019. Validation of novel relative orientation and inertial sensor-to-segment alignment algorithms for estimating 3D hip joint angles. Sensors (Switzerland) 19. https://doi.org/10.3390/s19235143

Al-Amri, M., Nicholas, K., Button, K., Sparkes, V., Sheeran, L., Davies, J., 2018. Inertial Measurement Units for Clinical Movement Analysis: Reliability and Concurrent Validity. Sensors 18, 719. https://doi.org/10.3390/s18030719

Andersen, K.A., Grimshaw, P.N., Kelso, R.M., Bentley, D.J., 2016. Musculoskeletal lower limb injury risk in army populations. Sport. Med. - Open 2, 22. https://doi.org/10.1186/s40798-016-0046-z

Attwells, R.L., Birrell, S.A., Hooper, R.H., Mansfield, N.J., 2006. Influence of carrying heavy loads on soldiers' posture, movements and gait. Ergonomics 49, 1527–1537. https://doi.org/10.1080/00140130600757237

Billing, D.C., Silk, A.J., Tofari, P.J., Hunt, A.P., 2015. Effects of military load carriage on susceptibility to enemy fire during tactical combat movements. J. Strength Cond. Res. 29, S134–S138. https://doi.org/10.1519/JSC.0000000000001036

Chapman, R.M., Torchia, M.T., Bell, J.E., Van Citters, D.W., 2019. Assessing shoulder biomechanics of healthy elderly individuals during activities of daily living using inertial measurement units: high maximum elevation is achievable but rarely used. J. Biomech. Eng. 141, 1–7. https://doi.org/10.1115/1.4042433

Cutti, A.G., Giovanardi, A., Rocchi, L., Davalli, A., Sacchetti, R., 2008. Ambulatory measurement of shoulder and elbow kinematics through inertial and magnetic sensors. Med. Biol. Eng. Comput. 46, 169–178. https://doi.org/10.1007/s11517-007-0296-5

de Vries, W.H.K., Veeger, H.E.J., Baten, C.T.M., van der Helm, F.C.T., 2009. Magnetic distortion in motion labs, implications for validating inertial magnetic sensors. Gait Posture 29, 535–541. https://doi.org/10.1016/j.gaitpost.2008.12.004

Ferrari, A., Cutti, A.G., Garofalo, P., Raggi, M., Heijboer, M., Cappello, A., Davalli, A., 2010. First in vivo assessment of "outwalk": A novel protocol for clinical gait analysis based on inertial and magnetic sensors. Med. Biol. Eng. Comput. 48, 1–15. https://doi.org/10.1007/s11517-009-0544-y

Hunt, A.P., Tofari, P.J., Billing, D.C., Silk, A.J., 2016. Tactical combat movements: inter-individual variation in performance due to the effects of load carriage. Ergonomics 59, 1232–1241. https://doi.org/10.1080/00140139.2015.1132780

Karatsidis, A., Jung, M., Schepers, H.M., Bellusci, G., de Zee, M., Veltink, P.H., Andersen, M.S., 2019. Musculoskeletal model-based inverse dynamic analysis under ambulatory conditions using inertial motion capture. Med. Eng. Phys. 65, 68–77. https://doi.org/10.1016/j.medengphy.2018.12.021

Laudanski, A., Brouwer, B., Li, Q., 2013. Measurement of lower limb joint kinematics using inertial sensors during stair ascent and descent in healthy older adults and stroke survivors. J. Healthc. Eng. 4, 555–576. https://doi.org/10.1260/2040-2295.4.4.555

Lin, J.F.S., Kulić, D., 2012. Human pose recovery using wireless inertial measurement units. Physiol. Meas. 33, 2099–2115. https://doi.org/10.1088/0967-3334/33/12/2099

Majumdar, Deepti, Pal, M.S., Majumdar, Dhurjati, 2010. Effects of military load carriage on kinematics of gait. Ergonomics 53, 782–791. https://doi.org/10.1080/00140131003672015

Morrow, M.M.B., Lowndes, B.R., Fortune, E., Kaufman, K.R., Susan Hallbeck, M., Kern, P.E., Hallbeck, S.M., 2017. Validation of inertial measurement units for upper body kinematics. J. Appl. Biomech. 33, 227–232. https://doi.org/10.1123/jab.2016-0120

Ohtaki, Y, Sagawa, K, Inooka, H., 2001. A method for gait analysis in a daily living environment by body-mounted instruments. JSME Int. J. 44, 1125–1132. https://doi.org/https://doi.org/10.1299/jsmec.44.1125

Orr, R.M., Johnston, V., Coyle, J., Pope, R., 2015. Reported load carriage injuries of the Australian army soldier. J. Occup. Rehabil. 25, 316–322. https://doi.org/10.1007/s10926-014-9540-7

Robert-Lachaine, X., Mecheri, H., Larue, C., Plamondon, A., 2017a. Validation of inertial measurement units with an optoelectronic system for whole-body motion analysis. Med. Biol. Eng. Comput. 55, 609–619. https://doi.org/10.1007/s11517-016-1537-2

Robert-Lachaine, X., Mecheri, H., Larue, C., Plamondon, A., 2017b. Accuracy and repeatability of single-pose calibration of inertial measurement units for whole-body motion analysis. Gait Posture 54, 80–86. https://doi.org/10.1016/j.gaitpost.2017.02.029

Robert-Lachaine, X., Parent, G., Fuentes, A., Hagemeister, N., Aissaoui, R., 2020. Inertial motion capture validation of 3D knee kinematics at various gait speed on the treadmill with a double-pose calibration. Gait Posture 77, 132–137. https://doi.org/10.1016/j.gaitpost.2020.01.029

Roetenberg, D., Luinge, H., Slycke, P., 2013. Xsens MVN: Full 6DOF Human Motion Tracking Using Miniature Inertial Sensors. XSens Technol. 1–9.

Roy, T.C., 2011. Diagnoses and Mechanisms of Musculoskeletal Injuries in an Infantry Brigade Combat Team Deployed to Afghanistan Evaluated by the Brigade Physical Therapist. Mil. Med. 176, 903–908. https://doi.org/10.7205/MILMED-D-11-00006

Schepers, M., Giuberti, M., Bellusci, G., 2018. Xsens MVN: Consistent tracking of human motion using inertial sensing. Xsens Technol. B.V. 1–8. https://doi.org/10.13140/RG.2.2.22099.07205

Seel, T., Raisch, J., Schauer, T., 2014. IMU-based joint angle measurement for gait analysis. Sensors 14, 6891–6909. https://doi.org/10.3390/s140406891

Supej, M., 2010. 3D Measurements of alpine skiing with an inertial sensor motion capture suit and GNSS RTK system. J. Sports Sci. 28, 759–769. https://doi.org/10.1080/02640411003716934

Teufl, W., Miezal, M., Taetz, B., Frohlichi, M., Bleser, G., 2019. Validity of inertial sensor based 3D joint kinematics of static and dynamic sport and physiotherapy specific movements. PLoS One 14, 1–18. https://doi.org/10.1371/journal.pone.0213064

Weygers, I., Kok, M., Konings, M., Hallez, H., De Vroey, H., Claeys, K., 2020. Inertial sensor-based lower limb joint kinematics: a methodological systematic review. Sensors (Basel). 20, 1–23. https://doi.org/10.3390/s20030673

Zhang, J.T., Novak, A.C., Brouwer, B., Li, Q., 2013. Concurrent validation of Xsens MVN measurement of lower limb joint angular kinematics. Physiol. Meas. 34, N63–N69. https://doi.org/10.1088/0967-3334/34/8/N63

Zügner, R., Tranberg, R., Timperley, J., Hodgins, D., Mohaddes, M., Kärrholm, J., 2019. Validation of inertial measurement units with optical tracking system in patients operated with total hip arthroplasty. BMC Musculoskelet. Disord. 20, 1–8. https://doi.org/10.1186/s12891-019-2416-4

Chapter 4: A Data-driven Framework for Assessing Soldier Performance, Health, and Survivability

Applied Ergonomics, 2022, 104, 103809. https://doi.org/10.1016/j.apergo.2022.103809

4.1 Abstract

Presented is a framework that uses pattern classification methods to incrementally morph whole-body movement patterns to investigate how personal (sex, military experience, and body mass) and load characteristics affect the survivability tradespace: performance, musculoskeletal health, and susceptibility to enemy action. Sixteen civilians and 12 soldiers performed eight military-based movement patterns under three body-borne loads: ~5.5 kg, ~22 kg, and ~38 kg. Our framework reduces dimensionality using principal component analysis and uses linear discriminant analysis to classify groups and morph movement patterns. Our framework produces morphed whole-body movement patterns that emulate previously published changes to the survivability tradespace caused by body-borne loads. Additionally, we identified that personal characteristics can greatly impact the tradespace when carrying heavy body-borne loads. Using our framework, military leaders can make decisions based on objective information for armour procurement, employment of armour, and battlefield performance, which can positively impact operational readiness and increase overall mission success.

4.2 Introduction

During training and combat, infantry soldiers are required to carry heavy body-borne loads comprising of protection, weapons, communications and sensor equipment, as well as sustainment and mission specific combat supplies (Bossi et al., 2020). Collectively, these items are designed to aid and protect the soldier; however, they also contribute to soldier burden (Bossi et al., 2020;

Karakolis and Bossi, 2017). Soldier burden is often discussed in the context of the magnitude of a body-borne load; however, many other factors can burden the soldier. Recently, Bossi et al. (Bossi et al., 2020) provided a broader definition of soldier burden that incorporates burden caused by the environment, metabolic demands, body-borne load, equipment properties (i.e., mass, mass distribution, coverage, bulk, stiffness, breathability, and thermal resistance), and psychological stressors.

The broad definition of soldier burden is not reflected in the current guidelines for the maximum load that should be carried, which is doctrinally set at 30%-45% of body mass across most North Atlantic Treaty Organization (NATO) nations (Drain et al., 2012; Marshal, 1980), nor does it consider many personal characteristics of the soldier (e.g., sex, fitness, experience) or their operating environment (Drain et al., 2012). Even this threshold may be set too high, as Roy et al. (Roy et al., 2012) discussed that carrying loads greater than 25% of body mass increases the risk of musculoskeletal injury. Additionally, these guidelines may not reflect actual usage (Bossi et al., 2020; Drain et al., 2012; Oudenhuijzen et al., 2021). In a report consisting of nine NATO nations, countries reported body-borne loads of 48% to 85% of a soldier's body mass for the same hypothetical operational scenarios (Oudenhuijzen et al., 2021). Although some load burden will always characterize the dismounted soldier, it is unclear what threshold is acceptable to prevent musculoskeletal injuries and traumatic events while preserving performance on the battlefield (Drain et al., 2012; Fish and Scharre, 2018). The uncertainty of the relationships between soldier characteristics, what they wear (e.g., body armour, generic equipment), the impact of these on task performance (e.g., mobility), and the consequent impact on health and susceptibility to enemy action is known as the integrated survivability tradespace (Bossi et al., 2020, 2017; Fish and Scharre, 2018).

Integrated survivability does not solely depend on armour protection. Researchers (Bossi et al., 2014; Guzie, 2004) have referred to the survivability "onion" or layered approach to survivability, where the advice is that protection should be the very last line of defence. Despite this, the historical response to novel threats has focussed on adding protection (i.e., to prevent penetration of rounds). This approach may worsen survivability because that protection, and the extra weight associated with it, can impair a soldier's ability to detect and appropriately react to threats in their combat environment (Drain et al., 2012). Heavy body-borne loads negatively impact the outer "onion" layers, quantified through whole-body joint kinematics and kinetics (Attwells et al., 2006; Brown et al., 2014b; Liew et al., 2016b, 2016a; Ramsay et al., 2016), greater physiological demands (Beekley et al., 2007; Holewijn, 1990; Park et al., 2014; Phillips et al., 2016; Ricciardi et al., 2008), decrements in performance (Bossi et al., 2017, 2016; Karakolis et al., 2017; Laing-Treloar and Billing, 2011; Pandorf et al., 2002; Vitali et al., 2019), and increased susceptibility to enemy action (Billing et al., 2015; Hunt et al., 2016; Morton et al., n.d.; Oudenhuijzen et al., 2021), all of which work in concert to increase the likelihood of a soldier being seen, targeted, and potentially hit. Additionally, there are a number of personal characteristics that can influence an individual's carrying capacity and the integrated survivability tradespace (Drain et al., 2012; Sanderson et al., 2021). Previous literature has identified lower limb strength (Baker et al., 1994; Billing et al., 2015; Dziados et al., 1987; Hunt et al., 2016; Knapik et al., 1990; Mello et al., 1988), whole-body strength (Koerhuis et al., 2009), VO_{2max} (Knapik et al., 1990; Lyons et al., 2005), body composition (Lyons et al., 2005), and sex (Laing-Treloar and Billing, 2011; Ricciardi et al., 2007) as confounding factors that influence performance during both long-duration low-intensity adaptive tasks (e.g., marching) and short-duration high-intensity reactive tasks (e.g., sprinting). By taking into account all layers of the survivability onion and by

understanding the integrated survivability tradespace of soldier load, performance, health, and susceptibility, we can potentially reduce the risk of soldiers developing musculoskeletal injuries caused by overloading (Roy et al., 2013, 2012), reduce traumatic events by reducing susceptibility to enemy action (Billing et al., 2015; Hunt et al., 2016), and optimize performance, all of which will positively impact operational readiness by having more soldiers available, fit, and ready to fight, which increases their operational effectiveness and increases the chances of overall mission success.

Fully understanding the trade-offs/tradespace requires a modelling approach to represent a wide range of soldier characteristics (e.g., fitness, sex, body mass, experience), across an infinite amount of body-borne load characteristics (e.g., magnitude, bulk, stiffness, distribution), environmental conditions (e.g., temperature, ground type, incline), physiological parameters (e.g., metabolic demand, heat dissipation) and psychological stressors. Pattern classification and machine learning methods can be used to create morphable movement patterns that can incrementally represent a vast array of personal characteristics and burdens that were not or cannot be collected (e.g., incrementally represent body-borne load magnitudes not originally collected; incrementally represent a mover with more or less military experience, which cannot be collected). This method has been used in visual perception research, where gait movement patterns were iteratively expressed to behave as individuals who are more male/female (Troje, 2002), depressed/never-depressed (Michalak et al., 2009), and sad/happy (Michalak et al., 2009). This method has also been used in sports research to classify novice versus elite athletes (Ross et al., 2018).

The goal of the present study is to demonstrate how an objective data-driven framework can be used to iteratively represent operationally-relevant military movement patterns based on

personal and body-borne load characteristics to assess the survivability tradespace. Our proposed framework (Figure 4.1) is designed to concurrently understand the effects of burden and personal characteristics on movement performance, musculoskeletal loading, and susceptibility to enemy action. Provided are use cases to display that our framework can be used to iteratively calculate the impact of soldier burden (i.e., load magnitude) and personal characteristics (i.e., military experience, sex, and body mass) on each aspect of the tradespace: task performance (i.e., velocity, exposure time), musculoskeletal health (i.e., inferred through joint kinetics), and susceptibility to enemy action (i.e., likelihood of getting hit by enemy action). Additionally, this framework is being used to develop a graphical user interface (GUI) that will be available to defence scientists and military leaders from allied nations, which will allow them to morph, visualize, and export movement patterns along with the tradespace results.

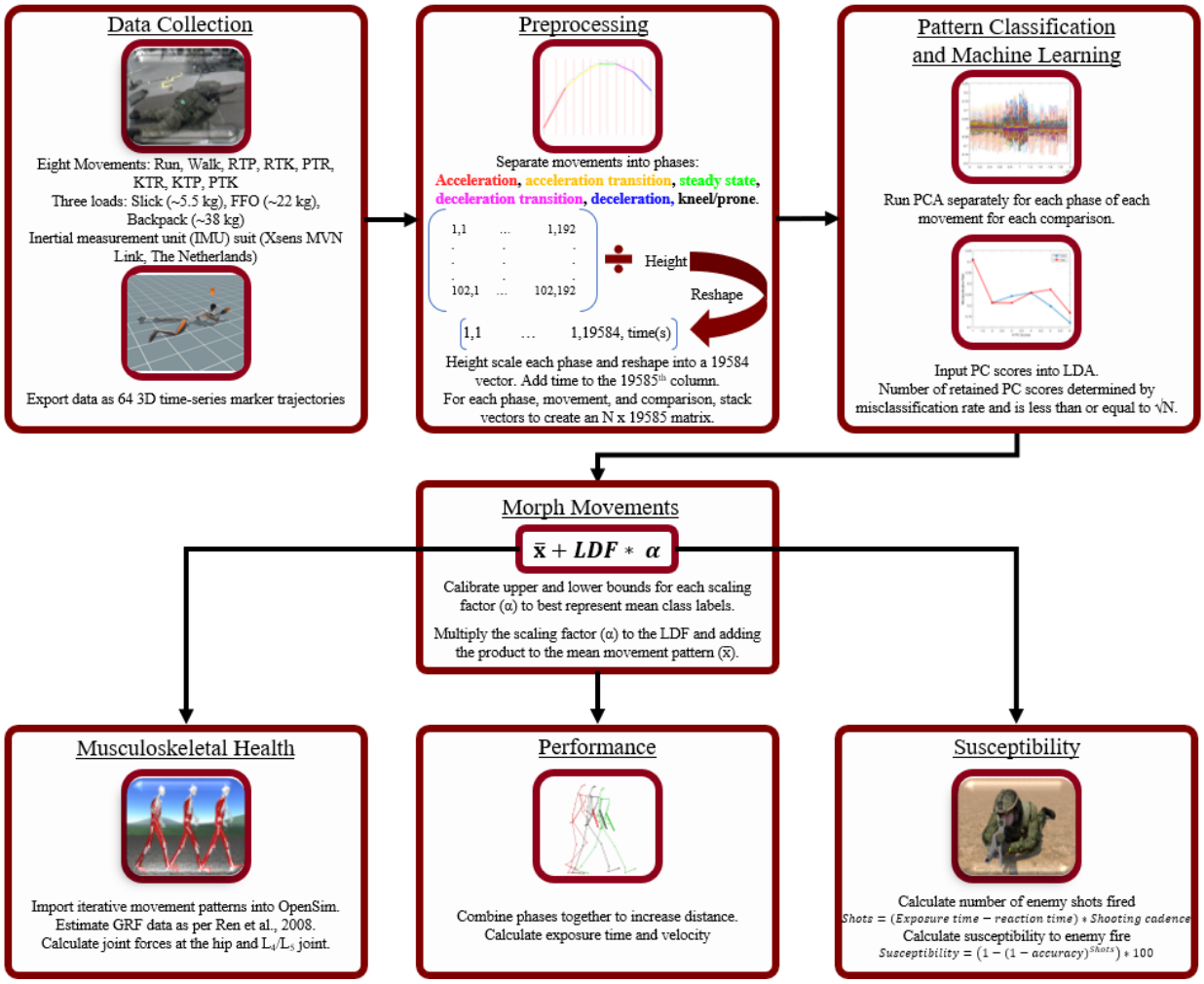

Figure 4.1. Framework Outline. Whole body movement data are collected using an inertial measurement unit suit. Those data are preprocessed into movement phases, scaled, and reshaped into vector form. Those vectors are stacked into matrices and analyzed through principal component analysis and linear discriminant analysis. The linear discriminant function is used to morph the movement patterns to represent different personal and load characteristics. These morphed movers can then be used to incrementally analyze how characteristics affect musculoskeletal health, performance, and susceptibility to enemy direct fire threats

4.3 Methods

4.3.1 Participants and Procedures

4.3.1.1 Participants

For proof of principle of our framework, 12 male reservist soldiers (Army; 1 Private, 10 Corporals, 1 Master Corporal) from the Canadian Armed Forces (CAF) and 16 civilians (12 male; 4 female) were recruited; participant sex distribution reflects that of the CAF (~14% female (Government of Canada, 2022)). Participant mean height, mass, age, and years served (soldiers) were 181.0 cm (±8.77), 79.5 kg (±11.1), 25.9 years (±5.23), and 3.61 years of service (±1.52), respectively. Demographic information is presented in Table 4.1. All experimental protocols followed the Declaration of Helsinki and were approved by the University of Ottawa (H-06-18-721) and Defence Research and Development Canada (2019-026) Research Ethics Boards. All participants provided free and informed consent prior to participating in these protocols.

Table 4.1. Participant demographics.

Demographic	Age (years)	Mass (kg)	Height (cm)	Number of Participants
Soldiers	25.9 (7.71)	81.9 (6.86)	183 (10.5)	12
Civilians	25.9 (3.16)	78.1 (13.0)	179 (7.30)	16
Males	26.2 (5.62)	82.5 (9.12)	182 (8.18)	24
Females	24.3 (1.71)	63.6 (6.06)	172 (8.32)	4
Top 50% Body Mass	25.3 (3.61)	87.2 (5.35)	184 (9.12)	13
Bottom 50% Body Mass	25.9 (3.56)	69.1 (6.94)	175 (6.93)	12
All	25.9 (5.23)	79.5 (11.1)	181 (8.77)	28

Note: demographic information was missing for three soldiers and thus were excluded from the body mass comparisons.

4.3.1.2 Equipment

Participants performed a series of movements under three load conditions: 1) Slick ~5.5 kg, comprising of a CAF helmet, a replica C7A2 rifle, a tunic, and trousers (soldiers)/athletic shirt and pants (civilians); 2) Full Fighting Order (FFO) ~22 kg, comprising of slick + CAF issued fragmentation protective vest (with 2 in-service ballistic plates) + a fully loaded tactical vest (2 replica grenades, 2 replica smoke grenades, 4 replica C7 magazines, a simulated canister of C9

ammunition, 2 field dressings, and a water filled 1 L canteen); and 3) Backpack 38 kg, comprising FFO + a loaded CAF daypack weighing 16 kg. For all conditions, participants' whole-body movement patterns were recorded at 240 Hz using an inertial measurement unit (IMU) suit validated for military-based tasks (MVN Link, Xsens, Netherlands (Mavor et al., 2020; Chapter 3)).

4.3.1.3 Experimental Protocol

Soldiers performed two repetitions and civilians performed three repetitions of eight military-based movements under the three load conditions described above: run, run-to-kneel (RTK), run-to-prone (RTP), kneel-to-run (KTR), prone-to-run (PTR), kneel-to-prone (KTP), prone-to-kneel (PTK), and walk. Trial order and weight conditions were randomized for each participant. Soldiers performed 48 movement trials (8 movements * 2 repetitions * 3 conditions = 48 movements) and civilians performed 72 movement trials (8 movements * 3 repetitions * 3 conditions = 72 movements). Soldiers performed fewer repetitions because their data collection was part of a larger data collection protocol outside of the scope of the current investigation, thus to avoid fatigue the number of repetitions was reduced.

All movements requiring forward progression were done in a straight line measuring ten metres and all movements began/ended with the participant in standing. To account for IMU drift, participants' initial foot position was outlined and the global coordinate system was reset before each trial in MVN Analyze 2019.1 (Xsens, Netherlands).

4.3.2 Data Preprocessing

IMU data were processed in Xsens MVN Analyze 2019.2.1 (Xsens, Netherlands) using the high-definition (HD) reprocessing tool. Data were visually inspected and segment contact data were manually adjusted when necessary. All IMU data were exported to 64 marker trajectory

coordinate 3D (.c3d) files with a T-pose. Marker position data were then imported into Matlab using the Biomechanical Toolkit (BTK (Barre and Armand, 2014)).

Movements with a walk/run portion were separated into individual gait cycles (toe-off to toe-off). These gait cycles were categorized into five phases using the pelvis' acceleration and their location within the overall movement pattern: acceleration (first gait cycle/first gait cycle after a transitional task), acceleration transition (second gait cycle/acceleration halfway between acceleration and steady-state), steady-state (acceleration of ~0 m/s^2), deceleration transition (second last gait cycle/acceleration halfway between steady-state and deceleration), and deceleration (last gait cycle/one gait cycle before a transitional movement). Transitional movements (into or out of kneeling/prone), were dynamically time-warped (DTW) based on key movement anchors and included 0.25 seconds worth of a kneel/prone, the ascending/descending transitional movement, plus one gait cycle of the kneeling leg either before or after the transitional movement (Helwig et al., 2011), when applicable. DTW anchors are explained in Appendix C Table C1.

Each movement's phases were normalized to 101 data points using a Piecewise Cubic Hermite Interpolating Polynomial (PCHIP). A T-pose was then added as the first frame of each movement's phase, which was used for height scaling and musculoskeletal model building. The phases were then scaled by dividing out each participant's height, and reshaped to 1 x 19584 vectors (64 markers * 3 axes * 102 data points). The time to complete each movement phase (normalized as a percentage of maxim observed time) was added as the last column of the reshaped vector (i.e., now 19585 columns).

4.3.3 Creation of Morphable Models

4.3.3.1 Principal Component Analysis and Linear Discriminant Analysis

Data were classified based on load and personal class labels: Slick vs. FFO, FFO vs. Backpack, Male vs. Female (for each body-borne load), Civilian vs. Soldier (for each body-borne load), and Top 50% body mass vs. and Bottom 50% body mass (for each body-borne load). Females were removed from the Civilian vs. Soldier comparison since there were no females present in the soldier class. For each classification, principal component analysis (PCA) was performed and the resulting principal component (PC) scores were used as input for linear discriminant analysis (LDA). To avoid overfitting and to increase generalizability, the maximum number of retained PCs for each classification was limited to the square root of the number of unique trials; however, the number of retained PCs were mainly driven by the accuracy of the LDA. Each LDA was cross-validated using a leave-one-out approach where all the trials that were contributed by a participant were removed (i.e., if participant one contributed three trials for a given classification all of their trials were removed, the model was retrained, and the excluded trials were projected back into the model for classification. This was repeated until all participants' trials were removed and classified (Ross et al., 2018)). Since there were a relatively small number of unique participants, only the most frequently used side of the body was used for classification (i.e., only gait cycles that started with the left leg or only kneelers with their right leg on the ground were analyzed), which resulted in 396 LDAs (36 phases across 8 movements * 11 classifications = 396 LDAs). LDA performance was evaluated using accuracy (i.e., number of correctly classified trials divided by total number of trials), precision (i.e., number of true positives divided by the number of trials classified as positive), and recall (i.e., all true positives divided by the number of trials in the positive class).

4.3.3.2 Morphing Movement Patterns

To create morphed movement patterns, the mean movement for each classification was added to the linear discriminant function (LDF) multiplied by a scaling factor (Equation 4.1):

$$Morphed\ movement = \bar{x} + LDF * \alpha \quad \text{(Eq. 4.1)}$$

where $\bar{x}$ represents the mean movement trajectory, LDF represents the linear discriminant function, and α represents the scaling factor used to morph the movement pattern. Each morphed movement was reshaped back into a 102 x 192 matrix, time normalized to the morphed time component at 30 Hz, and was height normalized to the mean height across all participants using the T-pose (i.e., to ensure the same height across phases).

Root mean squared error (RMSE) was calculated between the morphed and the mean movement pattern for a given class label (e.g., mean civilian, mean female, or mean Backpack mover) to determine the scaling factor's optimal upper and lower bounds. Morphed movers were created by iteratively changing the scaling factor to be between -4 to +4 using 0.01 increments. The scaling factor with the lowest RMSE value across all marker trajectories in three dimensions for a given class label was chosen as the bounds for the morphed movement. Once the scaling bounds were identified, 100 intermediary movement patterns were created. Each movement pattern represents an additional body-borne load (Slick vs. FFO and FFO vs. Backpack), a unit of military experience (civilian vs. soldier), a unit of representative sex (male vs. female), or additional body mass (top 50% (87 kg) vs. bottom 50% body mass (69 kg)). Calibrating to the mean movement pattern was chosen so that known values could be used to represent changes in performance, musculoskeletal health, and susceptibility.

To make our results comparable to previous literature and to represent the tradespace metrics as a factor of distance, systematic combinations of phases were combined to represent the movement tasks at different distances: 1, 2, 3, 4, 5, 10, 15, 20, 25, and 30 metres. These combinations of phases were informed by having a single external participant (female, 28 years old, 65 kg, 163 cm, civilian) run at each distance unloaded while wearing accelerometers attached to their pelvis, left ankle, and right ankle (Dot, Xsens, Netherlands).

4.3.4 Assessment of Trade-offs

4.3.4.1 Performance

For each forward progressing movement, exposure time (i.e., the total time to complete the movement task) and velocity were calculated at each distance by systematically combining phases as described above. When combining phases, distances cannot be exactly matched. Therefore, the distance differential was calculated and exposure time was added/removed using the velocity of the steady-state phase. Velocity was calculated for only the forward progressing movements by using the distance travelled divided by the adjusted exposure time. To represent the change in performance metrics, 100 intermediary movers were created for each classification. Linear relationships were calculated to represent the effects of each kilogram of body-borne load, unit of military experience, unit of sex, and kilogram of body mass has on exposure time and velocity. Linear relationships were selected as it has been previously reported by Hunt et al., (Hunt et al., 2016) that linear regressions best describe the increase in exposure time due to body borne loads ranging from 10-30 kg.

4.3.4.2 Susceptibility to Enemy action

Susceptibility to enemy action was calculated for each movement type (Equation 4.2). For each movement with a forward progression, susceptibility was calculated using the adjusted

exposure time for each distance and was interpolated using 0.01-metre intervals with a PCHIP to represent a continuous value. For the KTP and PTK tasks, the total time to complete the movement was used. The number of shots fired was calculated using Equation 4.2:

$$Shots = (Exposure\ Time - Reaction\ Time) * Shooting\ Cadence \quad \text{(Eq. 4.2)}$$

where reaction time was set to one second and shooting cadence was set to 1.3 shots per second (Billing et al., 2015; Blount et al., 2011). Given the number of shots fired, susceptibility was calculated with a shooting accuracy of 10% (Equation 4.3 (Billing et al., 2015; Blount et al., 2011)):

$$Susceptibility = (1 - (1 - Accuracy)^{Shots}) * 100 \quad \text{(Eq. 4.3)}$$

where susceptibility is represented as a percentage chance of being hit by the number of shots calculated in Equation 4.2.

To represent the change in susceptibility, 100 intermediary movers were created for each classification. Linear relationships were calculated to represent the effects of each kilogram of body-borne load, unit of military experience, unit of sex, and kilogram of body mass has on susceptibility.

4.3.4.3 Musculoskeletal Health

Eleven morphed walking movements created from the Slick-FFO and FFO-Backpack LDFs were imported into OpenSim 3.3 (SimTK, USA). Each walk consisted of three steady-state gait cycles. The Gait 2392 model (Delp et al., 2007) was used to calculate forces at the hip joint and the lifting full-body model (LFB (Beaucage-Gauvreau et al., 2019)) was used to calculate forces on the L_4-L_5 intervertebral joint. Equipment and backpack mass were incrementally added to the scaled mass of the torso (Slick-FFO: 0 – 22 kg; FFO-Backpack: 22 – 38 kg).

Static Optimization and Joint Reaction Analysis in OpenSim 3.3 were employed to calculate muscle forces and joint loads. When using the LFB model, ground reaction forces and moments (GRF&Ms) could be used to assess the dynamic inconsistencies in the model, but they are not required to calculate back muscle forces and joint loads; therefore, the LFB model can be used to estimate spinal joint loads during all tasks. However, GRF&Ms are required when using the Gait 2392 model to calculate the lower extremities' joint loads. Estimating GRF&Ms using solely motion data is a challenging problem tackled in many studies (Muller et al., 2020). In the present study, the methods presented by Ren et al. (2008), were implemented into the OpenSim pipeline. To form the equations of motion, space-fixed and body-fixed velocities were obtained using the Body Kinematics Analysis Tool, and the information regarding joint centres and the segments' centre of mass during the motions were gathered using the OpenSim Application Programming Interface (Akhavanfar et al., 2019).

To represent the change in hip and spinal loads, the average forces were scaled to body mass and then used to create a linear relationship that represents the effect of each kilogram of body-borne load on musculoskeletal health.

4.4 Results

Linear relationships are presented for exposure time, velocity, and susceptibility for movements travelling 30 metres. For the KTP and PTK movements, the linear relationship represents the total time to complete the movement.

4.4.1 Creation of Morphable Models

4.4.1.1 Linear Discriminant Analysis

The LDFs created to model changes in movement patterns caused by body-borne load (Slick vs. FFO movers and FFO vs. Backpack movers) had an average of 5.57 (±2.77) retained

PCs, an average accuracy of 73.6% (±8.80), an average precision of 74.6% (±10.8), and an average recall of 72.5% (±9.45) across 72 analyses.

The LDFs created to model changes in movement patterns caused by military experience (civilian vs. soldier movers) across all three load conditions had an average of 3.40 (±1.31) retained PCs, an average accuracy of 87.4% (±6.63), an average precision of 88.5% (±7.90), and an average recall of 89.0% (±8.49) across 108 analyses.

The LDFs created to model changes in movement patterns caused by sex (male vs. female movers) across all three load conditions had an average of 3.52 (±2.00) retained PCs, an average accuracy of 67.1% (±10.4), an average precision of 66.4% (±10.7), and an average recall of 90.9% (±10.4) across 108 analyses.

The LDFs created to model changes in movement patterns caused by body mass (top 50% (~ 87 kg) vs. bottom 50% (~69 kg) movers) across all three load conditions had an average of 2.31 (±1.81) retained PCs, an average accuracy of 70.7% (±12.9), an average precision of 71.8% (±16.3), and an average recall of 75.9% (±16.6) across 108 analyses.

4.4.2 Assessment of Trade-offs

4.4.2.1 Performance and Susceptibility to Enemy action

Tables 4.2–4.4 summarize the results for all classifiers across all movements. Each table represents the percent change in exposure time, velocity, or susceptibility per one kilogram of body-borne load, one unit of military experience (100 units separate civilians and soldiers), one unit of sex (100 units separate males and females), and one kilogram of body mass. Figures 4.2–4.3 graphically display how susceptibility to enemy action changes as a factor of personal and load characteristics over a 30-metre distance.

Table 4.2. Percent change in exposure time per unit of load, military experience, sex, and body mass.

Classifier	Load Condition	Task							
		Walk (%)	Run (%)	KTR (%)	PTR (%)	RTK (%)	RTP (%)	KTP (%)	PTK (%)
Load	Slick → FFO	0.01	0.15	0.20	0.82	0.10	0.26	0.38	0.50
	FFO → Backpack	0.10	0.17	0.26	0.88	0.88	0.19	-0.04	-0.14
Civilian → Soldier	Slick	0.01	-0.11	-0.12	-0.14	-0.11	-0.10	-0.37	-0.40
	FFO	0.00	-0.20	-0.18	-0.21	-0.11	-0.22	-0.45	-0.37
	Backpack	0.03	-0.08	-0.03	-0.23	-0.10	-0.21	-0.44	-0.32
Female → Male	Slick	0.13	-0.11	-0.13	-0.16	-0.22	-0.11	-0.09	-0.17
	FFO	0.14	-0.03	-0.11	-0.09	-0.08	-0.08	-0.17	-0.14
	Backpack	0.13	-0.01	-0.06	-0.21	-0.06	-0.05	-0.13	-0.19
69 kg → 87 kg	Slick	0.80	-0.94	-1.10	-0.54	-1.45	-0.62	-0.13	-1.24
	FFO	0.62	-0.51	-0.41	-0.38	-0.57	-0.35	0.14	0.03
	Backpack	0.52	-0.70	-0.56	-0.79	-0.36	-0.43	-0.58	-0.02

Note: 100 intermediary movers were created to establish the percent change in exposure time. → denotes the direction of change from one class label to another. Slick = ~5.5 kg, FFO = ~22 kg, Backpack = ~38 kg. KTR = Kneel-to-run, PTR = prone-to-run, RTK = run-to-kneel, RTP = run-to-prone, KTP = kneel-to-prone, PTK = prone-to-kneel. All movements except KTP and PTK represent 30 metres.

Table 4.3. Percent change in velocity per unit of load, military experience, sex, and body mass.

Classifier	Load Condition	Task							
		Walk (%)	Run (%)	KTR (%)	PTR (%)	RTK (%)	RTP (%)	KTP (%)	PTK (%)
Load	Slick → FFO	-0.01	-0.14	-0.19	-0.71	-0.10	-0.25	-	-
	FFO → Backpack	-0.10	-0.17	-0.25	-0.79	-0.78	-0.19	-	-
Civilian → Soldier	Slick	-0.01	0.13	0.13	0.17	0.12	0.11	-	-
	FFO	0.00	0.24	0.21	0.27	0.12	0.28	-	-
	Backpack	-0.03	0.09	0.03	0.29	0.12	0.26	-	-
Female → Male	Slick	-0.12	0.13	0.14	0.19	0.29	0.12	-	-
	FFO	-0.12	0.03	0.12	0.10	0.09	0.09	-	-
	Backpack	-0.11	0.01	0.06	0.26	0.06	0.05	-	-
69 kg → 87 kg	Slick	-0.93	0.80	0.91	0.49	1.15	0.56	-	-
	FFO	-0.70	0.47	0.38	0.35	0.51	0.33	-	-
	Backpack	-0.58	0.62	0.51	0.69	0.34	0.40	-	-

Note: 100 intermediary movers were created to establish the percent change in velocity. → denotes the direction of change in class label. Slick = ~5.5 kg, FFO = ~22 kg, Backpack = ~38 kg. KTR = Kneel-to-run, PTR = prone-to-run, RTK = run-to-kneel, RTP = run-to-prone, KTP = kneel-to-prone, PTK = prone-to-kneel. All movements except KTP and PTK represent 30 metres.

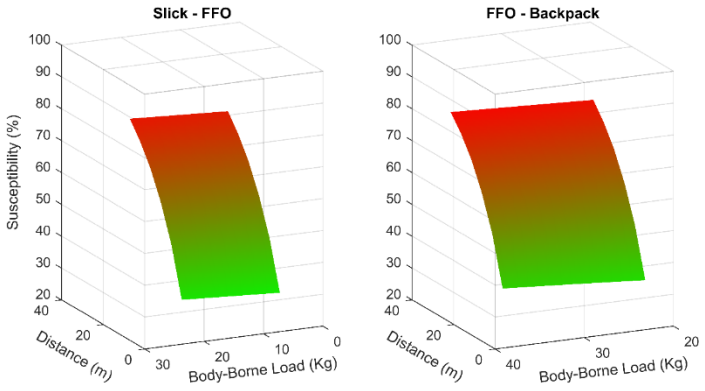

Figure 4.2. Body-borne load's affect on susceptibility to enemy fire. Displayed is the average susceptibility values across all movement types for each distance. The surface graph changes from green to red as the participant becomes more susceptible. Slick = ~5.5 kg, FFO = ~22 kg, Backpack = ~38 kg.

Table 4.4. Percent change in susceptibility per unit of load, military experience, sex, and body mass.

Classifier	Load Condition	Task							
		Walk (%)	Run (%)	KTR (%)	PTR (%)	RTK (%)	RTP (%)	KTP (%)	PTK (%)
Load	Slick → FFO	0.00	0.08	0.11	0.37	0.05	0.11	0.37	0.50
	FFO → Backpack	0.02	0.09	0.13	0.34	0.40	0.07	-0.04	-0.14
Civilian → Soldier	Slick	0.00	-0.08	-0.07	-0.08	-0.06	-0.05	-0.40	-0.43
	FFO	0.00	-0.12	-0.11	-0.11	-0.06	-0.10	-0.46	-0.38
	Backpack	0.00	-0.05	-0.02	-0.11	-0.05	-0.09	-0.44	-0.32
Female → Male	Slick	0.02	-0.07	-0.07	-0.08	-0.12	-0.05	-0.09	-0.17
	FFO	0.03	-0.02	-0.06	-0.04	-0.04	-0.03	-0.16	-0.14
	Backpack	0.02	0.00	-0.03	-0.08	-0.03	-0.02	-0.11	-0.17
69 kg → 87 kg	Slick	0.15	-0.53	-0.61	-0.27	-0.68	-0.28	-0.13	-1.33
	FFO	0.11	-0.28	-0.21	-0.16	-0.28	-0.14	0.14	0.03
	Backpack	0.09	-0.35	-0.27	-0.28	-0.16	-0.14	-0.53	-0.02

Note: 100 intermediary movers were created to establish the percent change in susceptibility. → denotes the direction of change from one class label to another. Slick = ~5.5 kg, FFO = ~22 kg, Backpack = ~38 kg. KTR = Kneel-to-run, PTR = prone-to-run, RTK = run-to-kneel, RTP = run-to-prone, KTP = kneel-to-prone, PTK = prone-to-kneel. All movements except KTP and PTK represent 30 metres.

Across all tasks, the Slick vs. FFO LDF models calculated that per kilogram of on-body load, exposure time increased by 0.30% (±0.26), velocity decreased by 0.23% (±0.25), and susceptibility increased by 0.20% (±0.19).

Across all tasks, the FFO vs. Backpack LDF models calculated that per each kilogram of increased backpack load, exposure time increased by an average of 0.29% (±0.39), velocity

decreased by an average of 0.38% (±0.32) and susceptibility increased by an average of 0.11% (±0.18). The LDFs for the KTP and PTK tasks incorrectly expressed a decrease in exposure time and susceptibility per kilogram added.

The LDFs classifying civilians and soldiers identified that civilians had higher exposure times, lower velocities, and were more susceptible than soldiers for all tasks and load conditions except for walking. Across all tasks, per iteration towards a representative soldier movement pattern, exposure time decreased by 0.17% (±0.14) 0.22% (±0.14), and 0.17% (±0.16) for the Slick, FFO and Backpack conditions respectively; velocity increased by 0.11% (±0.06), 0.19 (±0.11) and 0.13% (±0.13) for the Slick, FFO, and Backpack conditions respectively; and susceptibility decreased by 0.15% (±0.17), 0.17% (±0.16), and 0.13% (±0.16) for the Slick, FFO, and Backpack conditions respectively.

The LDFs classifying sex identified that females had higher exposure times, lower velocities, and higher susceptibilities than males for all tasks except for walking. Across all tasks, per iteration towards a representative male movement pattern, exposure time decreased by 0.11% (±0.10), 0.07% (±0.10), and 0.07% (±0.11) for the Slick, FFO, and Backpack conditions, respectively; velocity increased by 0.13% (±0.13), 0.05% (±0.09), and 0.06% (±0.12) for the Slick, FFO, and Backpack conditions, respectively; and susceptibility decreased by 0.08% (±0.06), 0.06% (±0.06), and 0.05% (±0.06) for the Slick, FFO, and Backpack conditions, respectively.

The LDFs classifying movers with the Top 50% (~87 kg) and Bottom 50% (~69 kg) body mass identified that lighter individuals had higher exposure times, lower velocities, and higher susceptibilities than heavier individuals for all tasks except for walking. Across all tasks, per additional kilogram of body mass, exposure time decreased by 0.65% (±0.72), 0.18% (±0.41), and 0.36% (±0.43) for the Slick, FFO, and Backpack conditions respectively; velocity increased by

0.49% (±0.74), 0.22% (±0.46), and 0.33% (±0.46) for the Slick, FFO, and Backpack conditions, respectively; and susceptibility decreased by 0.46% (±0.44), 0.10% (±0.17), and 0.21% (±0.19) for the Slick, FFO, and Backpack conditions, respectively.

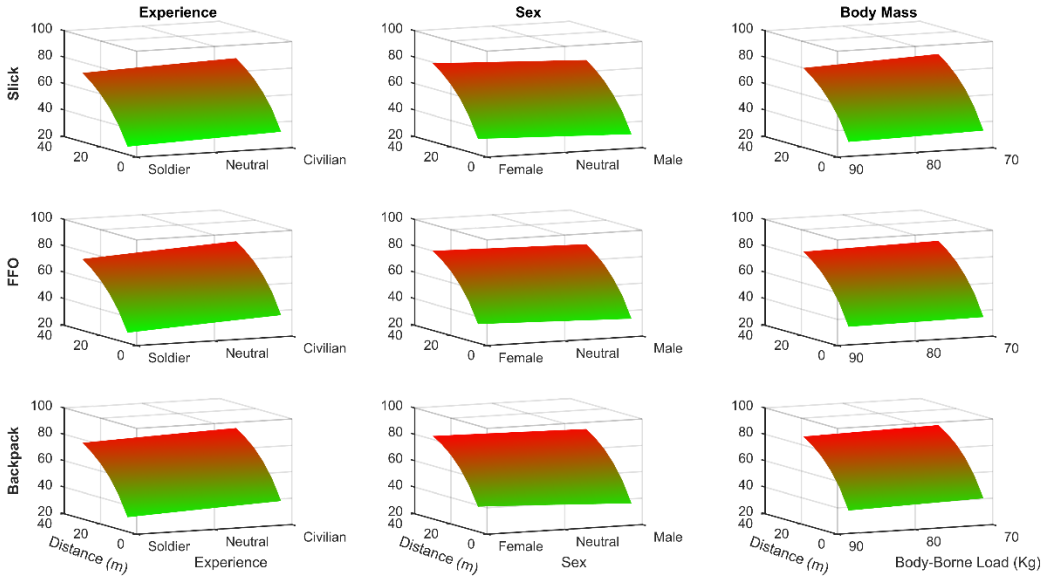

Figure 4.3. Personal factors' affect on susceptibility to enemy action for each body-borne load. Displayed is the average susceptibility values across all movement types for each distance. The surface graph changes from green to red as the participant becomes more susceptible. Slick = ~5.5 kg, FFO = ~22 kg, Backpack = ~38 kg.

4.4.2.2 Musculoskeletal Health

When represented as a linear relationship, average hip forces increased by 1.13% in the axial plane, 1.26% in the mediolateral plane, and 0.93% in the anteroposterior plane per kilogram of on-body load. For each kilogram of backpack load, hip forces increased by 1.47% in the axial plane, 0.30% in the mediolateral plane, and 1.46% in the anteroposterior plane. While forces exerted on the L_4-L_5 intervertebral joint increased by 2.81% in the axial plane, 11.11% in the mediolateral plane, and -37.79% (-0.05 N) in the anteroposterior plane per kilogram of on-body load. For each kilogram of backpack load, L_4-L_5 forces increased by 1.35% axial plane, 4.30% in the mediolateral plane, and 2.98% in the anteroposterior plane. Average forces normalized to body mass and their respective linear trends are visually displayed in Figure 4.4.

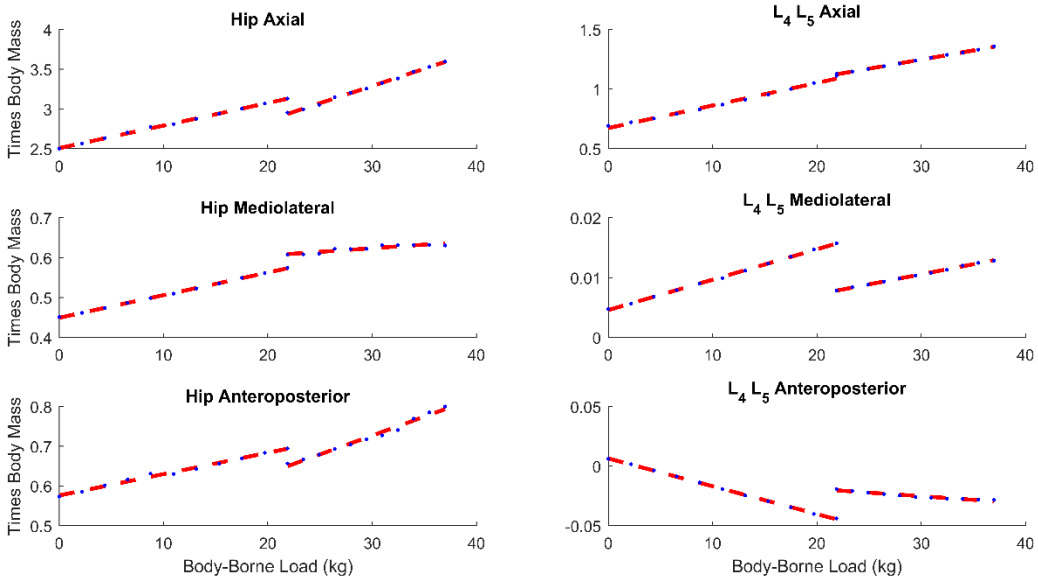

Figure 4.4. Average Hip and L_4-L_5 forces normalized to body mass. Blue dots represent each of the 11 morphed movers. Red dashed lines represent the linear relationships for the Slick-FFO and FFO-Backpack linear discriminant functions, respectively.

4.5 Discussion

Body-borne loads are a necessary soldier burden. Soldiers must carry weapons, communications and sensing equipment, personal protective equipment, and critical combat supplies (e.g., ammunition, water, food). However, it is documented that there is a trade-off in terms of performance (Billing et al., 2015; Hunt et al., 2016; Laing-Treloar and Billing, 2011), musculoskeletal health (Attwells et al., 2006; Sturdy et al., 2021), and susceptibility (Billing et al., 2015; Hunt et al., 2016) as body-borne loads progressively increase (Oudenhuijzen et al., 2021; Sanderson et al., 2021). It has also been documented that personal characteristics such as lower limb power (Billing et al., 2015; Hunt et al., 2016) and sex (Laing-Treloar and Billing, 2011) can exacerbate these negative responses to load. Additionally, there are many more factors that burden the soldier such as the environment, physiology, and psychological stressors (Bossi et al., 2020), which, in terms of the survivability tradespace, are poorly understood. To address this, we created a data-driven framework to calculate tradespace metrics using morphed movement patterns based

on personal and load characteristics. To maximize knowledge translation, we are developing a decision-making tool in the form of a GUI based on our framework that will allow members from allied nations to morph, visualize, and export movement patterns and calculate tradespace metrics.

In line with previous research (Billing et al., 2015; Hunt et al., 2016; Laing-Treloar and Billing, 2011), using our framework we identified decrements to the tradespace based on both load and personal characteristics. On average, across all tasks there was an average decrement in velocity of 0.30% (±0.28), an increase in an exposure time of 0.30% (±0.32) and an increase in susceptibility of 0.15% (±0.18) per kilogram of body-borne load. The framework identified that the most affected movement was the PTR task, which caused participants to increase their exposure time by 0.82% per kilogram of on-body load and 0.88% per kilogram of backpack load when simulated over a 30-metre distance. The presented results translate to a 1.6 second increase in exposure time between Slick and FFO and an additional 1.6 second increase in exposure time between FFO and Backpack. These PTR results are similar to previous research endeavours that investigated a 30-metre break contact simulation (i.e., starting in prone and maximally sprinting 30 metres (Billing et al., 2015; Hunt et al., 2016; Laing-Treloar and Billing, 2011)), who reported exposure time increases of 1.5%(Laing-Treloar and Billing, 2011) and 0.80% (Billing et al., 2015; Hunt et al., 2016) per kilogram of body-borne load.

Using our framework, we identified that personal characteristics can affect the response to body-borne loads. Similar investigations have reported that females are more affected by an increase in load than their male counterparts (Laing-Treloar and Billing, 2011). Liang-Treloar et al. (Laing-Treloar and Billing, 2011) reported a 1.7 second (1.33%/kg; 36%) and a 2.5 second (1.63%/kg; 29%) increase in exposure time for males and females respectively when completing a break contact simulation wearing 21.6 kg versus unloaded. Billing et al. (Billing et al., 2015)

sub-grouped their participants into “fast” and “slow” groups whose exposure time increased by 0.6%/kg and 1.0%/kg respectively when completing a 30-metre break contact simulation; only peak vertical jump height was significant between groups (Billing et al., 2015; Hunt et al., 2016). To be comparable to previous literature, we will focus on results from the PTR task. In the present investigation, we found that between the Slick and FFO loads, females’ exposure time increased by 1.69 seconds (0.84%/kg; 14%) whereas males’ exposure time increased by 2.36 seconds (1.39%/kg; 23%); however, between the FFO and Backpack conditions, females’ exposure time increased by 2.62 seconds (1.18%/kg; 19%) and males’ exposure time increased by 0.49 seconds (0.24%/kg; 3.9%). At low body-borne loads, males appear to be more affected than females, which may be driven by the lower exposure time in the Slick condition (10.27 seconds) compared to females (12.16 seconds), causing a floor effect. However, once body-borne loads surpass 50% of the body mass of females (FFO: 35%; Backpack: 59.7%), their performance is more impaired than the their male counterparts. Investigating the impact of body mass on performance supports that performance is moderately affected when carrying loads below 50% of body mass compared to carrying loads greater than 50% of body mass. Exposure time similarly increased between the Slick and FFO conditions for the Top 50% (1.94 s, 1.11%/kg, 18%) and Bottom 50% body mass groups (1.77 s, 0.92%/kg, 15%). However, between the FFO and Backpack conditions, the Bottom 50% group maintained a similar 0.92%/kg decrement to exposure time (1.98 s; 14%) while the Top 50% group had a much lower decrement of 0.45%/kg (0.91 s; 7%). Notably, the Bottom 50% body mass group consisted of majority civilians while the Top 50% group was more balanced. Our framework identified that experience greatly contributes to exposure time degradation when carrying heavy body-borne loads. Between Slick and FFO, civilians were much more affected by the increase in body-borne load (2.60 s, 1.45%/kg, 23.9%) and the soldiers (1.28 s, 0.83%/kg,

13.7%). Both civilians and soldiers demonstrated further, increases in exposure time between the FFO and Backpack conditions (Civilian: 0.48 s, 0.22%/kg, 3.57%; Soldier: 0.23 s 0.14%/kg, 2.17%). Our framework shows that sex, body mass, and experience can all affect task performance and thus susceptibility. It appears that lighter individuals (including females) can accommodate body-borne loads at relatively lower percentages of their body mass; however, once the load approaches/surpasses 50% of their body mass, these lighter individuals are more negatively affected than heavier individuals regardless of sex. Additionally, military experience appears to contribute greatly to the ability to perform these operationally-relevant movement patterns under high loads. However, the individuals who maintain performance when carrying heavy loads are not immune to the forces that are applied to their body.

Using our framework to morph movement patterns based on load magnitude, we produced quality data that were used for biomechanical analyses. Using the method outlined by Ren et al. (Ren et al., 2008), we estimated GRF&M data similar to what is expected at the loads carried. Using the equation presented by Birrell et al. (Birrell et al., 2007), our peak forces for FFO and Backpack should be 1.51- and 1.72-times body mass, respectively. Following Ren et al. (Ren et al., 2008), our calculated peak GRFs were similar albeit slightly higher at 1.64- and 1.87-times body mass, likely due to the higher velocity of our walkers (~3 m/s vs. ~1.5 m/s). The calculated joint loads at the hip suggest that the average axial forces increase by 1.13% and a 1.30% per kilogram of on-body and backpack loads respectively. Likewise, the average L_4-L_5 axial forces, were found to increase by 2.81% and 1.35% for on-body and backpack loads respectively. The presented values are larger but similar to what was previously reported by Sturdy et al. (2021), whose results can be translated to 1.03%/kg of average hip axial forces and 1.61%/kg of average L_4-L_5 axial forces. The difference between values can be attributable to differences between

biomechanical models and the velocity of the walkers. Of note is that the both the Slick vs. FFO and FFO vs. Backpack models did not produce the same joint forces when representing a mover carrying FFO (Figure 4.4); the kinematics are not identical thus parameters such as muscle moment arms are not consistent. This is due to the inherent workings of our method: the mean movement pattern and the LDF are influenced by their associative data. Therefore, the representative FFO mover created by the Slick vs. FFO model is influenced by a more upright posture and deep hip flexion present in Slick movements while the representative FFO mover created by the FFO vs. Backpack model is influenced by a more flexed posture and shallower hip flexion present in Backpack movements.

In the present study, we provide use cases for how a data-driven framework can be used to identify trends within movement patterns and to apply these trends to the survivability tradespace while producing quality movement patterns that can be applied to biomechanical analyses. Using these movement patterns, we were able to produce comparable results to those previously reported and have the ability to represent a vast array of personal and load characteristics without collecting them individually, which can help researchers overcome the issue of recruiting matching participants to identify trends (e.g., recruiting males and females with the same height, mass, and experience). Despite the successes of our work, our framework has several limitations. Our participant pool is relatively small, only consists of four females and lacks the diversity present in the Canadian Armed Forces. To account for this, females were excluded from the Civilian vs. Soldier comparison and all data were height normalized to reduce the influence of stature within our framework. It is important to note that infantry reservist soldiers were used in this investigation. Readers should be aware that trends presented here may differ for active soldiers and those in different occupations, which could be interesting class labels to use to morph

movement patterns in the future (e.g., Reservist vs. Active-duty, Infantry vs. Air Force, etc.). Our investigation focuses on changes due to load magnitude; however, there are many factors that can burden a soldier. It is possible to use our framework to ask these research questions by collecting the appropriate data (e.g., environmental conditions, terrain, fatigue, etc.). We approached this framework using an LDF method as it has been successfully implemented in previous research to separate movement patterns (Michalak et al., 2009; Ross et al., 2018; Troje, 2002) and ultimately provided acceptable results; however, future research could implement non-linear methods to achieve similar goals. A single external participant was used to inform decisions on what series of phases to combine to reach each desired distance (i.e., to avoid using only steady-state phases to complete the distance) as only 10-metre movements were collected. Future work should refine these decisions by having a number of participants perform the movements at different distances to ensure the optimal combination of phases are selected. We currently only include a small subset of the operationally relevant tasks performed by soldiers, and only a subset of the burdens experienced by them. We aim to address these limitations by expanding our participant pool, increase the number of tasks modelled, include outdoor simulated drills, investigating a number of burdens experienced, and increase the number of class labels from each participant. Additionally, we aim to include body morphology into our framework since it has been highlighted that stature may affect performance during military-based tasks (Sanderson et al., 2021).

We believe that our framework will be integral to addressing all layers of the integrated survivability model. As such, we are creating a GUI available to defence scientists and military leaders from allied nations to give them the ability to morph movement patterns, visualize changes to the tradespace metrics, and export movement patterns for further analysis. This will give defence scientists and military leaders the ability to investigate many types of soldier burden to provide

them with informed, objective information to make decisions from armour procurement to employment of armour, and battlefield performance, which can positively impact operational readiness and increase overall mission success.

4.5.1 Data Accessibility

All LDA classification metrics and tradespace results for all movements at 5, 10, 15, 20, 25, and 30 metres (when applicable) can be found in the supplementary file "Study_Two_Supplementary_Data.xlsx". Susceptibility values are graphically displayed for all movements at all distances in Figures C1-C32 in Appendix C.

4.5.2 Declaration of Competing Interests

The authors declare that they have no known competing financial interests or personal relationships that could have appeared to influence the work reported in this paper.

4.5.3 Acknowledgements

This work was funded by the Canadian Department of National Defence (DND) contract number [W7719-195460/001/TOR]. Authors of this work from the Defence Research and Development Canada (DRDC), an agency of DND, contributed to the study design, manuscript editing, data collection, provided the military equipment and IMU suit, and hosted a data collection space.

4.6 References

Akhavanfar, M.H., Brandon, S.C.E., Brown, S.H.M., Graham, R.B., 2019. Development of a novel MATLAB-based framework for implementing mechanical joint stability constraints within OpenSim musculoskeletal models. J. Biomech. 91, 61–68.

Attwells, R.L., Birrell, S.A., Hooper, R.H., Mansfield, N.J., 2006. Influence of carrying heavy loads on soldiers' posture, movements and gait. Ergonomics 49, 1527–1537. https://doi.org/10.1080/00140130600757237

Baker, D., Wilson, G., Carlyon, B., 1994. Generality versus specificity: a comparison of dynamic and isometric measures of strength and speed-strength. Eur. J. Appl. Physiol. Occup. Physiol. 68, 350–355. https://doi.org/10.1007/BF00571456

Barre, A., Armand, S., 2014. Biomechanical ToolKit: Open-source framework to visualize and process biomechanical data. Comput. Methods Programs Biomed. 114, 80–87. https://doi.org/10.1016/j.cmpb.2014.01.012

Beaucage-Gauvreau, E., Robertson, W.S.P., Brandon, S.C.E., Fraser, R., Freeman, B.J.C., Graham, R.B., Thewlis, D., Jones, C.F., 2019. Validation of an OpenSim full-body model with detailed lumbar spine for estimating lower lumbar spine loads during symmetric and asymmetric lifting tasks. Comput. Methods Biomech. Biomed. Engin. 22, 451–464.

Beekley, M.D., Alt, J., Buckley, C.M., Duffey, M., Crowder, T.A., 2007. Effects of heavy load carriage during constant-speed, simulated, road marching. Mil. Med. 172, 592–595. https://doi.org/10.7205/MILMED.172.6.592

Billing, D.C., Silk, A.J., Tofari, P.J., Hunt, A.P., 2015. Effects of military load carriage on susceptibility to enemy fire during tactical combat movements. J. Strength Cond. Res. 29, S134–S138. https://doi.org/10.1519/JSC.0000000000001036

Birrell, S.A., Hooper, R.H., Haslam, R.A., 2007. The effect of military load carriage on ground reaction forces. Gait Posture 26, 611–614. https://doi.org/10.1016/j.gaitpost.2006.12.008

Blount, E.M., Ringleb, S.I., Tolk, A., Bailey, M., Onate, J.A., 2011. Incorporation of physical fitness in a tactical infantry simulation. J. Def. Model. Simul. 10, 235–246. https://doi.org/10.1177/1548512911421343

Bossi, L., Karakolis, T., Jones, M., 2020. Rationalizing the approach to mitigate soldier physical burden are Iron Man or Captain America the magic bullet?, in: Transhumanizing War: Performance Enhancement and the Implications for Policy, Society, and the Soldier. McGill-Queen's University Press, Montreal, Quebec, pp. 119–151.

Bossi, L.L.M., Jones, M.L.H., Kelly, A., Tack, D.W., 2016. A Preliminary Investigation of the Effect of Protective Clothing Weight, Bulk and Stiffness on Combat Mobility Course Performance, in: Proceedings of the Human Factors and Ergonomics Society 2016 Annual Meeting. Washington DC, pp. 701–705.

Bossi, L.L.M., Morton, A., Keefe, A., Karakolis, T., Mitchell, K.B., Sy, A., Keefe, A., Karakolis, T., Jones, M., 2017. Understanding the trade-offs between protection, performance and integrated survivability. J. Sci. Med. Sport 20S, S137–S139. https://doi.org/10.1016/j.jsams.2017.09.509

Bossi, L.L.M., Richter, M., Tack, D., Kelly, A., Patterson, M., Lafiandra, M., 2014. Load Effects Assessment Program (LEAP): a Systematic Multinational Approach to Understand and Address Soldier Physical Burden.

Brown, T.N., O'Donovan, M., Hasselquist, L., Corner, B.D., Schiffman, J.M., 2014. Body borne loads impact walk-to-run and running biomechanics. Gait Posture 40, 237–242. https://doi.org/10.1016/j.gaitpost.2014.04.001

Delp, S.L., Anderson, F.C., Arnold, A.S., Loan, P., Habib, A., John, C.T., Guendelman, E., Thelen, D.G., 2007. OpenSim: Open-source software to create and analyze dynamic simulations of movement. IEEE Trans. Biomed. Eng. 54, 1940–1950. https://doi.org/10.1109/TBME.2007.901024

Drain, J., Orr, R., Attwells, R., Billing, D., 2012. Load Carriage Capacity of the Dismounted Combatant - A Commander's Guide. Australian Defence Science and Technology Organization (DSTO) Report No. DSTO-TR-2765. Fishermans Bend.

Dziados, J., Damokosh, A., Mello, R.P., Vogel, J.A., Farmer, K.L.J., 1987. Physiological determinants of load bearing capacity (No. USARIEM-T-19-87). Natic MA.

Fish, L., Scharre, P., 2018. The soldier's heavy load, Center for a New American Security.

Government of Canada, 2022. Statistics of women in the Canadian Armed Forces [WWW Document]. URL https://www.canada.ca/en/department-national-defence/services/women-in-the-forces/statistics.html (accessed 7.12.21).

Guzie, G.L., 2004. Integrated survivability assessment. White Sands Missile Range, New Mexico.

Helwig, N.E., Hong, S., Hsiao-Wecksler, E.T., Polk, J.D., 2011. Methods to temporally align gait cycle data. J. Biomech. 44, 561–566. https://doi.org/10.1016/j.jbiomech.2010.09.015

Holewijn, M., 1990. Physiological strain due to load carrying. Eur. J. Appl. Physiol. 61, 237–245.

Hunt, A.P., Tofari, P.J., Billing, D.C., Silk, A.J., 2016. Tactical combat movements: inter-individual variation in performance due to the effects of load carriage. Ergonomics 59, 1232–1241. https://doi.org/10.1080/00140139.2015.1132780

Karakolis, T., Bossi, L.L.M., 2017. Viability of using a wearable assistive device to reduce soldier burden. J. Sci. Med. Sport 20S, S99–S102. https://doi.org/10.1016/j.jsams.2017.09.456

Karakolis, T., Sinclair, B.A., Kelly, A., Terhaar, P., Bossi, L.L.M., 2017. Determination of orientation and practice requirements when using an obstacle course for mobility performance assessment. Hum. Factors 59, 535–545. https://doi.org/10.1177/0018720816686611

Knapik, J., Stabb, J., Bahrke, M., O'Connor, J., Sharp, M., Frykman, P.N., Mello, R.P., Reynolds, K., Vogel, J.A., 1990. Relationship of soldier load carriage to physiological factors, military experience and mood states (No. USARIEM-T17-90). Natic MA.

Koerhuis, C.L., Veenstra, B.J., Van Dijk, J.J., Delleman, N.J., 2009. Predicting marching capacity while carrying extremely heavy loads. Mil. Med. 174, 1300–1307. https://doi.org/10.7205/MILMED-D-00-7508

Laing-Treloar, A.K., Billing, D.C., 2011. Effect of load carriage on performance of an explosive, anaerobic military task. Mil. Med. 176, 1027–1031. https://doi.org/10.7205/MILMED-D-11-00017

Liew, B.X., Morris, S., Netto, K., 2016a. Joint power and kinematics coordination in load carriage running: Implications for performance and injury. Gait Posture 47, 74–79. https://doi.org/10.1016/j.gaitpost.2016.04.014

Liew, B.X., Morris, S., Netto, K., 2016b. The effects of load carriage on joint work at different running velocities. J. Biomech. 49, 3275–3280. https://doi.org/10.1016/j.jbiomech.2016.08.012

Lyons, J., Allsopp, A., Bilzon, J., 2005. Influences of body composition upon the relative metabolic and cardiovascular demands of load-carriage. Occup. Med. (Chic. Ill). 55, 380–384. https://doi.org/10.1093/occmed/kqi087

Marshal, S.L.A., 1980. The soldier's load and the mobility of a nation. The Marine Corps Association, Quantico, Virginia.

Mavor, M.P., Ross, G.B., Clouthier, A.L., Karakolis, T., Graham, R.B., 2020. Validation of an IMU suit for military-based tasks. Sensors 20, 1–14. https://doi.org/10.3390/s20154280

Mello, R., Damokosh, A., Reynolds, K., Witt, E., Vogel, J., 1988. The physiological determinants of load bearing performance at different march distances (No. USARIEM-T-15-88). Natic MA.

Michalak, J., Troje, N.F., Fischer, J., Vollmar, P., Heidenreich, T., Schulte, D., 2009. Embodiment of sadness and depression-gait patterns associated with dysphoric mood. Psychosom. Med. 71, 580–587. https://doi.org/10.1097/PSY.0b013e3181a2515c

Morton, A., Bray-Miners, J., Tack, D., n.d. Charactizing marksmanship performance against moving targets in a simulated gap crossing shoooting task(U). DRDC Tracking No. C21-0325-04984. [C-NCG]. Ottawa, Ontario, Canada.

Muller, A., Pontonnier, C., Dumont, G., 2020. Motion-based prediction of hands and feet contact efforts during asymmetric handling tasks. IEEE Trans. Biomed. Eng. 67, 344–352. https://doi.org/10.1109/TBME.2019.2913308

Oudenhuijzen, A.J.K., Bossi, L.L.M., Koerhuis, C.L., 2021. Chapter 3 - Work package 1: characterizing dismounted soldier burden, Reducing the Burden on the Dismounted Soldier. NATO AC/323(HFM-238)TP/950 STO TECHNICAL REPORT TR-HFM-238. NATO CSO, Neuilly sur Seine.

Pandorf, C.E., Harman, E.A., Frykman, P.N., Patton, J.F., Mello, R.P., Nindl, B.C., 2002. Correlates of load carriage and obstacle course performance among women. Work 18, 179–189.

Park, H., Branson, D., Kim, S., Warren, A., Jacobson, B., Petrova, A., Peksoz, S., Kamenidis, P., 2014. Effect of armor and carrying load on body balance and leg muscle function. Gait Posture 39, 430–435. https://doi.org/10.1016/j.gaitpost.2013.08.018

Phillips, D.B., Stickland, K.M., Lesser, I.A., Petersen, S.R., 2016. The effects of heavy load carriage on physiological responses to graded exercise. Eur. J. Appl. Physiol. 116, 275–280. https://doi.org/10.1007/s00421-015-3280-z

Ramsay, J.W., Hancock, C.L., O'Donovan, M.P., Brown, T.N., 2016. Soldier-relevant body borne loads increase knee joint contact force during a run-to-stop maneuver. J. Biomech. 49, 3868–3874. https://doi.org/10.1016/j.jbiomech.2016.10.022

Ren, L., Jones, R.K., Howard, D., 2008. Whole body inverse dynamics over a complete gait cycle based only on measured kinematics. J. Biomech. 41, 2750–2759.

Ricciardi, R., Deuster, P.A., Talbot, L.A., 2008. Metabolic demands of body armor on physical performance in simulated conditions. Mil. Med. 173, 817–824. https://doi.org/10.7205/milmed.173.9.817

Ricciardi, R., Deuster, P.A., Talbot, L.A., 2007. Effects of gender and body adiposity on physiological responses to physical work while wearing body armor. Mil. Med. 172, 743–748. https://doi.org/10.7205/MILMED.172.7.743

Ross, G.B., Dowling, B., Troje, N.F., Fischer, S.L., Graham, R.B., 2018. Objectively differentiating movement patterns between elite and novice athletes. Med. Sci. Sports Exerc. 50, 1457–1464. https://doi.org/10.1249/MSS.0000000000001571

Roy, T.C., Knapik, J.J., Ritland, B.M., Murphy, N., Sharp, M.A., 2012. Risk factors for musculoskeletal injuries for soldiers Deployed to Afghanistan. Aviat. Sp. Environ. Med. 83, 1060–1066. https://doi.org/10.3357/ASEM.3341.2012

Roy, T.C., Lopez, H.P., Piva, S.R., 2013. Loads worn by soldiers predict episodes of low back pain during deployment to afghanistan. Spine (Phila. Pa. 1976). 38, 1310–1317. https://doi.org/10.1097/BRS.0b013e31829265c4

Sanderson, P.W., Faulkner, S., Fordy, G., Garcia-Vicencio, Sebastian Malgoyre, A., Reilly, T., 2021. Chapter 4 – Work Package 2: Literature Review on Soldier Load., Reducing the Burden on the Dismounted Soldier. NATO AC/323(HFM-238)TP/950 STO TECHNICAL REPORT TR-HFM-238. NATO CSO, Neuilly sur Seine.

Sturdy, J.T., Sessoms, P.H., Silverman, A.K., 2021. A backpack load sharing model to evaluate lumbar and hip joint contact forces during shoulder borne and hip belt assisted load carriage. Appl. Ergon. 90, 103277. https://doi.org/https://doi.org/10.1016/j.apergo.2020.103277

Troje, N.F., 2002. Decomposing biological motion: A framework for analysis and synthesis of human gait patterns. J. Vis. 2, 371–387. https://doi.org/10.1167/2.5.2

Vitali, R. V, Cain, S.M., Ojeda, L. V, Potter, M. V, Zaferiou, A.M., Davidson, S.P., Coyne, M.E., Hancock, C.L., Mendoza, A., Stirling, L.A., Perkins, N.C., 2019. Body-worn IMU array reveals effects of load on performance in an outdoor obstacle course. PLoS One 14, 1–30. https://doi.org/10.1371/journal.pone.0214008

Chapter 5: Assessing the Soldier Survivability Tradespace Using a Single IMU

5.1 Abstract

Soldier burden is influenced by the environment, metabolic demands, equipment properties, and psychological stressors; however, much of our knowledge on soldier burden is in the context of body-borne load mass in controlled laboratory environments. Thus, to further our understanding of how all aspects of soldier burden affect the survivability tradespace (i.e., performance, health, and susceptibility), field-based motion capture methods are needed. We developed a human activity recognition method using the deep convolutional long short-term memory neural network architecture, trained using a single inertial measurement unit on the upper back, to identify eleven tactical movement patterns commonly performed by soldiers. Using a two-step logical algorithm, real-world constraints are forced, and class labels are expanded to 19 movements. Presented are three models based on Indoor, Section Attack (outdoors), and a General approach. Across all three approaches, we obtained an average accuracy of 90.0%. Further, we used these predictions to calculate meaningful tradespace metrics, which had an excellent agreement to calculations using the true labels. Military leaders and defence scientists can use this approach to quantify tradespace metrics in the field, as a preprocessing tool to supplement other technology, and make data-driven decisions that will improve performance, decrease susceptibility, and increase overall mission success.

5.2 Introduction

Military personnel perform a variety of tactical movement patterns during training and deployment. Typically, these movements are performed while subjected to various aspects of soldier burden: environmental conditions, metabolic demands, equipment properties (i.e., mass, mass distribution, coverage, bulk, stiffness, breathability, and thermal resistance), and psychological stressors (Armstrong and Bossi, 2021). However, during biomechanical research investigations, soldiers often perform movement protocols in a controlled indoor motion capture laboratory with a narrow focus on the mass of the body-borne load. Using this data collection framework, previous literature has unanimously identified many negative kinematic (Attwells et al., 2006; Brown et al., 2014), kinetic (Liew et al., 2016a, 2016b; Ramsay et al., 2016), and performance (Bossi et al., 2017, 2016; Karakolis et al., 2017; Laing-Treloar and Billing, 2011; Pandorf et al., 2002; Vitali et al., 2019) outcomes due to heavy body-borne load mass. Although these investigations are essential to our fundamental understanding of the underlying phenomena that affect a soldier's movement patterns, they do not fully reflect the movement patterns of soldiers in the field as influenced by the mission, threat, environment, and commander's intent. Thus, to truly understand a soldier's movements within the operational environment and the impact soldier burden has on these movements, a motion capture method that can efficiently and reliably collect meaningful data in the field is needed.

One technology that is suitable for field use is inertial measurement units (IMUs). IMUs are small wearable devices that typically include an accelerometer, gyroscope, and magnetometer. These devices are highly transportable, can collect over long periods of time, and can be combined with a biomechanical model to calculate joint angles (Laidig et al., 2017; Schepers et al., 2018). Previous work in our laboratory validated a 17-sensor IMU suit (Mavor et al., 2020) and used data

from this suit to morph movement patterns to represent intermediary body-borne loads and personal characteristics (Mavor et al., 2022). While such a suit can provide a tremendous amount of biomechanical information and drive many essential research questions, it is not practical for widespread usage as it is costly, must be set up and calibrated correctly by trained individuals, and is susceptible to damage in an operational environment (e.g., wires can get pulled/frayed, the onboard computer can breakdown if struck, and one of the many sensors can move, nullifying the calibration). An alternative method is to use a single IMU that does not need to be calibrated to a biomechanical model and can be easily outfitted on the participant. Although it is impossible to determine gross kinematic differences caused by soldier burden, a single IMU is field-deployable, is relatively inexpensive, enables the measurement of multiple participants simultaneously, and could be used for gathering performance and susceptibility metrics. Previous military investigations using single IMUs have been able to determine performance degradations due to body-borne load and personal characteristics (Billing et al., 2015; Hunt et al., 2016) and have been used to recognize operationally-relevant movement patterns in the field (Clements et al., 2012; Wyss and Mäder, 2010).

Human activity recognition (HAR) is a domain of machine learning research that typically uses deep neural networks (DNNs) to recognize movement patterns based on data obtained from various wearable sensors: a single IMU setup (Lockhart et al., 2013; Russell et al., 2021), multiple IMU setup (Ordóñez and Roggen, 2016), IMUs + heart rate monitor (Wyss and Mäder, 2010), IMU + EMG (Bangaru et al., 2021), optical motion capture systems (Clouthier et al., 2020), and smartphones (Ankita et al., 2021; Ronao and Cho, 2016), among others. Researchers have applied HAR to these various data types to recognize hand gestures (Ordóñez and Roggen, 2016), activities of daily living (Ankita et al., 2021; Ordóñez and Roggen, 2016; Russell et al., 2021), non-specific

sporting movements (Clouthier et al., 2020), workplace postures (Abobakr et al., 2019) and tasks (Bangaru et al., 2021), and military activities (Clements et al., 2012; Papadakis et al., 2020; Wyss and Mäder, 2010), among many others. Using the knowledge obtained from the HAR algorithms, researchers have been able to perform workplace ergonomic assessments (Abobakr et al., 2019; Antwi-Afari et al., 2020) and at-home monitoring of activities of daily living (Lockhart et al., 2013). In a military context, by using a single IMU to recognize what activities soldiers are performing, with or without combining other wearable technology, there is potential to advance other fields of study within defence science, such as fatigue research (e.g., knowing what activities lead up to sustained heart rate or the evaluation of performance decline over time), ergonomics (e.g., task frequency, rest, interaction with objects), team-based interactions, training (i.e., digitize drills to visualize), and survivability (i.e., firing at digitized avatars, calculation of exposure time), among others.

This work aimed to investigate the efficacy of using a single IMU sensor to recognize key military movements and calculate tradespace metrics. Presented are a series of DNNs, trained to recognize operationally-relevant movement patterns using data from a single IMU, obtained from data collected in an indoor laboratory and during an outdoor two-person 60-metre simulated section attack drill. Three types of DNN architectures, 1) convolutional neural network (CNN), 2) fully connected DNN (FC), and 3) deep convolutional long short-term memory neural network (DeepConvLSTM), were trained using three approaches: indoor-specific, section attack-specific, and general (i.e., both indoor and section attack data). Predictions made by the DNNs were processed through a two-step logical algorithm to ensure predictions adhered to real-world constraints and to expand the number of class labels from 11 to 19. We present our models' performance using traditional machine learning metrics (i.e., accuracy and F1-scores) and compare

the survivability tradespace metrics (i.e., exposure time, susceptibility to enemy action) calculated using the predicted labels versus the true labels for our test participants.

5.3 Methods

5.3.1 Participants and Procedures

5.3.1.1 Participants

Seventeen male dismounted combat arms reserve force soldiers (consisting of Privates, Corporals, and Master Corporals) from the Canadian Armed Forces (CAF) were recruited. Participants' mean height, mass, age, and years served were 1.83 m (±8.9), 81.7 kg (±9.2), 26.6 years (±7.2), and 3.8 years of service (±2.2), respectively. All experimental protocols followed the Declaration of Helsinki and were approved by the University of Ottawa (H-06-18-721) and Defence Research and Development Canada (2019-026) Research Ethics Boards. All participants provided free and informed consent prior to participating in these protocols.

5.3.1.2 Equipment

Participants performed a series of movements under four load conditions: 1) ***Slick*** ~5.5 kg, comprising of a CAF helmet, a replica C7A2 rifle, and the temperate combat clothing ensemble (T-shirt, combat shirt, combat trousers, combat boots); 2) ***Full Fighting Order (FFO)*** ~22 kg, comprising Slick + CAF issued fragmentation protective vest (with 2 in-service ballistic plates, front and back) + a fully loaded tactical vest (2 replica grenades, 2 replica smoke grenades, 4 replica C7 magazines, a simulated canister of C9 ammunition, 2 field dressings, and a water-filled 1 L canteen); 3) ***Backpack*** 38 kg, comprising FFO + a loaded CAF daypack weighing 16 kg; and 4) ***Pockets*** 38 kg, comprising of FFO + 16 kg worth of non-ferrous plates added to the fragmentation vest (section attack only). Participants' whole-body movement patterns were recorded at 240 Hz for all conditions using an Xsens IMU suit (MVN Link, Xsens, Netherlands)

validated for military-based tasks (Mavor et al., 2020). Concurrently, movement patterns were collected at 100 Hz using a single IMU (S5, Catapult Sports Pty Ltd., Australia) designed for high-performance activities. The IMU was placed on the back of the upper torso using a specialized sports pinnie.

5.3.1.3 Experimental Protocol

5.3.1.3.1 Indoor Laboratory

Twelve soldiers performed two repetitions of eight military-based movements under the Slick, FFO, and Backpack load conditions described above: run, run-to-kneel (RTK), run-to-prone (RTP), kneel-to-run (KTR), prone-to-run (PTR), kneel-to-prone (KTP), prone-to-kneel (PTK), and walk. Trial order and weight conditions were randomized for each participant; a total of 48 movement trials (8 movements * 2 repetitions * 3 conditions = 48 movements) were performed. All movements requiring forward progression were done in a straight line measuring ten metres and all movements began/ended with the participant in standing.

5.3.1.3.2 Outdoor Section Attack

Ten soldiers performed two repetitions of fireteam pairs within the context of a simulated 60-metre section attack under the four load conditions (i.e., Slick, FFO, Backpack, and Pockets). For each repetition, team members alternated between fireteam leader and follower roles. Fireteam pairs began by patrolling (walking and watching for threats) for at least 10 m in open grassy terrain. At the command of a Section Commander (non-participant), fireteam pairs began advancing towards the threat and adopted tactical movements (i.e., bounding rushes, wherein one soldier dashes from one point of cover to another while simulated covering fire is provided by the fireteam partner and vice versa) until the desired distance was reached (~40 metres). Soldiers then completed a simulated assault on the objective for the remaining distance (~20 metres). These

tactical movements replicate the individual movements and postures captured during the laboratory data collection (run, RTK, KTR, PTR, KTR, PTK, walk).

5.3.2 Data Processing

5.3.2.1 Preprocessing

Xsens IMU data were processed in Xsens MVN Analyze 2019.2.1 (Xsens, Netherlands) using the high-definition (HD) reprocessing tool. Data were visually inspected, and segment contact data were manually adjusted when necessary. Files were exported in both .mvnx and .c3d file formats.

Catapult IMU data were downloaded and processed through Sprint 5.1.7 (Catapult, Australia) to produce comma-separated variable (CSV) files hosting the sensor's triaxial acceleration, triaxial gyroscope, and triaxial magnetometer data; GPS data were available outdoors but were not used for this investigation. The output data were a continuous stream hosting the entire data collection protocol thus, data were cropped and recombined to only include data when the Xsens suit was collecting. This was done so that all input data for the DNNs could be accurately labelled with ground truth labels.

Before each load condition, a jumping task was performed to synchronize the Catapult and Xsens IMU systems. Specifically, the peak vertical acceleration from the Catapult and Xsens (T8 segment) systems were used to align the data in time using the serial date number calculated through Matlab's (MathWorks, USA) datenum function.

5.3.2.2 Ground Truth Labels

Ground truth labels were visually identified using Matlab 2016b by a single labeller who plotted the Catapult IMU's vertical accelerometer and yaw gyroscope data, along with Xsens'

vertical virtual marker position of the T8 spinal process and used Matlab's ginput function to select the bounds of each movement type. The labeller also visualized the whole-body movement patterns using the .c3d files to gain additional information on the movements.

The labeller manually identified two class label sets: original and expanded. The original set was used as ground truth labels for the DNNs and consisted of eleven class labels: stand, jump, descend, ascend, prone, kneel, stand-to-run (STR), run, walk, crawl, and null. By processing the DNNs' predictions through a two-step logical algorithm, they were expanded to give context to the ascend and descend classes, resulting in 19 class labels (Table 5.1). The null class was used as a catch-all for any movement the participant performed that did not fit into any other movement; examples include, but are not limited to: bending over, shuffling feet while standing, and turning.

Table 5.1. Original and Expanded Class Labels

Original	**Expanded**
Stand	Stand
Jump	Jump
Descend	Run-to-prone Run-to-kneel Stand-to-prone Stand-to-kneel Kneel-to-prone
Ascend	Prone-to-run Kneel-to-run Prone-to-stand Kneel-to-stand Prone-to-kneel
Kneel	Kneel
Prone	Prone
Stand-to-run	Stand-to-run
Run	Run
Walk	Walk
Crawl	Crawl
Null	Null

The original labels were predicted by the DNNs. The expanded labels were generated through a two-step algorithm to give context to the descend and ascend class labels.

5.3.3 Deep Neural Network-based Human Activity Recognition

A hold-out testing approach was employed to train and evaluate the DNNs for activity recognition. Three approaches to model development were employed: Indoor-specific, Section

Attack-specific, and General. The Indoor and Section Attack approaches were used to develop models to classify only indoor or section attack data, respectively. The General approach was used to develop models to classify activities from either scenario. For each approach, three neural network architectures were employed (3 approaches * 3 architectures = 9 models).

5.3.3.1 Data Preparation

The data were divided into training, validation, and test subsets by participant (i.e., samples from one participant were always kept together in the same subset), shown in Table 5.2. The same subsets for a given approach were used across all models (i.e., CNN, FC, and DeepConvLSTM) to allow for direct comparisons. Across all approaches, the validation and test participants were not exposed during training to provide an unbiased estimate of model generalizability. In the General approach, indoor and section attack data were represented in the validation and test subsets with a distribution similar to the training subset.

For all approaches, a single matrix was created for each subset by concatenating data from all movement trials and conditions performed by the participants in that subset. Normalization was conducted on a feature-by-feature basis by subtracting the mean and dividing by the standard deviation of all data frames across participants and movements in the corresponding subset (Clouthier et al., 2021). A sliding window approach was used to divide the data into segments containing an equal number of data frames (i.e., 64 or 128), where the step size was set to ¼ of the window size. Each segment was assigned a label according to the movement performed for the majority of that segment. The length and width of the input data was the window size and nine features (x, y, and z component of the linear accelerometer, gyroscope, and magnetometer data from the Catapult IMU), respectively.

Table 5.2. Datasets used for each approach.

	Total samples	Training subset	Validation subset	Test subset
Indoor	628,063 (12 participants)	477,929 (76.1%) (9 participants)	47,866 (7.6%) (1 participant)	102,268 (16.3%) (2 participants)
Section Attack	1,032,177 (10 participants)	812,402 (78.7%) (8 participants)	109,889 (10.7%) (1 participant)	109,886 (10.7%) (1 participant)
General	1,660,240 (22 participants)	1,337,335 (80.6%) (18 participants)	157,755 (9.5%) (2 participants)	165,150 (9.9%) (2 participants)

Note: The general dataset was comprised of the indoor and section attack datasets, and both indoor and section attack data were represented in the validation and test subsets. Seventeen unique participants were recruited for this study; however, 5 of the same participants performed both the indoor and section attack protocols. Each sample consisted of 9 features (3*accelerometer, 3*gyroscope, 3*magnetometer).

5.3.3.2 Model Architectures, Hyperparameter Optimization, and Training

To perform activity recognition, three neural network architectures based on previous work were implemented in Python 3.8.12 (Van Rossum and Drake, 2009) using Tensorflow 2.3.0 (Abadi et al., 2016): shallow CNN (Ignatov, 2018), FC (Kwapisz et al., 2011), and DeepConvLSTM (Ordóñez and Roggen, 2016). All machine learning development was synchronously distributed using a mirrored strategy across three, Nvidia Titan RTX GPUs (Nvidia, USA) with 24 GB of GDDR6 memory each. This was performed on a server running Ubuntu 18.04 powered by two, Intel Xeon Gold 6248 CPUs @ 2.50GHz (Intel, USA) and 384 GB of DDR4 RAM.

A combination of reliance on previous work and hyperparameter optimization was used to select the hyperparameters for each model. Hyperparameter optimization was performed using the indoor dataset and KerasTuner library (O'Malley et al., 2019) with the objective of maximizing validation accuracy. Bayesian hyperparameter optimization was implemented to search the hyperparameter spaces defined for each model (Snoek et al., 2012), presented in Table 5.3. The resulting hyperparameters were used to train the models for all approaches.

Table 5.3. The hyperparameter search spaces for each architecture. The values for the CNN channels, input units, and LSTM cells were held constant across layers within a model. SGD = stochastic gradient descent; LSTM = long short-term memory; RMSProp = root mean squared propagation.

	Hyperparameters
CNN	Window size = [64, 128] CNN channels = [32, 64, 96] Kernel size = [5, 7, 9, 11] SGD learning rate = [0.0001, 0.001, 0.01, 0.1, 1] SGD momentum = [0.7, 0.9, 0.95, 0.98]
FC	Window size = [64, 128] Input units = [64, 128, 192, 256, 320] SGD learning rate = [0.0001, 0.001, 0.01, 0.1, 1] SGD momentum = [0.7, 0.9, 0.95, 0.98]
DeepConvLSTM	Window size = [64, 128] CNN channels = [32, 64, 96] Kernel size = [5, 7, 9, 11] LSTM cells = [64, 128, 192] RMSProp learning rate = [0.0001, 0.001, 0.01, 0.1, 1]

CNN = convolutional neural network, FC = fully connected neural network, DeepConvLSTM = deep convolutional long short-term memory neural network

All models were trained using a batch size of 100 samples, a maximum epoch of 500, and early stopping was implemented via monitoring the training accuracy with a patience of three. The categorical cross-entropy function was used to compute loss for all models and was minimized using either stochastic gradient descent (SGD) or root mean squared propagation (RMSProp). When training was stopped, the weights from the epoch with the smallest validation loss were retained and used to classify all samples in the test set. Loss, accuracy, and weighted average F1-score were computed to evaluate test performance. The architectures and hyperparameter optimization procedures for each model are described in the following sections.

5.3.3.3 Convolutional Neural Network

The CNN was comprised of an input layer, a convolutional layer with a rectified linear unit (ReLU) activation function, and a dense layer with a softmax activation function (Figure 5.1). During training, the model parameters were optimized using SGD. The SGD hyperparameters (i.e.,

learning rate and momentum), the number of convolutional filters, and the convolutional kernel size were tuned during hyperparameter optimization (Table 5.3).

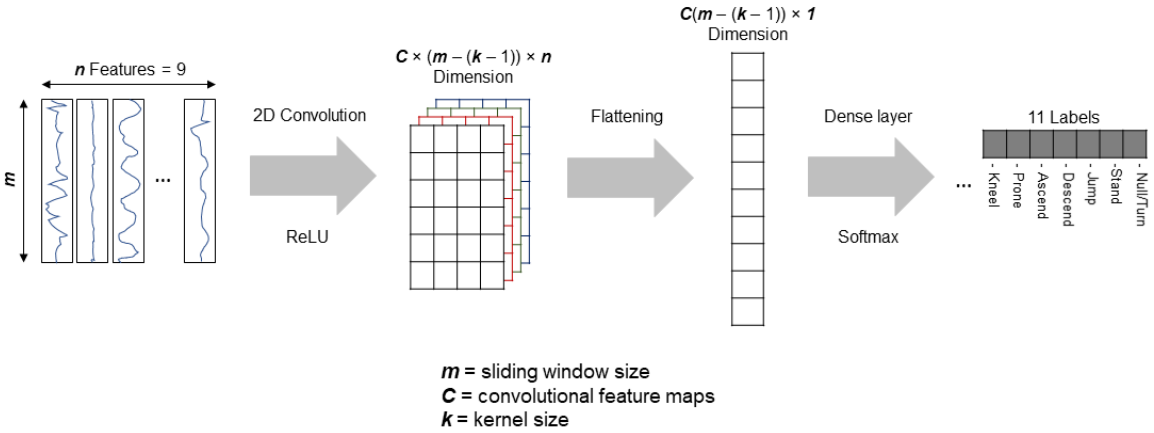

Figure 5.1. Convolutional neural network architecture. The nine features were the x, y, and z components of the accelerometer, gyroscope, and magnetometer signals from the inertial measurement unit. The sliding window size, the number of convolutional feature maps (i.e., number of filters), and the kernel size were tuned during hyperparameter optimization. ReLU = rectified linear unit.

5.3.3.4 Fully Connected Neural Network

The FC neural network was comprised of an input layer, three dense (i.e., fully-connected) layers with ReLU activation functions, and a dense output layer with a softmax activation function (Figure 5.2). As a form of regularization, a drop-out operator with a probability set to $p = 0.5$ was implemented on the output of the dense layers. Model parameters were optimized during training using SGD. The SGD hyperparameters (i.e., learning rate and momentum) and the number of input units in the dense layers were tuned during hyperparameter optimization (Table 5.3).

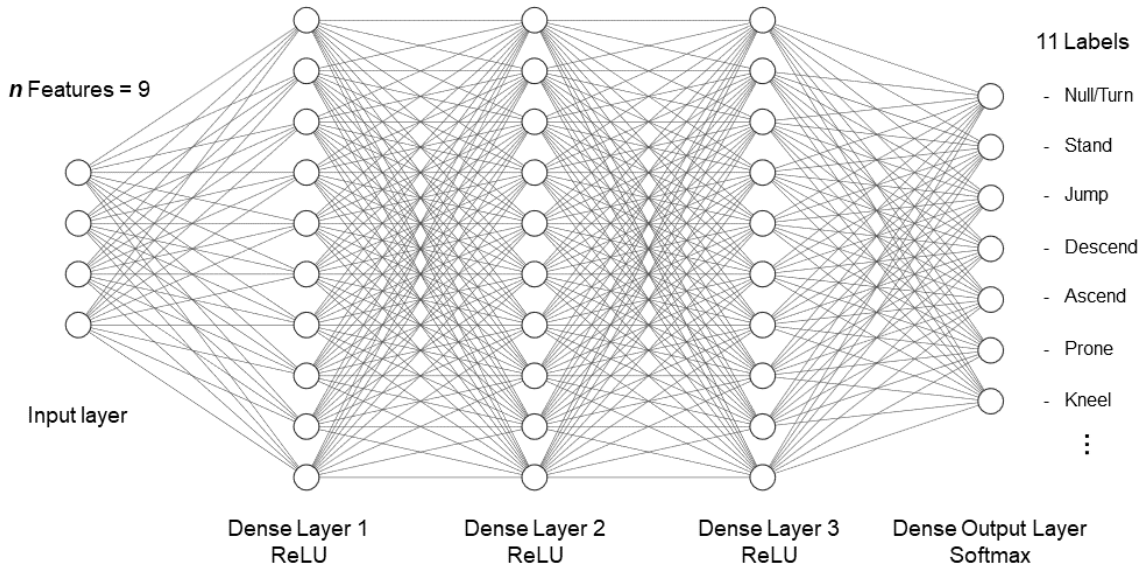

Figure 5.2. Fully connected neural network architecture. The nine features were the x, y, and z components of the accelerometer, gyroscope, and magnetometer signals from the inertial measurement unit. The sliding window size and the number of input units in each dense (i.e., fully-connected) layer were tuned during hyperparameter optimization. ReLU = rectified linear unit.

5.3.3.5 Deep Convolutional Long Short-term Neural Network

The DeepConvLSTM model was comprised of an input layer, four convolutional layers with ReLU activation functions, two long short-term memory recurrent layers with hyperbolic tangent (tanh) activation functions, and a dense layer with a softmax activation function (Figure 5.3). A drop-out operator was implemented on the inputs of the recurrent layers with a probability set to $p = 0.5$.

Following procedures outlined by Ordóñez and Roggen (2016), the model parameters were optimized during training by minimizing the cross-entropy loss function using batch gradient descent and the RMSProp update rule. For RMSProp, the decay factor was set to $\rho = 0.9$, and the momentum was set to 0.0. The RMSProp learning rate, the number of convolutional filters, the convolutional kernel size, and the number of long short-term memory (LSTM) cells in the LSTM recurrent layers were tuned during hyperparameter optimization (Table 5.3).

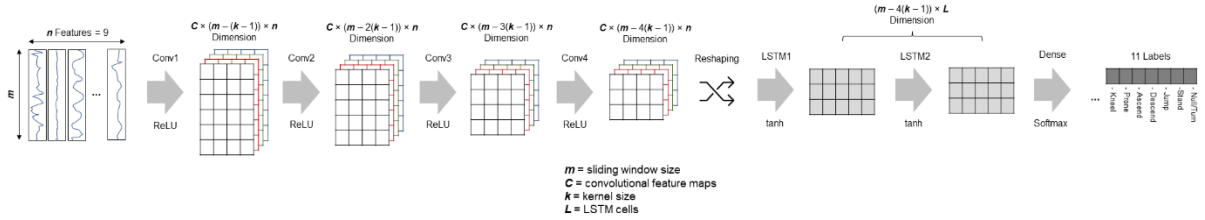

Figure 5.3. Deep convolutional long short-term memory neural network architecture. The nine features were the x, y, and z components of the accelerometer, gyroscope, and magnetometer signals from the inertial measurement unit. The sliding window size, the number of convolutional feature maps (i.e., number of filters), the kernel sizes, and the number of long short-term memory (LSTM) cells in each recurrent layer were tuned during hyperparameter optimization. Conv = convolutional layer; ReLU = rectified linear unit; tanh = hyperbolic tan function.

5.3.4 Prediction Processing

5.3.4.1 Logical Algorithm

The predictions from the DNNs were processed through a two-step logical algorithm implemented in Matlab 2016b. In step one, the initial predictions from the DNN were processed to update the original label set to ensure that the predictions adhere to real-world constraints. Examples of constraints are: no standing after a descend, no standing before an ascend, kneel/prone must be preceded by a descend if the previous label is a stand, walk, or run, etc. The input to the logical algorithm was a 3 x 5 matrix where the columns were the class labels (rows 1 and 2 corrected; rows 3-5 predicted), the number of windows for each class label (i.e., multiple windows can contribute to the class labels), and the mean probability for those windows for that class. The current step for the logical algorithm was row three such that the algorithm could consider the previous two and future two class labels. Considering real-world constraints and the DNN's confidence in those labels, the logical algorithm altered the current (i.e., 3 row) class label, which was fed into the next step. If the step failed, the logical algorithm was given the last and next five labels, window sizes, and probabilities to make a decision and could alter any previous label if real-world constraints were violated.

After completing the first step, the second step iterates through the updated original label set to generate the expanded label set (Table 5.1). To expand the labels, the algorithm was shown the similarly structured 3 x 5 matrix described above; however, the algorithm only made changes to the ascend and descend classes based on what the previous and next class labels were. For example, if the current class was a descend with a previous class of running and a next class of kneeling, the current class descend would be altered to a run-to-kneel.

The logical algorithms were run on an Acer Laptop with Intel® Core™ i7-8750H CPU @ 2.20GHz 2.21 GHz, 16 GB of RAM..

5.3.3.2 Survivability Tradespace

Using the expanded label set, the survivability tradespace metrics were calculated: exposure time, number of enemy shots fired, and susceptibility to enemy action. For the current investigation, the exposure time for each movement was calculated with the assumption that while the participant was on the ground (i.e., kneel, prone, crawl, KTP, PTK), they were considered to be not exposed. For all other movements, participants were considered exposed to enemy action.

Due to the nature of the protocol (especially during the indoor collections), participants stood at the starting and finish line for a variable amount of time. Therefore, all laboratory-based movement trials were cropped to exclude the standing portion at the start or end of the movement (i.e., calculations started at the first movement following a stand and ended at the last movement before a stand). Using the same rationale, the section attack data were cropped between the first descend into a kneel/prone after the initial patrol, and the last ascend before the simulated assault. For the indoor movements, the exposure time was calculated for each individual movement and averaged within each load condition. For the section attack, the exposure time was individually

calculated at each instance of exposure between two periods when the participant was unexposed (i.e., one instance of exposure can be represented as KTR, run, RTK, kneel).

The calculated exposure time for each movement was used to determine the number of enemy shots that could be fired at the participant using Equation 5.1 (Billing et al., 2015; Blount et al., 2011):

$$Shots = (Exposure\ Time - Reaction\ Time) * Shooting\ Cadence \quad \text{(Eq. 5.1)}$$

where reaction time was set to one second and shooting cadence was set to 1.3 shots per second (Billing et al., 2015; Blount et al., 2011). Given the number of shots fired, susceptibility was calculated with a shooting accuracy of 10% (Equation 5.2 (Billing et al., 2015; Blount et al., 2011)):

$$Susceptibility = (1 - (1 - Accuracy)^{Shots}) * 100 \quad \text{(Eq. 5.2)}$$

where susceptibility is represented as a percentage chance of being hit by the number of shots calculated in Equation 5.1.

5.4.0 Results

Model performance results represent the whole time series, while the tradespace metrics represent the cropped labels as described in section 5.3.3.2. Model performance was evaluated using the windowed true labels described above, while the original true labels were used for tradespace calculations (i.e., the true labels manually identified by the research team before windowing).

5.4.1 Deep Neural Network Performance

The performance of the DNNs for activity recognition is presented for the original label set only. Across all approaches, the DeepConvLSTM architecture had less loss, greater accuracy, and greater weighted average F1-score compared to the CNN and FC models when evaluated using the test subsets (Table 5.4). The training and prediction time on the general dataset (i.e., indoor and section attack data combined) were longest for the DeepConvLSTM (24.5 minutes), followed by the FC (5.72 minutes) and CNN (1.77 minutes) models (Table 5.5). For the general dataset, the logical algorithms took 10.76 seconds to process 109,886 frames of data. The remainder of the results are computed using the output from the DeepConvLSTM models.

Table 5.4. Human activity recognition performance for all architectures across all approaches.

	Indoor	Outdoor	General
CNN	Loss = 0.688 Accuracy = 79.86% F1-score = 79.52%	Loss = 0.657 Accuracy = 82.10% F1-score = 82.97%	Loss = 0.638 Accuracy = 81.48% F1-score = 81.41%
FC	Loss = 0.610 Accuracy = 82.26% F1-score = 81.86%	Loss = 0.509 Accuracy = 83.58% F1-score = 84.80%	Loss = 0.481 Accuracy = 84.81% F1-score = 84.58%
DeepConvLSTM	Loss = 0.486 Accuracy = 85.87% F1-score = 86.11%	Loss = 0.406 Accuracy = 87.06% F1-score = 87.36%	Loss = 0.459 Accuracy = 85.88% F1-score = 86.14%
DeepConvLSTM after Logical Algorithm	Accuracy = 91.72% F1-Score = 91.79%	Accuracy = 90.64% F1-Score = 91.11%	Accuracy = 87.70% F1-Score = 87.86%

CNN = convolutional neural network, FC = fully connected neural network, DeepConvLSTM = deep convolutional long short-term memory neural network, F1-score = weighted average F1-score.

Table 5.5. Training and test set prediction times on the general dataset for all three deep neural network architectures.

	Epochs before early stopping	Total training time	Average time per epoch	Prediction time on test set
CNN	59	73.93 s (1.23 min)	1.25 s	0.867 s
FC	99	588.65 s (9.81 min)	5.94 s	1.768 s
DeepConvLSTM	99	944.68 s (15.74 min)	9.54 s	1.932 s

CNN = convolutional neural network, FC = fully connected neural network, DeepConvLSTM = deep convolutional long short-term memory neural network. Times are based on a mirrored strategy across three, Nvidia Titan RTX GPUs (Nvidia, USA) with 24 GB of GDDR6 memory each, performed on a server running Ubuntu 18.04 powered by two, Intel Xeon Gold 6248 CPUs @ 2.50GHz (Intel, USA) and 384 GB of DDR4 RAM.

5.4.2 Logical Algorithm

Once the predictions were analyzed through the logical algorithm, on average, across all three model approaches, accuracy and weighted F1 scores were 90.0% and 90.3%, respectively (Table 5.4). This represents an average increase in accuracy and weighted F1-scores of 3.75% and 3.72%, respectively. The General model had a slightly lower overall accuracy (87.7%) compared to the Indoor (91.7%) and Section Attack (90.6%) models. Load condition did not appear to greatly influence the performance of the models (Table 5.6). The worst classified load condition was the

General model classifying the Slick condition (accuracy: 82.3%; F1: 82.9%), while the Pocket condition classified by the General model was the best (accuracy: 93.1%; F1: 93.8%).

Table 5.6. Accuracy and weighted average F1-scores across load conditions.

Approach	Metric	Slick	FFO	Backpack	Pockets
Indoor	Accuracy	90.91	92.86	87.87	-
	F1-Score	90.88	92.93	87.90	-
Section Attack	Accuracy	85.72	90.01	93.02	93.03
	F1-Score	87.13	90.61	93.20	93.26
General	Accuracy	82.26	91.50	85.49	93.15
	F1-Score	82.89	91.47	85.47	93.76
Mean	Accuracy	86.29	91.46	88.79	93.09
SD	F1-Score	4.355	1.423	3.852	0.080

All values are expressed as a percentage. The indoor data do not have a Pockets condition.

5.4.3 Tradespace Metrics

For the four unique test participants, all models identified an increase in exposure time with an increase in body-borne load. On average, across all trials/instances of exposure, compared to the true labels, the predicted labels had an absolute difference in exposure time of 0.17 s, 0.13 s, and 0.16 s for the Indoor, Section Attack, and General models, respectively. This difference in exposure time between true and predicted labels across all trials/instances of exposure led to an average absolute difference in the number of shots fired of 0.17, 0.16, and 0.21 for the Indoor, Section Attack, and General models, respectively. Ultimately, these differences between the predicted and true labels led to an average absolute difference in susceptibility of 1.25%, 1.20%, and 1.09% for the Indoor, Section Attack, and General models, respectively, across all trials/instances of exposure. Differences in tradespace metrics between the true and predicted labels can be visualized in Figure 5.4.

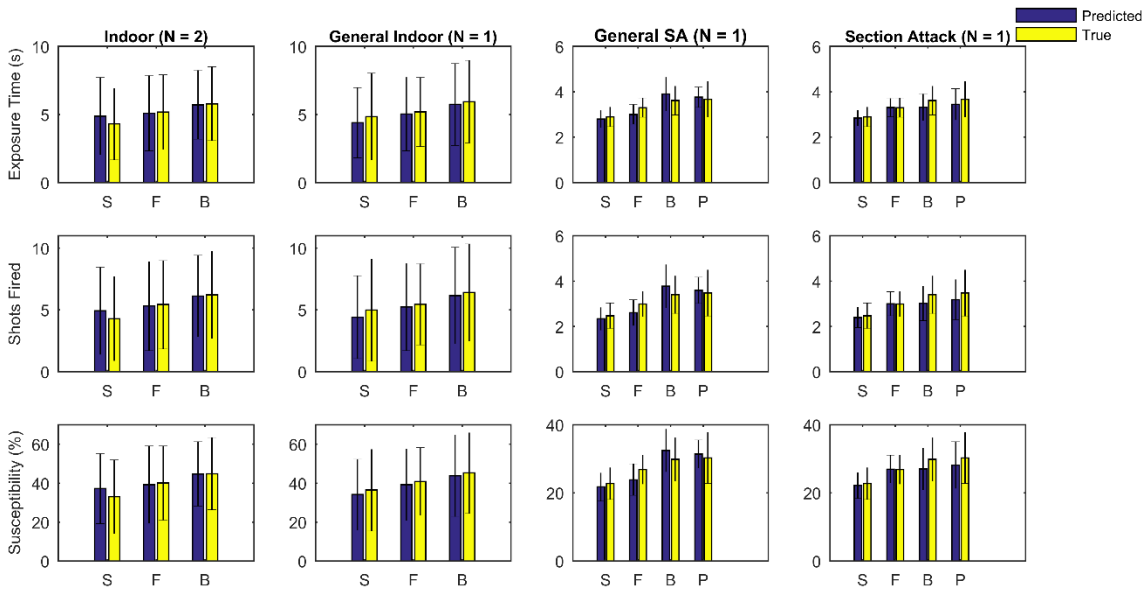

Figure 5.4. Tradespace results for four unique test participants across all approaches. S = Slick, F = Full Fighting Order (FFO), B = Backpack, P = Pockets, General SA = the General model's results on the section attack data, General Indoor = the General model's results of the indoor data, N = the number of test participants included in each comparison. Error bars represent standard deviation of the mean for each trial performed indoors or each instance of exposure during the section attack.

5.5 Discussion

To further our knowledge into how survivability tradespace metrics are impacted by soldier burden, methods are needed to collect soldiers' movement patterns in their operational environment. These methods need to use technology that is simple (i.e., does not need extensive expertise to operate), cost-effective (i.e., so multiple soldiers can be collected at once), highly transportable (i.e., can be deployed anywhere), and provides meaningful information that can be disseminated to military leaders. Current methods of calculating soldier survivability metrics include timing gates (Laing-Treloar and Billing, 2011), and GPS + accelerometer values on pre-setup courses (Billing et al., 2015; Hunt et al., 2016). While these studies have helped establish foundational knowledge, these methods are suitable for targeted data collections rather than in-the-wild soldier monitoring. In the current work, we have shown how we can address the needs of the military and build on previous work by using a single IMU that is placed on the upper back combined with a DNN to perform HAR addresses these needs.

Our investigation found that the DeepConvLSTM architecture was best at predicting our eleven movement classes. This was likely influenced by the data type (i.e., time series) and the node architecture allowing LSTM nodes to retain memory from previous data windows (Ordóñez and Roggen, 2016), whereas the CNN and FC models interpret data windows as unique inputs. A benefit of employing models with less complex architectures (i.e., CNN and FC) is shorter training and prediction times. However, considering the intended use cases for this analytical framework, model performance is valued over training time, and the DeepConvLSTM prediction time (i.e., ~2 s) is still suitable for field-based processing. Thus, the remainder of this discussion will focus on results from the DeepConvLSTM models. Through this investigation, we used three approaches to model development: Indoor-specific, Section Attack-specific, and General. Although not substantial, the Indoor and Section Attack-specific models were more accurate than the General model (90.9% and 90.2% vs. 87.9%, respectively) for classifying the movements. Since data distribution can have adverse effects on a DNN's accuracy (Johnson and Khoshgoftaar, 2019), the reduced performance in the General model may be caused by the distribution of the Indoor and Section Attack data within the General model's training set (62% Section Attack, 38% Indoor) and that the data collection and preparation methods between Indoor and Section Attack were different (i.e., a structured protocol cropped into individual movements compared to a continuous movement protocol).

To ensure that our prediction adhered to real-world movement constraints, we processed the original predictions through a two-step logical algorithm, which, on average, increased our models' accuracies by 3.45% for the original labels (i.e., 86.4% vs. 89.8%). When expanding the original labels to the expanded label set (i.e., all 19 labels to give meaning to ascend and descend), accuracy dropped slightly to 87.0% on average, which represents a small accuracy improvement

of 0.6% from the original predictions, with the additional contextual benefit of eight labels. With this additional context, combined with the time dependencies, we could produce digital reconstructions of the movement patterns (e.g., Mavor et al., 2022; Chapter 4), which can be imported into battle simulators, animation software, and musculoskeletal models.

Soldiers can be tasked to carry a variety of body-borne loads; therefore, to increase generalizability, we trained our models on three common body-borne load conditions (Slick, FFO, Backpack) and one hypothetical load condition (Pockets). All approaches were sensitive enough to identify an increase in exposure time due to body-borne load, a well-established phenomenon (Sanderson et al., 2021). Across all approaches, there were no meaningful performance differences between load conditions; however, across all approaches, the Pocket (93.1%) and FFO (91.5%) conditions tended to have higher accuracies than the Slick (86.3%) and Backpack (88.8%) conditions. Given that the IMU was placed on the upper back, the differences seen could possibly be due to the movement patterns in the FFO and Pockets condition being in a "sweet spot" between an upright posture in the Slick and a more flexed posture in the Backpack condition.

Previous literature using HAR models for military movements have reported higher overall accuracies than the presented work. These investigations used a single IMU (Papadakis et al., 2020), a single triaxial accelerometer and GPS data (Clements et al., 2012), and a uniaxial accelerometer with a heart rate monitor (Wyss and Mäder, 2010); the authors collectively report overall accuracies ranging from 87.5% to 98.5%. The accuracy differences between previous literature and the present work are primarily attributable to the amount and types of movements studied (i.e.., walking, running, jumping, and loaded marching), representing a small subset of the movements that soldiers typically perform, and fewer than the number of movements included in the present study. Wyss and Mäder (2010) included manual materials handling tasks (lifting and

lowering, carrying, and digging) in their HAR model; however, their model only achieved an average accuracy of 54% for these tasks. Across our three approaches, the DeepConvLSTM architecture trained on data from a single IMU produced movement-specific accuracies of 89.1% for walking and 88.6% for running following our two-step logical algorithm, whih are comparable to previous literature. Aside from Null (66%), the least accurate movement class was Descend at 81.2%, while the most accurate label was Standing at 95.2%. This tight range of accuracies between class labels highlights that by using a DeepConvLSTM architecture, all our movements are identifiable with a consistently high level of accuracy, building on the large range of accuracies previously reported.

Although the presented results are promising, there are several limitations to the current work. The sliding window method was employed to create segments of 128 frames to train the DNNs. This method reduced our resolution, as movements that were performed in less than 65 frames (i.e., the majority of 128-frame window) are not captured. This primarily affected descend movements during the section attack, which negatively affected the model performance metrics. That is, when the models correctly predicted descend, they were evaluated as errors when the majority of the windowed true label was not a descend. To overcome this limitation, model predictions used to calculate the tradespace metrics (computed after the logical algorithm) were compared to the un-windowed true labels to ensure that all movements were captured. The “null” class label was used as a catch-all for all movements that did not fit into other classes thus, there was a large amount of variability for this label, which had a negative impact on performance (i.e., accuracy for this label was 66%). Future work should aim to collect greater samples of these underrepresented movements to avoid the need for a null label. In the present work, we used a DNN approach; however, there are less computationally expensive approaches that have been

deployed to HAR. A DNN approach was used to avoid the need for feature engineering to simplify the utilization of our methods for future end users, who may not have the necessary expertise in signal processing/domain knowledge.

The goal of the current work was to display the efficacy of using a single IMU for recognizing tactical movement patterns. As such, there is much more work to be done to realize the full potential of this field of research. Future work should aim to collect more movements as part of realistic situations (i.e., collecting during drills/simulated combat), diversify the movement patterns (e.g., manual materials handling, stair/ladder climbing, window vaulting, etc.), diversify the type of soldier burden experienced by the soldier (e.g., environmental conditions, equipment properties, etc.), diversify the operational environment (e.g., terrain, weather, closeness to operationally-relevant equipmwnt), and diversify the training population (i.e., sex, occupation, rank, experience, etc.). By diversifying the data collection and integrating real-world tactical situations, it will make any developed HAR algorithm more generalizable to the diverse soldier population who operate in various environments around the world. In order to provide defence scientists with recommendations on the optimal number and location of IMUs to use to perform HAR for military movements, future work should focus on a sensitivity analysis using different combinations of all sensors from the Xsens whole-body IMU suit, uncoupled from a biomechanical model.

Presented is a HAR method for identifying military-based movements during a variety of body-borne loads using a single deployable IMU that is being widely used by the Canadian Armed Forces and allied nations. We used the predictions from DeepConvLSTM models to calculate tradespace metrics to produce meaningful information with a high degree of accuracy. Defence scientists and military leaders can employ our method to directly calculate tradespace metrics, use

it as a preprocessing tool to supplement other technologies (e.g., heart rate monitor, temperature probes, motion capture), perform workplace assessments (e.g., work-to-rest ratios), identify how the same soldier burden is affecting different soldiers, or as a monitoring tool during deployment, among other applications. The ability to collect meaningful information in the field will accelerate our understanding of the survivability tradespace (i.e., soldier burden factors and their influence on soldier performance, vulnerability, and operational effectiveness). Filling knowledge gaps in this tradespace will also inform the development and employment of modular, scalable protection systems, and data-driven decision support tools to aid military leaders with risk-based trade-off decisions during mission planning.

5.6 References

Abadi, M., Barham, P., Chen, J., Chen, Z., Davis, A., Dean, J., Devin, M., Ghemawat, S., Irving, G., Isard, M., Kudlur, M., Levenberg, J., Monga, R., Moore, S., Murray, D.G., Steiner, B., Tucker, P., Vasudevan, V., Warden, P., Wicke, M., Yu, Y., Zheng, X., 2016. Tensorflow: A system for large-scale machine learning, in: 12th {USENIX} Symposium on Operating Systems Design and Implementation. pp. 265–283.

Abobakr, A., Nahavandi, D., Hossny, M., Iskander, J., Attia, M., Nahavandi, S., Smets, M., 2019. RGB-D ergonomic assessment system of adopted working postures. Appl. Ergon. 80, 75–88. https://doi.org/10.1016/j.apergo.2019.05.004

Ankita, Rani, S., Babbar, H., Coleman, S., Singh, A., Aljahdali, H.M., 2021. An efficient and lightweight deep learning model for human activity recognition using smartphones. Sensors 21, 1–17. https://doi.org/10.3390/s21113845

Antwi-Afari, M.F., Li, H., Umer, W., Yu, Y., Xing, X., 2020. Construction Activity Recognition and Ergonomic Risk Assessment Using a Wearable Insole Pressure System. J. Constr. Eng. Manag. 146, 04020077. https://doi.org/10.1061/(asce)co.1943-7862.0001849

Armstrong, N., Bossi, L.L.M., 2021. Chapter 1 – INTRODUCTION, Reducing the Burden on the Dismounted Soldier. NATO AC/323(HFM-238)TP/950 STO TECHNICAL REPORT TR-HFM-238. NATO CSO, Neuilly sur Seine.

Attwells, R.L., Birrell, S.A., Hooper, R.H., Mansfield, N.J., 2006. Influence of carrying heavy loads on soldiers' posture, movements and gait. Ergonomics 49, 1527–1537. https://doi.org/10.1080/00140130600757237

Bangaru, S.S., Wang, C., Busam, S.A., Aghazadeh, F., 2021. ANN-based automated scaffold builder activity recognition through wearable EMG and IMU sensors. Autom. Constr. 126, 103653. https://doi.org/10.1016/j.autcon.2021.103653

Billing, D.C., Silk, A.J., Tofari, P.J., Hunt, A.P., 2015. Effects of military load carriage on susceptibility to enemy fire during tactical combat movements. J. Strength Cond. Res. 29, S134–S138. https://doi.org/10.1519/JSC.0000000000001036

Blount, E.M., Ringleb, S.I., Tolk, A., Bailey, M., Onate, J.A., 2011. Incorporation of physical fitness in a tactical infantry simulation. J. Def. Model. Simul. 10, 235–246. https://doi.org/10.1177/1548512911421343

Bossi, L.L.M., Jones, M.L.H., Kelly, A., Tack, D.W., 2016. A Preliminary Investigation of the Effect of Protective Clothing Weight, Bulk and Stiffness on Combat Mobility Course Performance, in: Proceedings of the Human Factors and Ergonomics Society 2016 Annual Meeting. Washington DC, pp. 701–705.

Bossi, L.L.M., Morton, A., Keefe, A., Karakolis, T., Mitchell, K.B., Sy, A., Keefe, A., Karakolis, T., Jones, M., 2017. Understanding the trade-offs between protection, performance and integrated survivability. J. Sci. Med. Sport 20S, S137–S139. https://doi.org/10.1016/j.jsams.2017.09.509

Brown, T.N., O'Donovan, M., Hasselquist, L., Corner, B.D., Schiffman, J.M., 2014. Body borne loads impact walk-to-run and running biomechanics. Gait Posture 40, 237–242. https://doi.org/10.1016/j.gaitpost.2014.04.001

Clements, C.M., Buller, M.J., Welles, A.P., Tharion, W.J., 2012. Real time gait pattern classification from chest worn accelerometry during a loaded road march, in: Proceedings of the Annual International Conference of the IEEE Engineering in Medicine and Biology Society, EMBS. IEEE, pp. 364–367. https://doi.org/10.1109/EMBC.2012.6345944

Clouthier, A.L., Ross, G.B., Graham, R.B., 2020. Sensor data required for automatic recognition of athletic tasks using deep neural networks. Front. Bioeng. Biotechnol. 7, 1–8. https://doi.org/10.3389/fbioe.2019.00473

Clouthier, A.L., Ross, G.B., Mavor, M.P., Coll, I., Boyle, A., Graham, R.B., 2021. Development and Validation of a Deep Learning Algorithm and Open-Source Platform for the Automatic Labelling of Motion Capture Markers. IEEE Access 9, 36444–36454. https://doi.org/10.1109/ACCESS.2021.3062748

Hunt, A.P., Tofari, P.J., Billing, D.C., Silk, A.J., 2016. Tactical combat movements: inter-individual variation in performance due to the effects of load carriage. Ergonomics 59, 1232–1241. https://doi.org/10.1080/00140139.2015.1132780

Ignatov, A., 2018. Real-time human activity recognition from accelerometer data using Convolutional Neural Networks. Appl. Soft Comput. J. 62, 915–922. https://doi.org/10.1016/j.asoc.2017.09.027

Johnson, J.M., Khoshgoftaar, T.M., 2019. Survey on deep learning with class imbalance. J. Big Data 6. https://doi.org/10.1186/s40537-019-0192-5

Karakolis, T., Sinclair, B.A., Kelly, A., Terhaar, P., Bossi, L.L.M., 2017. Determination of orientation and practice requirements when using an obstacle course for mobility performance assessment. Hum. Factors 59, 535–545. https://doi.org/10.1177/0018720816686611

Kwapisz, J.R., Weiss, G.M., Moore, S.A., 2011. Activity recognition using cell phone accelerometers. ACM SIGKDD Explor. Newsl. 12, 74–82. https://doi.org/10.1145/1964897.1964918

Laidig, D., Schauer, T., Seel, T., 2017. Exploiting kinematic constraints to compensate magnetic disturbances when calculating joint angles of approximate hinge joints from orientation estimates of inertial sensors. IEEE Int. Conf. Rehabil. Robot. 971–976. https://doi.org/10.1109/ICORR.2017.8009375

Laing-Treloar, A.K., Billing, D.C., 2011. Effect of load carriage on performance of an explosive, anaerobic military task. Mil. Med. 176, 1027–1031. https://doi.org/10.7205/MILMED-D-11-00017

Liew, B.X., Morris, S., Netto, K., 2016a. The effects of load carriage on joint work at different running velocities. J. Biomech. 49, 3275–3280. https://doi.org/10.1016/j.jbiomech.2016.08.012

Liew, B.X., Morris, S., Netto, K., 2016b. Joint power and kinematics coordination in load carriage running: Implications for performance and injury. Gait Posture 47, 74–79. https://doi.org/10.1016/j.gaitpost.2016.04.014

Lockhart, T.E., Soangra, R., Zhang, J., Wu, X., 2013. Wavelet based automated postural event detection and activity classification with single IMU. Biomed. Sci. Instrum. 49, 224–233.

Mavor, M.P., Gruevski, K.M., Ross, G.B., Akhavanfar, M., Clouthier, A.L., Bossi, L.L.M., Karakolis, T., Graham, R.B., 2022. A data-driven framework for assessing soldier performance, health, and survivability. Appl. Ergon. 104, 103809. https://doi.org/10.1016/j.apergo.2022.103809

Mavor, M.P., Ross, G.B., Clouthier, A.L., Karakolis, T., Graham, R.B., 2020. Validation of an IMU suit for military-based tasks. Sensors 20, 1–14. https://doi.org/10.3390/s20154280

Mavor, M.P., Gruevski, K.M., Ross, G.B., Akhavanfar, M., Clouthier, A.L., Bossi, L.L.M., Karakolis, T., Graham, R.B., 2022. A data-driven framework for assessing soldier performance, health, and survivability. Appl. Ergon. 104, 103809. https://doi.org/10.1016/j.apergo.2022.103809

O'Malley, T., Elie Bursztein, James Long, François Chollet, Haifeng Jin, Luca Invernizzi, 2019. Keras Tuner.

Ordóñez, F.J., Roggen, D., 2016. Deep convolutional and LSTM recurrent neural networks for multimodal wearable activity recognition. Sensors 16. https://doi.org/10.3390/s16010115

Pandorf, C.E., Harman, E.A., Frykman, P.N., Patton, J.F., Mello, R.P., Nindl, B.C., 2002. Correlates of load carriage and obstacle course performance among women. Work 18, 179–189.

Papadakis, N., Havenetidis, K., Papadopoulos, D., Bissas, A., 2020. Employing body-fixed sensors and machine learning to predict physical activity in military personnel. BMJ Mil. Heal. 0–16. https://doi.org/10.1136/bmjmilitary-2020-001585

Ramsay, J.W., Hancock, C.L., O'Donovan, M.P., Brown, T.N., 2016. Soldier-relevant body borne loads increase knee joint contact force during a run-to-stop maneuver. J. Biomech. 49, 3868–3874. https://doi.org/10.1016/j.jbiomech.2016.10.022

Ronao, C.A., Cho, S.B., 2016. Human activity recognition with smartphone sensors using deep learning neural networks. Expert Syst. Appl. 59, 235–244. https://doi.org/10.1016/j.eswa.2016.04.032

Russell, B., McDaid, A., Toscano, W., Hume, P., 2021. Moving the lab into the mountains: A pilot study of human activity recognition in unstructured environments. Sensors 21, 1–14. https://doi.org/10.3390/s21020654

Sanderson, P.W., Faulkner, S., Fordy, G., Garcia-Vicencio, Sebastian Malgoyre, A., Reilly, T., 2021. Chapter 4 – Work Package 2: Literature Review on Soldier Load., Reducing the Burden on the Dismounted Soldier. NATO AC/323(HFM-238)TP/950 STO TECHNICAL REPORT TR-HFM-238. NATO CSO, Neuilly sur Seine.

Schepers, M., Giuberti, M., Bellusci, G., 2018. Xsens MVN: Consistent tracking of human motion using inertial sensing. Xsens Technol. B.V. 1–8. https://doi.org/10.13140/RG.2.2.22099.07205

Snoek, J., Larochelle, H., Adams, R.P., 2012. Practical bayesian optimization of machine learning algorithms. Adv. Neural Inf. Process. Syst. 25, 1–9.

Van Rossum, G., Drake, F.L., 2009. Python 3 Reference Manual.

Vitali, R. V, Cain, S.M., Ojeda, L. V, Potter, M. V, Zaferiou, A.M., Davidson, S.P., Coyne, M.E., Hancock, C.L., Mendoza, A., Stirling, L.A., Perkins, N.C., 2019. Body-worn IMU array reveals effects of load on performance in an outdoor obstacle course. PLoS One 14, 1–30. https://doi.org/10.1371/journal.pone.0214008

Wyss, T., Mäder, U., 2010. Recognition of military-specific physical activities with body-fixed sensors. Mil. Med. 175, 858–864. https://doi.org/10.7205/MILMED-D-10-00023

Chapter 6: General Discussion

Soldier burden can come from various sources: the environment, metabolic demands, equipment properties (i.e., mass, mass distribution, coverage, bulk, stiffness, breathability, and thermal resistance), and psychological stressors (Bossi et al., 2020). However, most of these sources are not considered in doctrine guidelines nor seem to affect decisions when tasking soldiers with body-borne loads (Oudenhuijzen et al., 2021). In general, doctrine guidelines for NATO nations are set at 30% and 45% of body mass for fighting and marching loads, respectively, with no further discussion on combat conditions, equipment properties or personal characteristics (Drain et al., 2012; Oudenhuijzen et al., 2021). While it is likely that these recommendations are set too high since epidemiological evidence suggests that carrying body-borne loads greater than 25% of one's body mass increases the risk of musculoskeletal injury (Roy et al., 2012), the reality on the battlefield is that soldiers are carrying much heavier loads than what doctrine recommends. For three widely different hypothetical combat scenarios (i.e., differences in duration, temperature, threat, etc.), military leaders from five NATO nations consistently tasked their soldiers with heavy equipment that, on average, equated to 54 kg (±3.9 kg) or 68% of an average soldier's body-mass (Oudenhuijzen et al., 2021). One of the main contributors to these consistently high loads is the importance placed on weapons and protective equipment, which make up a staggering 63% of the body-borne load (Oudenhuijzen et al., 2021).

Most of our knowledge on soldier burden is in the context of the mass of the body-borne load. There is an overall consensus from this body of literature that heavy body-borne loads negatively impact all aspects of the survivability tradspace. Heavy body-borne loads decrease soldier performance (Billing et al., 2015; Bossi et al., 2017; Hunt et al., 2016; Laing-Treloar and Billing, 2011; Vitali et al., 2019), negatively alter kinematics (Attwells et al., 2006; Birrell and

Haslam, 2009; Brown et al., 2016, 2014b, 2014a; Wang et al., 2013) and kinetics (Birrell et al., 2007; Lidstone et al., 2017; Ramsay et al., 2016; Seymore et al., 2019; Sturdy et al., 2021), increase the demand on the cardio-respiratory system (Beekley et al., 2007; Dominelli et al., 2012; Lidstone et al., 2017), and increase susceptibility to enemy action (Billing et al., 2015; Hunt et al., 2016). Further, it has been documented that stiffness and bulk can independently and interact with each other (and mass) to degrade performance during an obstacle course (Gijsbertse et al., 2021). Beyond the body-borne load carried, it has been shown that personal characteristics such as sex (Laing-Treloar and Billing, 2011) and fitness (Billing et al., 2015; Hunt et al., 2016; Stein et al., 2022) can further impact performance in response to body-borne loads. This large body of literature has made it clear that body-borne loads negatively affect the human body and there are complex interactions between equipment properties and personal characteristics. Therefore, to further our understanding of soldier burden, we must assess all aspects of soldier burden while accounting for all possible personal characteristics. To feasibly achieve this goal, novel approaches are needed.

The objective of this dissertation was to establish novel approaches to assessing the soldier survivability tradespace. This was done through three studies that aimed to 1) validate an inertial measurement unit (IMU) suit for military-based movements, 2) develop a data-driven framework to morph movements to calculate tradespace metrics of intermediate load conditions and personal characteristics, and 3) to train a machine learning algorithm to identify tactical movements and calculate tradespace metrics from a single IMU.

6.1 Summary of Findings

Study one (Chapter 3), entitled “Validation of an IMU Suit for Military-based Tasks,” investigated the validity of an IMU suit compared to optical motion capture (OPT) system for

capturing tactical movement patterns. While wearing a whole-body IMU (MVN Link, Xsens, Netherlands) and optical motion capture (Vantage V5, Vicon, UK) suit, 18 civilian participants (nine male, nine female) completed a series of eight military movements: run, walk, run-to-prone (RTP), run-to-kneel (RTK), prone-to-run (PTR), kneel-to-run (KTR), kneel-to-prone (KTP), and prone-to-kneel (PTK). Joint angles were compared between systems using root mean squared error (RMSE), while time series marker trajectory data were compared using correlation coefficients of principal component (PC) scores.

It was found that, across all movements, RMSE values for lower limb joint angles were less than 8º while upper limb joint angles had an average RMSE value of 21.6º; however, through a procedure to align the biomechanical models, the upper limb joint angles can be reduced as much as 8.7º on average while maintaining the lower limb RMSE values. PC scores had an average correlation coefficient of +0.81. Of the 48 retained PCs, 38 (79%) had scores with a high or very high positive correlation (≥ +0.70) between the OPT and IMU systems, 15 (31%) of which had scores with a very high correlation (≥ +0.90).

Given the low RMSE values and the highly correlated PC scores, the IMU suit was deemed valid for collecting the eight military-based movements. This validation was of great importance as it allowed for the continuation of this work through study two (Chapter 4): "A Data-driven Framework for Assessing Soldiers' Performance, Health and Survivability." In this study, 16 civilians (four female) and 12 male dismounted reservist soldiers were recruited to perform the same eight movements as study one while wearing the validated IMU suit under three different body-borne load conditions: Slick (~5.5 kg), full fighting order (FFO; ~22 kg) and Backpack (~38 kg). This work aimed to create morphable movement patterns representing intermediary load conditions and personal characteristics to assess their effects on the survivability tradespace. By

applying principal component analysis (PCA) and linear discriminant analysis (LDA) to time series marker trajectories, linear discriminant functions (LDFs) were calculated. By applying a scaling factor (i.e., in standard deviations) to the LDFs, movement patterns were iteratively morphed to represent marker trajectories that behave more like one class label over another. For each movement type, two morphable model types were created for the body-borne load (Slick vs. FFO and FFO vs. Backpack), and nine were created for personal characteristics (Male vs. Female, Civilian vs. Soldier, Top 50% body mass vs. Bottom 50% body mass; one for each load condition). The iteratively morphed movement patterns were then used to calculate tradespace metrics: performance (i.e., exposure time, velocity), musculoskeletal health (i.e., hip and L_4-L_5 forces; body-borne load only), and survivability (i.e., number of enemy shots fired and susceptibility to enemy action).

In line with previous research, the morphable models calculated that performance decreases (exposure time +0.30 %/kg, velocity -0.30 %/kg), loading on the musculoskeletal system increases (hip 1.13 %/kg FFO load, 1.30 %/kg backpack load; L_4-L_5 2.81 %/kg FFO load, 1.35 %/kg backpack load), and susceptibility increases by 0.15 %/kg. Negative trends were also found for performance and survivability per representative unit of sex towards female, per representative unit of military experience towards civilian, and per kg of body mass towards lighter individuals. This project presents an analytical method that defence scientists can use to incrementally morph movement patterns to simulate conditions that were not collected or cannot be collected. This will greatly reduce the number of conditions needed to be tested and participants needing to be recruited to understand the broad spectrums of soldier burden. Displayed here is a proof of principle; if the appropriate data are collected, this method can be applied to practically any pair of signals with distinct class labels.

Study two outlines a sophisticated method for reproducing time series marker trajectories to calculate tradespace metrics. While marker trajectories are needed if musculoskeletal health is of interest to the researcher, a less intrusive data collection method can be used to calculate performance and standard survivability metrics. In Study 3 (Chapter 5), entitled "Assessing the Soldier Survivability Tradespace Using a Single IMU," data from study two and a simulated two-person 60-metre section attack were used to train deep convolutional long short-term neural networks (DeepConvLSTMs) to identify 11 class labels: stand, jump, descend, ascend, kneel, prone, stand-to-run, run, walk, crawl, and null. Combined with a two-step logical algorithm to ensure real-world constraints and to expand the context of ascend and descend, the Indoor-based, Section Attack-based, and General-based model achieved an accuracy of 91.7% (F1-score: 91.8%), 90.6% (F1-score: 91.1%), and 87.7% (F1-score: 87.9%), respectively. Being able to accurately identify what the soldier was doing and for how long allowed for the calculation of exposure time, defined as any movement that was not kneeling, prone, KTP, or PTK. All models identified that an increase in body-borne load resulted in an increase in exposure time and thus susceptibility to enemy fire. The absolute difference in exposure time and susceptibility across all models was 0.15 seconds and 1.18%, respectively, compared to the true labels.

Using the single IMU approach, movements were identified, and exposure time was calculated at a high level of accuracy, showing that the deployable and cost-effective technology can be used to calculate meaningful data in the field. The whole-body IMU approach in study two allows for the reconstruction of movement patterns in the form of time series marker trajectories, which can be used for musculoskeletal modelling, animation, exposure time, and susceptibility. Both approaches are catered to different research questions but have the potential to be used together. While not studied here, it is possible to understand which movement patterns are being

performed during a drill, for example, and reconstruct them *in silico* to perform musculoskeletal modelling or digitize them for visualization/advanced survivability modelling in a battle simulator. Therefore, there is potential for the methods developed throughout this dissertation to drive a tremendous amount of research questions in the defence science domain, which will help increase the quality of life of our soldiers and make our country more secure.

Chapter 7: Limitations

Considering that this dissertation focuses on proof of principal approaches, this work has several limitations. Aside from study one, this work has a relatively small sample size, and all studies lack the diversity present in the Canadian Armed Forces (CAF); therefore, the presented results are largely biased towards male dismounted combat arms reserve force soldiers. The movements assessed throughout were identified by members of the Department of National Defence as important to investigate; however, there are many more movement patterns that soldiers perform throughout their day-to-day work and during combat that are not presented here/validated for. Soldier burden comprises many factors (Bossi et al., 2020), but the body-borne load's mass was a large focus of this dissertation. The presented methods are not limited to assessing body-borne load mass, but rather it was chosen as the primary testing variable because of the wealth of knowledge surrounding military movement patterns and body-borne load mass.

Study one used optical motion capture (OPT) as a "gold standard"; thus, several constraints had to be adhered to in order to use this technology. As such, movements could not be performed entirely within the calibrated volume; therefore, participants had to exit and enter the collection space during the protocol. This may under-represent the true differences between the IMU suit and the OPT system. Study one did not introduce body-borne loads when evaluating the systems, although studies two and three used the IMU suit under load. This limitation was accepted because

reflective markers cannot be placed on the skin when wearing body-borne loads unless the marker set is reduced (i.e., the OPT system becomes less precise) or the equipment is modified (i.e., decreased generalizability). If markers were placed on the equipment, it would have resulted in the OPT system tracking the movement of the equipment while the IMU suit tracked the body.

Study two required a structured data collection protocol to develop the framework; thus, the reconstructed movements are biased toward a laboratory environment and the 10-metre distance that the movements were performed. To be comparable to previous research, the movements were extended to represent movements between 5 and 30 metres. However, the series of phases used to alter the distances were selected based on a single person running/walking each distance. An ideal approach would be to collect movements during drills/simulated combat scenarios such that the appropriate distances can be teased out and collected in an operational environment. Joint forces were reported, but no ground reaction force (GRF) data were collected. To circumvent this, methods from Ren et al. (2008) were used to estimate GRF. A future user of the framework could import movement and GRF data together to simultaneously morph them to obtain more representative GRF vectors and thus joint loads.

In study three, a window size of 128 frames (1.28 seconds) was chosen. Although this window size provided the best accuracy, F1-scores, and loss values, movements that took less than 0.65 seconds were not represented in the training label set, which primarily affected the descend movement in the section attack data. This likely resulted in the HAR models' performance metrics being under-represented compared to the actual labels. This may become a recurring issue in the future and should be considered when continuing this research. It is impossible to have participants not fidget, gesture, or exactly match instructions on what to do at the start or end of a trial; therefore, a null label had to be created to capture a myriad of unstructured movements that

participants performed “outside” of the deliberate protocol. The null label was by far the most underperforming class label with an accuracy of 66% compared to the next worst accuracy of 81% (descend label), which likely decreased the overall performance metrics reported. Better controlling for these spontaneous movements at the data collection level or better integrating them into other labels may prove better for future iterations.

Chapter 8: Future Directions

I hope that the methods outlined within this dissertation inspire many future research endeavours. Researchers can expand on this work by increasing generalizability, including multiple data streams, and digitally representing movements. The methods outlined in this dissertation have the potential to be the foundation of a data-driven load planning decision-support tool as recommended by Oudenhuijzen et al. (2021). Such a tool will accelerate our collective understanding of tradespace metrics and improve our ability to disseminate information to military leaders, all of which will improve the well-being of our soldiers, make them more fit and able to fight, and increase overall mission success. Our laboratory has already made initial steps towards this by developing a database to integrate the collected data with future data and developing a software package to visualize, predict, and optimize soldier performance (Canadian Soldier Predictive Performance and Optimization Tool; CAN-SPPOT).

To increase generalizability, future researchers should add to the movements collected here. More sub-movements could be identified by observing soldiers performing their day-to-day activities, drills, and targeted obstacle courses. Once identified, attempts should be made to have soldiers perform these movements in a semi-structured way (e.g., as part of a drill) and after a long slow approach (i.e., simulate the approach before performing tactical movements). In these ways, movement patterns will be more representative of how they are performed in the field.

Diversifying every aspect of soldier burden will enhance any model developed through study two or three. I will highlight three: the environment, equipment properties, and population. By representing multiple environments, one HAR model may work across environments rather than developing site-specific models, while morphable movements could be developed to represent movements performed in an open field versus a sandy beach, for example. Mission-specific equipment can change dramatically depending on mission details (e.g., amount of time, enemy capabilities, goals, time of day, etc.); therefore, to increase generalizability, an array of operationally-relevant equipment should be used for morphable models that represent a body-borne load's mass, mass distribution, coverage, bulk, stiffness, breathability, and thermal resistance. Diversifying the testing population (e.g., fitness, mass, rank, experience, occupation, branch, etc.) will be key to ensuring that the models developed are not biased to one set of demographics and that all members of the CAF are representable through these methods.

Work from this dissertation can be expanded on by combining multiple data streams. The framework developed in study two is not limited to time-series marker trajectory data. Thus, researchers can use data from any technology (e.g., force plates, 3D scans) to morph those data by themselves or with movement patterns. These can be used to more accurately perform musculoskeletal modelling and represent body morphology, for example. The HAR algorithms developed in study three could be used as a preprocessing tool to segment out data collections that have whole-body movement data or physiological sensors. Alternatively, it can be a fundamental method for monitoring/understanding exertion in the field by combining other technology (e.g., temperature probes, heart rate monitors, etc.) to identify movements that are being performed at or lead to higher/lower levels of physiological excursion.

Digitizing movement patterns for animation can be an interesting avenue for future research. The models developed in study two can be exported as .c3d files, making them compatible with animation software. One could drive avatars in virtual environments to develop more sophisticated survivability metrics. One approach could be to digitize drills by combining methods from studies two and three. Such an approach would see a soldier performing the desired drill while wearing a single IMU. These data would be used to identify the series of movements performed, which would dictate what premade morphable movements need to be stitched together to represent the drill. In this way, depending on the morphable models available, a single participant can help answer how tradespace metrics during the drill change due to different personal, equipment, or environmental characteristics. Alternatively, the movements could be used to develop animations to disseminate knowledge to recruits about how to perform typical movements, to military leaders so they can visualize a 1% increase in exposure time or what a bulkier vest does to a movement pattern, for example, and to the academic community who are unfamiliar with what some tactical movements/drills are.

Future researchers should also know that models developed using study two can be combined to represent a more complex representation of an individual's characteristics or aspect of soldier burden. For example, if the data are appropriately collected, a user could combine several LDFs to reconstruct the movement pattern of a representative dismounted male soldier with five years of military experience who is walking in the sand while wearing a 15.27 kg of body-borne load that has a given stiffness and bulkiness value. This possibility allows for complex and niche research questions that could inform decisions on armour procurement and tasking when presented with different combat scenarios.

Chapter 9: References

Abobakr, A., Nahavandi, D., Hossny, M., Iskander, J., Attia, M., Nahavandi, S., Smets, M., 2019. RGB-D ergonomic assessment system of adopted working postures. Appl. Ergon. 80, 75–88. https://doi.org/10.1016/j.apergo.2019.05.004

Ankita, Rani, S., Babbar, H., Coleman, S., Singh, A., Aljahdali, H.M., 2021. An efficient and lightweight deep learning model for human activity recognition using smartphones. Sensors 21, 1–17. https://doi.org/10.3390/s21113845

Antwi-Afari, M.F., Li, H., Umer, W., Yu, Y., Xing, X., 2020. Construction Activity Recognition and Ergonomic Risk Assessment Using a Wearable Insole Pressure System. J. Constr. Eng. Manag. 146, 04020077. https://doi.org/10.1061/(asce)co.1943-7862.0001849

Armstrong, N., Bossi, L.L.M., 2021. Chapter 1 – INTRODUCTION, Reducing the Burden on the Dismounted Soldier. NATO AC/323(HFM-238)TP/950 STO TECHNICAL REPORT TR-HFM-238. NATO CSO, Neuilly sur Seine.

Armstrong, N.C., Gay, L.A., 2016. The effect of flexible body armour on pulmonary function. Ergonomics 59, 692–696. https://doi.org/10.1080/00140139.2015.1084052

Attwells, R.L., Birrell, S.A., Hooper, R.H., Mansfield, N.J., 2006. Influence of carrying heavy loads on soldiers' posture, movements and gait. Ergonomics 49, 1527–1537. https://doi.org/10.1080/00140130600757237

Bangaru, S.S., Wang, C., Busam, S.A., Aghazadeh, F., 2021. ANN-based automated scaffold builder activity recognition through wearable EMG and IMU sensors. Autom. Constr. 126, 103653. https://doi.org/10.1016/j.autcon.2021.103653

Beekley, M.D., Alt, J., Buckley, C.M., Duffey, M., Crowder, T.A., 2007. Effects of heavy load carriage during constant-speed, simulated, road marching. Mil. Med. 172, 592–595. https://doi.org/10.7205/MILMED.172.6.592

Bengio, Y., Delalleau, O., Roux, N.L., 2005. The curse of dimensionality for local kernel machines. Montreal, Quebec.

Benoit, D.L., Damsgaard, M., Andersen, M.S., 2015. Surface marker cluster translation, rotation, scaling and deformation: Their contribution to soft tissue artefact and impact on knee joint kinematics. J. Biomech. 48, 2124–2129. https://doi.org/10.1016/j.jbiomech.2015.02.050

Billing, D.C., Silk, A.J., Tofari, P.J., Hunt, A.P., 2015. Effects of military load carriage on susceptibility to enemy fire during tactical combat movements. J. Strength Cond. Res. 29, S134–S138. https://doi.org/10.1519/JSC.0000000000001036

Birrell, S.A., Haslam, R.A., 2009. The effect of military load carriage on 3-D lower limb kinematics and spatiotemporal parameters. Ergonomics 52, 1298–1304. https://doi.org/10.1080/00140130903003115

Birrell, S.A., Hooper, R.H., Haslam, R.A., 2007. The effect of military load carriage on ground reaction forces. Gait Posture 26, 611–614. https://doi.org/10.1016/j.gaitpost.2006.12.008

Bossi, L., Karakolis, T., Jones, M., 2020. Rationalizing the approach to mitigate soldier physical burden are Iron Man or Captain America the magic bullet?, in: Transhumanizing War: Performance Enhancement and the Implications for Policy, Society, and the Soldier. McGill-Queen's University Press, Montreal, Quebec, pp. 119–151.

Bossi, L.L.M., Jones, M.L.H., Kelly, A., Tack, D.W., 2016. A Preliminary Investigation of the Effect of Protective Clothing Weight, Bulk and Stiffness on Combat Mobility Course Performance, in: Proceedings of the Human Factors and Ergonomics Society 2016 Annual Meeting. Washington DC, pp. 701–705.

Bossi, L.L.M., Morton, A., Keefe, A., Karakolis, T., Mitchell, K.B., Sy, A., Keefe, A., Karakolis, T., Jones, M., 2017. Understanding the trade-offs between protection, performance and integrated survivability. J. Sci. Med. Sport 20S, S137–S139. https://doi.org/10.1016/j.jsams.2017.09.509

Bossi, L.L.M., Richter, M., Tack, D., Kelly, A., Patterson, M., Lafiandra, M., 2014. Load Effects Assessment Program (LEAP): a Systematic Multinational Approach to Understand and Address Soldier Physical Burden.

Brown, T.N., Loverro, K.L., Schiffman, J.M., 2016. Soldier-relevant body borne load impacts minimum foot clearance during obstacle negotiation. Appl. Ergon. 55, 56–62. https://doi.org/10.1016/j.apergo.2015.12.009

Brown, T.N., O'Donovan, M., Hasselquist, L., Corner, B., Schiffman, J.M., 2014a. Soldier-relevant loads impact lower limb biomechanics during anticipated and unanticipated single-leg cutting movements. J. Biomech. 47, 3494–3501. https://doi.org/10.1016/j.jbiomech.2014.09.002

Brown, T.N., O'Donovan, M., Hasselquist, L., Corner, B.D., Schiffman, J.M., 2014b. Body borne loads impact walk-to-run and running biomechanics. Gait Posture 40, 237–242. https://doi.org/10.1016/j.gaitpost.2014.04.001

Clements, C.M., Buller, M.J., Welles, A.P., Tharion, W.J., 2012. Real time gait pattern classification from chest worn accelerometry during a loaded road march, in: Proceedings of the Annual International Conference of the IEEE Engineering in Medicine and Biology Society, EMBS. IEEE, pp. 364–367. https://doi.org/10.1109/EMBC.2012.6345944

Clements, C.M., Moody, D., Potter, A.W., Seay, J.F., Fellin, R.E., Buller, M.J., 2013. Loaded and unloaded foot movement differentiation using chest mounted accelerometer signatures. 2013 IEEE Int. Conf. Body Sens. Networks, BSN 2013 1–5. https://doi.org/10.1109/BSN.2013.6575524

Clouthier, A.L., Ross, G.B., Graham, R.B., 2020. Sensor data required for automatic recognition of athletic tasks using deep neural networks. Front. Bioeng. Biotechnol. 7, 1–8. https://doi.org/10.3389/fbioe.2019.00473

Dominelli, P.B., Sheel, A.W., Foster, G.E., 2012. Effect of carrying a weighted backpack on lung mechanics during treadmill walking in healthy men. Eur. J. Appl. Physiol. 112, 2001–2012. https://doi.org/10.1007/s00421-011-2177-8

Drain, J., Orr, R., Attwells, R., Billing, D., 2012. Load Carriage Capacity of the Dismounted Combatant - A Commander's Guide. Australian Defence Science and Technology Organization (DSTO) Report No. DSTO-TR-2765. Fishermans Bend.

Du, J., Vong, C.M., Philip Chen, C.L., 2021. Novel efficient RNN and LSTM-like architectures: recurrent and gated broad learning systems and their applications for text classification. IEEE Trans. Cybern. 51, 1586–1597. https://doi.org/10.1109/TCYB.2020.2969705

Duda, R.O., Hart, P.E., Stork, D.G., Hard, P.E., Stork, D.G., Hart, P.E., Stork, D.G., 2001. Pattern classification, 2nd ed. John Wiley & Sons, Inc., New York.

Gijsbertse, K., Linssen, L., Woering, A., Catoire, M., 2021. The effects of mass, bulk and stiffness of personal protective equipment and clothing on physical performance when performing a military mobility obstacle course. Appl. Ergon. 95, 103448. https://doi.org/10.1016/j.apergo.2021.103448

Government of Canada, 2022. Statistics of women in the Canadian Armed Forces [WWW Document]. URL https://www.canada.ca/en/department-national-defence/services/women-in-the-forces/statistics.html (accessed 7.12.21).

Gruevski, K.M., Cameron, I.J., McGuinness, C., Sy, A., Best, K.L., Bouyer, L., Diamond-Ouellette, G., Graham, R.B., Karakolis, T., 2020. A Pilot Investigation of the Influence of a Passive Military Exoskeleton on the Performance of Lab-Simulated Operational Tasks. IISE Trans. Occup. Ergon. Hum. Factors 8, 195–203. https://doi.org/10.1080/24725838.2021.1912852

Guzie, G.L., 2004. Integrated survivability assessment. White Sands Missile Range, New Mexico.

Harper, W.H., Knapik, J.J., de Pontbriand, R., 1997. Equipment compatibility and performance of men and women during heavy load carriage, in: Proceedings of the Human Factors and Ergonomics Society. pp. 604–608. https://doi.org/10.1177/107118139704100133

Hunt, A.P., Tofari, P.J., Billing, D.C., Silk, A.J., 2016. Tactical combat movements: inter-individual variation in performance due to the effects of load carriage. Ergonomics 59, 1232–1241. https://doi.org/10.1080/00140139.2015.1132780

Karakolis, T., Sinclair, B.A., Kelly, A., Terhaar, P., Bossi, L.L.M., 2017. Determination of orientation and practice requirements when using an obstacle course for mobility performance assessment. Hum. Factors 59, 535–545. https://doi.org/10.1177/0018720816686611

Kessels, I., Koopman, B., Verdonschot, N., Marra, M., Gijsbertse, K., 2021. The Added Value of Musculoskeletal Simulation for the Study of Physical Performance in Military Tasks. Sensors 21, 5588. https://doi.org/10.3390/s21165588

Knapik, J.J., Reynolds, K.L., Harman, E., 2004. Soldier Load Carriage: Historical, Physiological, Biomechanical, and Medical Aspects. Mil. Med. 169, 45–56. https://doi.org/10.7205/milmed.169.1.45

Laing-Treloar, A.K., Billing, D.C., 2011. Effect of load carriage on performance of an explosive, anaerobic military task. Mil. Med. 176, 1027–1031. https://doi.org/10.7205/MILMED-D-11-00017

Lawal, I.A., Bano, S., 2020. Deep Human Activity Recognition with Localisation of Wearable Sensors. IEEE Access 8, 155060–155070. https://doi.org/10.1109/ACCESS.2020.3017681

Lidstone, D.E., Stewart, J.A., Gurchiek, R., Needle, A.R., Van Werkhoven, H., McBride, J.M., 2017. Physiological and biomechanical responses to prolonged heavy load carriage during level treadmill walking in females. J. Appl. Biomech. 33, 248–255. https://doi.org/10.1123/jab.2016-0185

Liew, B.X., Morris, S., Netto, K., 2016. The effects of load carriage on joint work at different running velocities. J. Biomech. 49, 3275–3280. https://doi.org/10.1016/j.jbiomech.2016.08.012

Lockhart, T.E., Soangra, R., Zhang, J., Wu, X., 2013. Wavelet based automated postural event detection and activity classification with single IMU. Biomed. Sci. Instrum. 49, 224–233.

Lyons, J., Allsopp, A., Bilzon, J., 2005. Influences of body composition upon the relative metabolic and cardiovascular demands of load-carriage. Occup. Med. (Chic. Ill). 55, 380–384. https://doi.org/10.1093/occmed/kqi087

Majumdar, D., Srivastava, K.K., Purkayastha, S.S., Pichan, G., Selvamurthy, W., 1997. Physiological effects of wearing heavy body armour on male soldiers. Int. J. Ind. Ergon. 20, 155–161. https://doi.org/10.1016/S0169-8141(96)00057-1

Martin, P.E., Nelson, R.C., 1986. The effect of carried loads on the walking patterns of men and women. Ergonomics 29, 1191–1202. https://doi.org/10.1080/00140138608967234

Mavor, M.P., Ross, G.B., Clouthier, A.L., Karakolis, T., Graham, R.B., 2020. Validation of an IMU suit for military-based tasks. Sensors 20, 1–14. https://doi.org/10.3390/s20154280

Michalak, J., Troje, N.F., Fischer, J., Vollmar, P., Heidenreich, T., Schulte, D., 2009. Embodiment of sadness and depression-gait patterns associated with dysphoric mood. Psychosom. Med. 71, 580–587. https://doi.org/10.1097/PSY.0b013e3181a2515c

Ordóñez, F.J., Roggen, D., 2016. Deep convolutional and LSTM recurrent neural networks for multimodal wearable activity recognition. Sensors 16. https://doi.org/10.3390/s16010115

Oudenhuijzen, A.J.K., Bossi, L.L.M., Koerhuis, C.L., 2021. Chapter 3 - Work package 1: characterizing dismounted soldier burden, Reducing the Burden on the Dismounted Soldier. NATO AC/323(HFM-238)TP/950 STO TECHNICAL REPORT TR-HFM-238. NATO CSO, Neuilly sur Seine.

Pandorf, C.E., Harman, E.A., Frykman, P.N., Patton, J.F., Mello, R.P., Nindl, B.C., 2002. Correlates of load carriage and obstacle course performance among women. Work 18, 179–189.

Papadakis, N., Havenetidis, K., Papadopoulos, D., Bissas, A., 2020. Employing body-fixed sensors and machine learning to predict physical activity in military personnel. BMJ Mil. Heal. 0–16. https://doi.org/10.1136/bmjmilitary-2020-001585

Phillips, D.B., Stickland, K.M., Lesser, I.A., Petersen, S.R., 2016. The effects of heavy load carriage on physiological responses to graded exercise. Eur. J. Appl. Physiol. 116, 275–280. https://doi.org/10.1007/s00421-015-3280-z

Pyke, A.J., Costello, J.T., Stewart, I.B., 2015. Heat strain evaluation of overt and covert body armour in a hot and humid environment. Appl. Ergon. 47, 11–15. https://doi.org/10.1016/j.apergo.2014.08.016

Ramsay, J.W., Hancock, C.L., O'Donovan, M.P., Brown, T.N., 2016. Soldier-relevant body borne loads increase knee joint contact force during a run-to-stop maneuver. J. Biomech. 49, 3868–3874. https://doi.org/10.1016/j.jbiomech.2016.10.022

Robert-Lachaine, X., Mecheri, H., Larue, C., Plamondon, A., 2017. Validation of inertial measurement units with an optoelectronic system for whole-body motion analysis. Med. Biol. Eng. Comput. 55, 609–619. https://doi.org/10.1007/s11517-016-1537-2

Robertson, D.G.E., Caldwell, G.E., Hamill, J., Kamen, G., Whittlesey, S.N., 2014. Research methods in biomechanics, 2nd ed. Human Kinetics, Champaign, Illinois.

Roetenberg, D., Luinge, H., Slycke, P., 2013. Xsens MVN: full 6DOF human motion tracking using miniature inertial sensors. Xsens Motion Technol. BV 1–7.

Ronneberger, O., Fischer, P., Brox, T., 2015. U-net: Convolutional networks for biomedical image segmentation, in: Lecture Notes in Computer Science (Including Subseries Lecture Notes in Artificial Intelligence and Lecture Notes in Bioinformatics). pp. 234–241. https://doi.org/10.1007/978-3-319-24574-4_28

Ross, G.B., Dowling, B., Troje, N.F., Fischer, S.L., Graham, R.B., 2018. Objectively differentiating movement patterns between elite and novice athletes. Med. Sci. Sports Exerc. 50, 1457–1464. https://doi.org/10.1249/MSS.0000000000001571

Roy, T.C., 2011. Diagnoses and Mechanisms of Musculoskeletal Injuries in an Infantry Brigade Combat Team Deployed to Afghanistan Evaluated by the Brigade Physical Therapist. Mil. Med. 176, 903–908. https://doi.org/10.7205/MILMED-D-11-00006

Roy, T.C., Knapik, J.J., Ritland, B.M., Murphy, N., Sharp, M.A., 2012. Risk factors for musculoskeletal injuries for soldiers Deployed to Afghanistan. Aviat. Sp. Environ. Med. 83, 1060–1066. https://doi.org/10.3357/ASEM.3341.2012

Roy, T.C., Lopez, H.P., Piva, S.R., 2013. Loads worn by soldiers predict episodes of low back pain during deployment to afghanistan. Spine (Phila. Pa. 1976). 38, 1310–1317. https://doi.org/10.1097/BRS.0b013e31829265c4

Russell, B., McDaid, A., Toscano, W., Hume, P., 2021. Moving the lab into the mountains: A pilot study of human activity recognition in unstructured environments. Sensors 21, 1–14. https://doi.org/10.3390/s21020654

Sammito, S., Hadzic, V., Karakolis, T., Kelly, K.R., Proctor, S.P., Stepens, A., 2021. Risk factors for musculoskeletal injuries in the military : a qualitative systematic review of the literature from the past two decades and a new prioritizing injury model. Mil. Med. Res. 1–40. https://doi.org/10.1186/s40779-021-00357-w

Sanderson, P.W., Faulkner, S., Fordy, G., Garcia-Vicencio, Sebastian Malgoyre, A., Reilly, T., 2021. Chapter 4 – Work Package 2: Literature Review on Soldier Load., Reducing the Burden on the Dismounted Soldier. NATO AC/323(HFM-238)TP/950 STO TECHNICAL REPORT TR-HFM-238. NATO CSO, Neuilly sur Seine.

Schepers, M., Giuberti, M., Bellusci, G., 2018. Xsens MVN: Consistent tracking of human motion using inertial sensing. Xsens Technol. B.V. 1–8. https://doi.org/10.13140/RG.2.2.22099.07205

Seel, T., Schauer, T., Raisch, J., 2012. Joint axis and position estimation from inertial measurement data by exploiting kinematic constraints. Proc. IEEE Int. Conf. Control Appl. 45–49. https://doi.org/10.1109/CCA.2012.6402423

Semeniuta, S., Severyn, A., Barth, E., 2016. Recurrent dropout without memory loss, in: 26th International Conference on Computational Linguistics. pp. 1757–1766. https://doi.org/10.5281/zenodo.546212

Seymore, K.D., Fain, A.L.C., Lobb, N.J., Brown, T.N., 2019. Sex and limb impact biomechanics associated with risk of injury during drop landing with body borne load. PLoS One 14, 1–16. https://doi.org/10.1371/journal.pone.0211129

Stein, J.A., Hepler, T.C., DeBlauw, J.A., Beattie, C.M., Beshirs, C.D., Holte, K.M., Kurtz, B.K., Heinrich, K.M., 2022. Lower-body muscular power and exercise tolerance predict susceptibility to enemy fire during a tactical combat movement simulation. Ergonomics 0, 1–11. https://doi.org/10.1080/00140139.2022.2025913

Sturdy, J.T., Sessoms, P.H., Silverman, A.K., 2021. A backpack load sharing model to evaluate lumbar and hip joint contact forces during shoulder borne and hip belt assisted load carriage. Appl. Ergon. 90, 103277. https://doi.org/https://doi.org/10.1016/j.apergo.2020.103277

Troje, N.F., 2008. BLM Walker [WWW Document]. URL https://www.biomotionlab.ca/html5-bml-walker/ (accessed 5.5.22).

Troje, N.F., 2002. Decomposing biological motion: A framework for analysis and synthesis of human gait patterns. J. Vis. 2, 371–387. https://doi.org/10.1167/2.5.2

Vitali, R. V, Cain, S.M., Ojeda, L. V, Potter, M. V, Zaferiou, A.M., Davidson, S.P., Coyne, M.E., Hancock, C.L., Mendoza, A., Stirling, L.A., Perkins, N.C., 2019. Body-worn IMU array reveals effects of load on performance in an outdoor obstacle course. PLoS One 14, 1–30. https://doi.org/10.1371/journal.pone.0214008

Wang, H., Frame, J., Ozimek, E., Leib, D., Dugan, E.L., 2013. The effects of load carriage and muscle fatigue on lower-extremity joint mechanics. Res. Q. Exerc. Sport 84, 305–312. https://doi.org/10.1080/02701367.2013.814097

Williamson, J.R., Dumas, A., Ciccarelli, G., Hess, A.R., Telfer, B.A., Buller, M.J., 2015. Estimating load carriage from a body-worn accelerometer, in: 2015 IEEE 12th International Conference on Wearable and Implantable Body Sensor Networks (BSN). IEEE, pp. 1–6. https://doi.org/10.1109/BSN.2015.7299356

Wills, J.A., Saxby, D.J., Glassbrook, D.J., Doyle, T.L.A., 2021a. Sex-Specific Physical Performance Adaptive Responses Are Elicited After 10 Weeks of Load Carriage Conditioning. Mil. Med. 00, 1–7. https://doi.org/10.1093/milmed/usab470

Wills, J.A., Saxby, D.J., Glassbrook, D.J., Doyle, T.L.A., 2019. Load-Carriage Conditioning Elicits Task-Specific Physical and Psychophysical Improvements in Males. J. Strength Cond. Res. 33, 2338–2343. https://doi.org/10.1519/JSC.0000000000003243

Wills, J.A., Saxby, D.J., Lenton, G.K., Doyle, T.L.A., 2021b. Lower Limb Biomechanical Responses During a Standardized Load Carriage Task are Sex Specific. Mil. Med. 186, 1157–1168. https://doi.org/10.1093/milmed/usab093

Wyss, T., Mäder, U., 2010. Recognition of military-specific physical activities with body-fixed sensors. Mil. Med. 175, 858–864. https://doi.org/10.7205/MILMED-D-10-00023

Zhang, J.T., Novak, A.C., Brouwer, B., Li, Q., 2013. Concurrent validation of Xsens MVN measurement of lower limb joint angular kinematics. Physiol. Meas. 34, N63–N69. https://doi.org/10.1088/0967-3334/34/8/N63

Appendix A: Research Consent Form

uOttawa

Université d'Ottawa

Faculté des sciences de la santé

École des sciences de l'activité physique

University of Ottawa

Faculty of Health Sciences

School of Human Kinetics

☎ 613-562-5853
613-562-5149

125 University Privat
Ottawa ON K1N 6N5 Canada

www.uOttawa.ca

Research Project Title: **A validation of an IMU suit for military-based movements**

Principal Investigator:
Dr. Ryan Graham
613-562-5800 X 1025; ryan.graham@uottawa.ca
University of Ottawa
Faculty of Health Sciences
Department of Human Kinetics
200 Lees Ave (E020)
Ottawa, ON K1N6N5

Background and Purpose of the Study:
To ensure that our Canadian Armed Forces (CAF) meets their vision of being strong, secure, and engaged here at home and around the world, soldiers undergo specialized training under a variety of combat scenarios in many different environments while wearing body-borne loads (i.e., helmet, boots, ballistic plated vests, backpacks, firearms). However, it is still unknown how body-borne loads affect a soldier's ability to perform occupationally relevant tasks. To be able to test these research questions, a suitable way to collect a soldier's kinematics first needs to be established.

Recently, there has been a large shift towards the field of wearable technology. Inertial measurement units (IMUs) are small sensors that can measure their orientation and acceleration about a coordinate system. However, to implement these sensors into future research with the CAF they must be deemed valid against a gold standard. Therefore, the purpose of this investigation is to test the agreement between and IMU based system (MVN Biomech, Xsens, Netherlands) against an optical motion capture system (V5, Vicon, UK) during military-based movements.

Description of Study Procedures:
You are invited to participate in a two-day motion analysis procedure for approximately 2 hours on day one and approximately 1 hour on day two at the University of Ottawa Human Movement Biomechanics Laboratory (200 Lees Avenue, E020). On day one, the first part of the study protocol consists of a series of randomly assigned military-based movements to be performed 3 times each with and without a firearm (19 movements x 3 repetition x 2 firearm conditions = 114 trials): run-to-down (run and then immediately assume a prone position), down-to-up (start in a prone position then stand up and begin running), crawl (in prone, stomach touches the ground and all 4 limbs contact the ground), stair ascent and descent (3 steps at 18 cm steps), ramp ascent and descent (9 metres at 7°), ladder climbing (approximately 2 metres vertical), drop-jumps (standing on an adjusted platform, you will drop off the platform, land on the force plates in front of you and immediately jump as high as you can), vertical jump (jump as high as you can from

standing), walking at a self-selected pace (8 metres), wall vault (climb over a 1 metre tall wall), slow marching (60 beats/minute), fast marching 120 beats/minute, and an agility run (self-selected run at perceived 80% maximal effort), run-to-kneel (running then transition to kneeling), kneel-to-run (kneeling then transition to run), prone-to-kneeling (laying down then transition to kneeling), kneel-to-prone (kneeling then transition to laying down). In an attempt to reduce fatigue, there will be a 30 second to 1 minute rest period after each trial. The second part of the study consists of 6 different movement screening tasks to be performed three times each to the best of your ability. The tasks will be performed bilaterally and consist of a bird-dog, hop-down, L-hop, step-down, T-balance, and lunge. Similar to the first section, there will be a 30 second to 1 minute rest period after each trial to reduce fatigue.

Upon arrival, you will be outfitted with 2 motion capture suits: an inertial measurement suit (IMU) and an optical motion capture suit. 1) Using neoprene bands and a custom shirt, IMUs will be placed on your lower limbs, upper limbs, trunk, pelvis, and head. These sensors will then connect to an on-board computer that will stream all the IMU data to the computer. 2) Using the same clothing as outlined in 1, reflective marker clusters and individual markers will be placed on the upper and lower limbs, trunk, pelvis, and head for the purpose of optical motion capture. Before the experimental trials can begin, you will be asked to perform two five-second static reference calibration trials and a functional range of motion trial, which will both be used to create an individualized biomechanical model. Additionally, a calibration procedure will be performed for the IMU system, which consists of standing in a neutral posture (N-pose), walk for 5 seconds forward, turning around, and returning to an N-pose at the origin. After these calibration trials are completed, some markers will be removed and the experimental trials will begin.

On day two, you will be asked to perform eight of the military-based tasks performed on day one with a simulated firearm: walking, running, prone-to-run, prone-to-kneeling, kneeling-to-run, kneeling-to-prone, run-to-kneeling, and run-to-prone. All tasks will be performed three times under three different loading conditions: 6 kg, 20 kg, and 40 kg (8 tasks x 3 repetitions x 3 loads = 72 movements). These loading conditions will be accomplished through backpacks and protective equipment similar to what the Canadian Armed Forces wear. Unlike the first day, only the IMU suit will be worn.

Possible Risks and Discomforts:

There are no significant risks associated with participating in this study. You may experience pain and fatigue due to the nature of the tasks; however, sufficient rest will be given to reduce these effects. The tape used to attach the individual reflective markers may cause minor skin irritation; similar to what it experienced with a bandage and typically fades within 2 to 3 days.

Should you experience any major discomfort, please tell us immediately and seek primary care from a medical professional on campus (100 Marie Curie, Ottawa, Tel.: 613-564-3950) or a medical professional of your choosing.

Possible Benefits:

You will not directly benefit from participating in this study. However, the results of this study will greatly add to our knowledge of the validity of motion capture systems during loaded military-based movements.

Voluntary Participation:

You are not obliged to participate in this study; you participation is voluntary. You may also withdraw from the study at any time with no penalty or coercion. You will be compensated up to the time of withdrawal and your data will be destroyed (i.e. it will not be used in the study).

Confidentiality:

All personal information is kept confidential. Information gained from this study will be stored electronically and will need a password to access, which will only be known to Dr. Ryan Graham and

Matthew Mavor. Paper study records are stored in a locked cabinet and will be destroyed after 5 years post publication; electronic records will be deleted and paper records will be shredded. You will not be identified by name in any reports of the completed study. Your anonymity will be strictly maintained – you will not be identified by your name, but will be determined by an independent study number.

Compensation:
You will receive $20 in compensation for your participation in this study.

Questions about the Study:
You are free to ask questions at any time during the protocol and by contacting the principal investigator by email: Dr. Ryan Graham (ryan.graham@uottawa.ca). The ethical components of this research project has been approved by the University of Ottawa research ethics board. If you have any questions regarding the ethical conduct of this study, you may contact the Protocol Officer for Ethics in Research, University of Ottawa, Tabaret Hall, 550 Cumberland Street, Room 154, Ottawa ON, K1N 6N5. Tel.: (613) 562-5387 Email: ethics@uottawa.ca. There are two copies of the consent form, one of which is yours to keep.

Research Project Title: **A validation of an IMU suit for military-based movements**

Consent:
I have read this consent form, and I agree to participate in the procedures of this study.

_____
Printed Name of Participant

_____ _____
Signature of Participant Date

Investigator Statement (or Person Explaining the Consent):
I have carefully explained to the research participant the nature of the above research study. To the best of my knowledge, the research participant signing this consent form understands the nature, demands, risks and benefits involved in participating in this study. I acknowledge my responsibility for the care and well-being of the above research participant, to respect the rights and wishes of the research participant, and to conduct the study according to applicable Good Clinical Practice guidelines and regulations.

_____
Name of Investigator/Delegate (printed)

_____ _____
Signature of Investigator/Delegate Date

Informed Consent to have Pictures Taken:
I consent to have side view pictures taken of myself completing the experiment, and understand that no pictures will be taken at any point without me knowing. I also understand that if any of these pictures are used in a subsequent presentation or publication, that my face and any other identifiers will be blurred. You can still participate in the research study without consenting to have pictures taken.

_____ _____
Name Date

_____
Signature

_____ _____
Witness Name Witness Signature

Future Participation:

- ☐ I am interested in being contacted to participate in future research performed by this laboratory (your email information will be saved in a password-protected file).

uOttawa

Université d'Ottawa
Faculté des sciences de la santé
École des sciences de l'activité physique

University of Ottawa
Faculty of Health Sciences
School of Human Kinetics

☎ 613-562-5853
613-562-5149

125 University Private
Ottawa ON K1N 6N5 Canada

www.uOttawa.ca

Formulaire de consentement à la recherche

Titre du projet de recherche: **Validation d'un costume avec unités de mesure inertielle (IMU) pour des mouvements militaires**

Chercheur principal:
Dr. Ryan Graham
613-562-5800 X 1025; ryan.graham@uottawa.ca
Université d'Ottawa
Faculté des sciences de la santé
École des sciences de l'activité physique
200 Lees Ave (E020)
Ottawa, ON K1N6N5

Contexte et objectif de l'étude:
Pour que les Forces armées canadiennes (FAC) répondent à leur vision d'être fortes, sécuritaires et engagées au Canada et ailleurs dans le monde, les soldats suivent un entraînement spécialisé dans divers scénarios de combat dans divers environnements tout en portant des charges corporelles (c'est-à-dire casque, bottes, gilets pare-balles, sacs à dos, armes à feu). Cependant, on ne sait toujours pas comment les charges corporelles affectent la capacité d'un soldat d'effectuer des tâches pertinentes professionnellement. Pour pouvoir tester ces questions de recherche, il faut d'abord établir une méthode appropriée pour collecter la cinématique d'un soldat.

Récemment, il y a eu un grand changement vers le domaine de la technologie portable. Les unités de mesure inertielles (IMU) sont de petits capteurs qui peuvent mesurer leur orientation et leur accélération autour d'un système de coordonnées. Toutefois, pour implémenter ces capteurs dans les recherches futures avec les FAC, ils doivent être jugés valables par rapport à un étalon-or. Par conséquent, le but de cette enquête est de tester l'accord entre un système basé sur IMU (MVN Biomech, Xsens, Pays-Bas) contre un système de capture de mouvement optique (V5, Vicon, Royaume-Uni) lors de mouvements militaires.

Description des procédures d'étude:
Vous êtes invité à participer à une procédure d'analyse de mouvement de deux jours pendant environ deux heures le premier jour et environ une heure le deuxième jour au Laboratoire de biomécanique du mouvement humain de l'Université d'Ottawa (200, avenue Lees, E020). Le premier jour, la première partie du protocole d'étude consiste en une série de mouvements militaires attribués au hasard, à exécuter trois fois chacun avec et sans arme à feu (19 mouvements x 3 répétitions x 2 armes à feu = 114 essais): de haut en bas (courir, puis prendre immédiatement une position couchée), de bas en haut (commencer dans une position couchée puis se lever et commencer

à courir), ramper (en position couchée, l'estomac touche le sol et les 4 membres entrent en contact avec le sol), descente (3 marches à 18 cm), montée et descente en rampe (9 mètres à 7 °), montée en échelle (environ 2 mètres à la verticale), sauts en chute libre (debout sur une plate-forme ajustée, descente en chute de la plate-forme, atterrissage sur les plaques de force en face de vous et sautez immédiatement aussi haut que possible), saut vertical (sauter aussi haut que possible de la position debout), marcher à un rythme choisi par vous-même (8 mètres), voûte murale (escalader un mur de un mètre de haut), marche lente (60 battements / minute), marche rapide 120 battements / minute, et une course d'agilité (course auto-vitesse à 80% d'effort maximal perçu) courir à genoux (courir puis passer à genoux), s'agenouiller à courir (s'agenouiller puis passer à courir), couché sur le ventre (couché puis passer à genoux), s'agenouiller à genoux (passage à genoux) couché). Dans le but de réduire la fatigue, il y aura une période de repos de 30 secondes à 1 minute après chaque essai, en dépendamment de l'intensité. La deuxième partie de l'étude consiste de 6 différents mouvements de test de dépistage à effectuer trois fois chacun au mieux de vos capacités. Les tâches seront effectuées bilatéralement et se composent d'un oiseau-chien, hop-down, L-hop, descente, T-balance et fente. Comme dans la première partie du protocole, il y aura une période de repos de 30 secondes à 1 minute après chaque essai, basée sur l'intensité pour réduire la fatigue.

À votre arrivée, vous serez équipé avec 2 différents costumes de capture de mouvement: un costume de mesure inertielle (IMU) et un costume de capture de mouvement optique. 1) En utilisant des bandes en néoprène et une chemise personnalisée, les IMU seront placées sur vos membres inférieurs, les membres supérieurs, le tronc, le bassin et la tête. Ces capteurs se connecteront ensuite à un ordinateur de bord qui diffusera toutes les données de l'IMU vers l'ordinateur. 2) En utilisant les mêmes vêtements que ceux indiqués au point 1, des groupes de marqueurs réfléchissants et des marqueurs individuels seront placés sur les membres supérieurs et inférieurs, le tronc, le bassin et la tête dans le but de capturer le mouvement optique. Avant que les essais expérimentaux puissent commencer, vous devrez effectuer deux essais de calibrage statiques de cinq secondes et un essai fonctionnel d'amplitude de mouvement, qui seront tous deux utilisés pour créer un modèle biomécanique individualisé. De plus, une procédure de calibrage sera effectuée pour le système IMU, qui consiste à se tenir dans une position neutre (pose N), marcher pendant 5 secondes en avant, se retourner et revenir à une pose N à l'origine. Une fois ces essais d'étalonnage terminés, certains marqueurs individuels seront retirés et les essais expérimentaux commenceront.

Le deuxième jour, vous serez invité à exécuter huit des tâches militaires du premier jour avec une arme à feu simulée: marcher, courir, sur le ventre, sur le ventre, sur le ventre, sur le dos à courir, à courir à genoux et à courir. Toutes les tâches seront effectuées trois fois dans trois conditions de chargement différentes: 6 kg, 20 kg et 40 kg (8 tâches x 3 répétitions x 3 charges = 72 mouvements). Ces conditions de chargement seront remplies par des sacs à dos et des équipements de protection similaires à ceux que portent les Forces armées canadiennes. Contrairement au premier jour, seul le costume IMU sera porté.

Risques possibles et inconforts:

Il n'y a pas de risques significatifs associés à la participation à cette étude. Vous pourriez ressentir de la douleur et de la fatigue en raison de la nature des tâches; cependant, suffisamment de repos sera donné pour réduire ces effets. Le ruban adhésif utilisée pour attacher les marqueurs réfléchissants individuels peut causer une légère irritation de la peau; similaire à ce qui est ressentis avec un bandage et disparaît généralement dans 2 à 3 jours. Si vous ressentez un inconfort majeur, veuillez-nous en informer immédiatement et demander des soins primaires auprès d'un

professionnel de la santé sur le campus (100 Marie Curie, Ottawa, 613-664-3950) ou d'un professionnel de la santé de votre choix.

Avantages possibles:
Vous ne bénéficierez pas directement de votre participation à cette étude. Cependant, les résultats de cette étude ajouteront beaucoup à notre connaissance de la validité des systèmes de capture de mouvement lors de mouvements militaires chargés.

Participation Volontaire:
Vous n'êtes pas obligé de participer à cette étude; Votre participation est volontaire. Vous pouvez également vous retirer de l'étude à n'importe quel moment, sans pénalité ni coercition. Vous serez compensé jusqu'au moment du retrait et vos données seront détruites (c'est-à-dire qu'elles ne seront pas utilisées dans l'étude).

Confidentialité:
Toutes les informations personnelles sont gardées confidentielles. Les informations tirées de cette étude seront stockées électroniquement et nécessiteront un mot de passe pour y accéder, qui ne sera connu que par Dr. Ryan Graham et Matthew Mavor. Les dossiers d'étude sur papier sont stockés dans une armoire verrouillée et seront détruits 5 ans après leur publication; les dossiers électroniques seront supprimés et les dossiers papier seront déchiquetés. Vous ne serez pas identifié par nom dans les rapports de l'étude terminée. Votre anonymat sera strictement maintenu - vous ne serez pas identifié par votre nom, mais sera déterminé par un numéro d'étude indépendant.

Compensation:
Vous recevrez une compensation de 20 $ pour votre participation à cette étude.

Questions sur l'étude:
Vous êtes libre de poser des questions à tout moment pendant le protocole et en communiquant avec le chercheur principal par courriel: Dr Ryan Graham (ryan.graham@uottawa.ca). Les composantes éthiques de ce projet de recherche ont été approuvées par le comité d'éthique de la recherche de l'Université d'Ottawa. Si vous avez des questions concernant la conduite éthique de cette étude, vous pouvez communiquer avec l'agente de protocole pour l'éthique de la recherche, Université d'Ottawa, Pavillon Tabaret, 550, rue Cumberland, pièce 154, Ottawa (Ontario) K1N 6N5. Tél .: (613) 562-5387 Courriel: ethics@uottawa.ca. Il y a deux copies du formulaire de consentement, dont l'une est à vous de conserver.

Titre du projet de recherche: Validation d'un costume avec unités de mesure inertielle (IMU) pour des mouvements militaires

Consentement:
J'ai lu ce formulaire de consentement et j'accepte de participer aux procédures de cette étude.

_____
Nom imprimé du participant

_____ _____
Signature du participant Date

Déclaration de l'investigateur (ou personne expliquant le consentement):
J'ai soigneusement expliqué au participant à la recherche la nature de l'étude de recherche ci-dessus. À ma connaissance, le participant à la recherche qui signe ce formulaire de consentement comprend la nature, les exigences, les risques et les avantages de participer à cette étude. Je reconnais ma responsabilité pour les soins et le bien-être du participant à la recherche ci-dessus, pour respecter les droits et les souhaits du participant à la recherche, et pour mener l'étude conformément aux directives et règlements applicables en matière de bonnes pratiques cliniques.

_____
Nom de l'enquêteur / délégué (imprimé)

_____ _____
Signature de l'enquêteur / délégué Date

Consentement pour la prise de photos:
Je consens à la prise de photos en complétant l'expérience, et je comprends qu'aucune photo ne sera prise à aucun moment sans que je le sache. Je comprends également que si l'une de ces images est utilisée dans une présentation ou une publication ultérieure, mon visage et tous les autres identifiants seront flous. Vous pouvez toujours participer à l'étude de recherche sans consentir à la prise de photos.

_____ _____
Nom Date

_____
Signature

_____ _____
Nom du témoin Signature du témoin

Participation future:

- ☐ Je suis intéressé à être contacté pour participer à de futures recherches effectuées par ce laboratoire (vos informations d'email seront sauvegardées dans un fichier protégé par mot de passe).

Appendix B: Study One Supplementary Material

Table B1. OPT and Xsens time series marker trajectories used for PCA.

Segment	OPT Marker	Xsens Marker
Head	Back of head	pBackOfHead
	Right side of head	pRightAuricularis
	Left side of head	pLeftAuricularis
Torso	Sternal Notch	pIJ
	Xyphoid process	pPX
	C7	pC7SpinalProcess
Left Upper Arm	Left acromion	pLeftAcromion
	Left lateral epicondyle of Humerus	pLeftArmLatEpicondyle
	Left medial epicondyle of Humerus	pLeftArmMedEpicondyle
Left Forearm	Left radial styloid process	pLeftRadialStyloid
	Left ulnar styloid process	pLeftUlnarStyloid
Right Upper Arm	Right acromion	pRightAcromion
	Right lateral epicondyle of Humerus	pRightArmLatEpicondyle
	Right medial epicondyle of Humerus	pRightArmMedEpicondyle
Right Forearm	Right radial styloid process	pRightRadialStyloid
	Right ulnar styloid process	pRightUlnarStyloid
Pelvis	Left ASIS	pLeftASI
	Left iliac crest	pLeftCSI
	Right ASIS	pRightASI
	Right iliac crest	pRightCSI
Left Thigh	Left greater trochanter	pLeftGreaterTrochanter
	Left lateral epicondyle of the femur	pLeftKneeLatEpicondyle
	Left medial epicondyle of the femur	pLeftKneeMedEpicondyle
Left Shank	Left lateral malleolus	pLeftLatMalleolus
	Left medial malleolus	pLeftMedMalleolus
Right Thigh	Right greater trochanter	pRightGreaterTrochanter
	Right lateral epicondyle of the femur	pRightKneeLatEpicondyle
	Right medial epicondyle of the femur	pRightKneeMedEpicondyle
Right Shank	Right lateral malleolus	pRightLatMalleolus
	Right medial malleolus	pRightMedMalleolus

Table B2. OPT and Xsens tracking markers used for Visual 3D biomechanical model.

Segment	OPT Tracking markers	Xsens Tracking Markers
Head	Back of head Front of head Left side of head Right side of head	pTopOfHead pRightAuricularis pLeftAuricularis pBackOfHead
Left Upper Arm	4 marker cluster placed over the lateral side of the left humerus	pLeftAcromion pLeftArmLatEpicondyle pLeftArmMedEpicondyle
Left Forearm	4 marker cluster placed over the dorsum of the left radius and ulna	pLeftArmLatEpicondyle pLeftArmMedEpicondyle pLeftUlnarStyloid pLeftRadialStyloid
Right Upper Arm	4 marker cluster placed over the lateral side of the right humerus	pRightAcromion pRightArmLatEpicondyle pRightArmMedEpicondyle
Right Forearm	4 marker cluster placed over the dorsum of the right radius and ulna	pRightArmLatEpicondyle pRightArmMedEpicondyle pRightUlnarStyloid pRightRadialStyloid
Thorax/Ab	4 marker cluster placed over the $T_{10} - T_{12}$ vertebrea	pPX pIJ pC7SpinalProcess pT12SpinalProcess pT4SpinalProcess pT8SpinalProcess pL3SpinalProcess pL5SpinalProcess
Pelvis	4 marker cluster placed over the sacrum	pHipOrigin pLeftASI pLeftCSI pLeftIschialTub pRightASI pRightCSI pRightIschialTub pSacrum
Left Thigh	4 marker cluster placed over the lateral side of the left femur	pLeftGreaterTrochanter pLeftKneeLatEpicondyle pLeftKneeMedEpicondyle pLeftPatella
Left Shank	4 marker cluster placed over the lateral side of the left fibula	pLeftLatMalleolus pLeftMedMalleolus pLeftTibialTub
Left Foot	Left heel 3 marker cluster placed over the dorsum of the left foot	pLeftFifthMetatarsal pLeftFirstMetatarsal pLeftHeelCenter pLeftHeelFoot pLeftPivotFoot pLeftToe
Right Thigh	4 marker cluster placed over the lateral side of the right femur	pRightGreaterTrochanter pRightKneeLatEpicondyle pRightKneeMedEpicondyle pRightPatella
Right Shank	4 marker cluster placed over the lateral side of the right fibula	pRightLatMalleolus pRightMedMalleolus pRightTibialTub
Right Foot	Right heel 3 marker cluster placed over the dorsum of the right foot	pRightFifthMetatarsal pRightFirstMetatarsal pRightHeelCenter pRightHeelFoot pRightPivotFoot pRightToe

Appendix C: Study Two Supplementary Material

Table C3. Dynamic Time Warping Anchors

Movement	Segment 1	Segment 2	Segment 3	Segment 4	Segment 5
Kneel-to-Prone	Start of the trial to when either the hands or sternum move	When either the hands or sternum move to when the first hand is planted on the ground	First hand planted on the ground to when the second hand is planted on the ground	Second hand planted on the ground to when the sternum is on the ground	Sternum on the ground to the end of the trial
Prone-to-Kneel	Start of the trial to when the hands or sternum or toes move	Hand or sternum or toes move to when the left foot is planted	Left foot planted to when right foot is on the ground	Right foot on the ground to when the hands stop become stationary	Hand stationary to the end of the trial
Run-to-Kneel	One heel strike before kneeling movement	Last heel strike to when second knee touches ground	Second knee touches ground to end of trial		
Kneel-to-Run	Start of the trial to when the hands or sternum or toes move	Hands or sternum or toes move to when the left hand drops back down	Left hand drops back down to first heel strike	First heel strike to second heel strike	
Run-to-Prone	One heel strike before prone movement	Fourth heel strike to first hand on the ground	First hand on the ground to second hand on the ground	Second hand on the ground to sternum on the ground	Sternum on the ground to end of trial
Prone-to-Run	Start of trial to sternum raised off the ground	Sternum raised off the ground to first foot plant	First foot plant to second foot plant	Second foot plant to first heel strike	First heel strike to second heel strike
Walking					
Running					

Note: Transitional movements (i.e., kneel/prone movements) were dynamically time warped based on the identified key segments of the movement. Greyed-out portions of the table are not applicable to that given movement. Gait cycles that are not part of the transitional movement were time normalized to 101 data points and are represented as phases of the movement based on the pelvis' acceleration and their sequence in the overall movement task: acceleration, acceleration transition, steady-state, deceleration transition, deceleration.

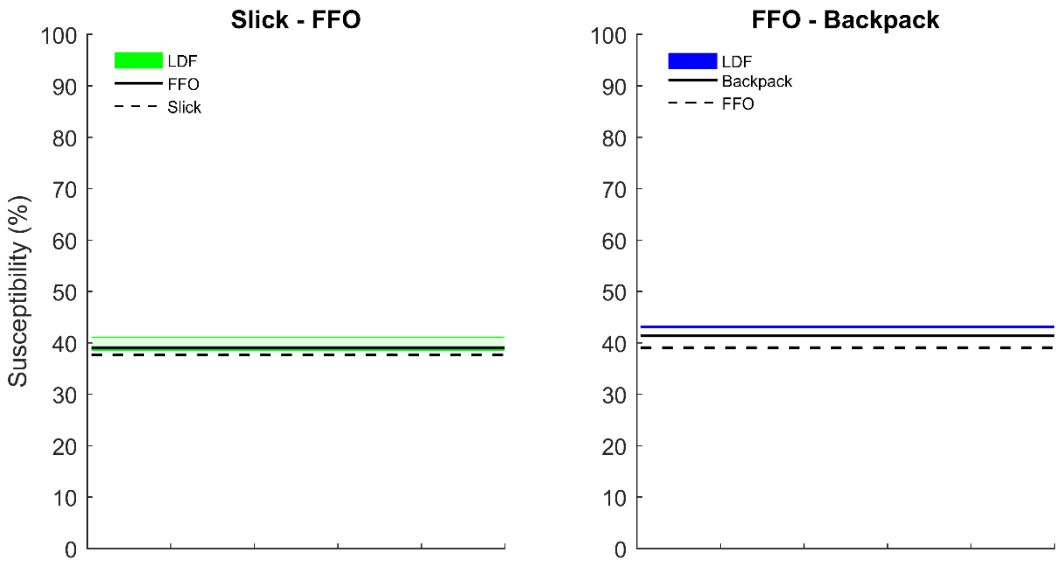

Figure C.1. Kneel-to-prone susceptibility as a factor of load. Linear discriminant functions (LDFs) were scaled to best represent the average Slick, FFO, and Backpack movers. LDFs were created for the Slick vs. FFO (~5.5 kg vs. ~22 kg), and FFO vs. Backpack (~22 kg vs. ~38 kg) conditions. Solid black lines in the Slick – FFO graph represent the average FFO mover and the dashed lines represent the average Slick mover. Solid black lines in the FFO – Backpack graph represent the average Backpack mover and the dashed lines represent the average FFO mover. Each coloured band represents the upper and lower bounds of the scaled LDF model to the average mover. Scaling is based on the sum of root mean squared error of all movement trajectories compared to the mean movement.

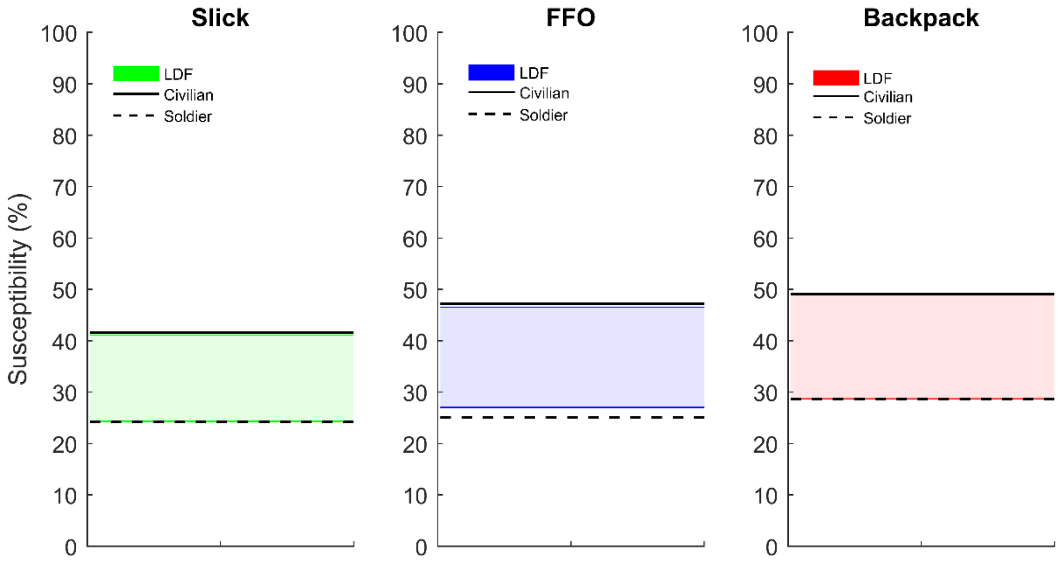

Figure C.2. Kneel-to-prone susceptibility as a factor of military experience. Linear discriminant functions (LDFs) were scaled to best represent the average civilian and soldier movers. LDFs were created for the Slick (~5.5 kg), FFO (~22 kg), and Backpack (~38 kg) conditions. Solid black lines represent the average civilian mover and the dashed lines represent the average soldier mover. Each coloured band represents the upper and lower bounds of the scaled LDF model to the average mover. Scaling is based on the sum of root mean squared error of all movement trajectories compared to the mean movement.

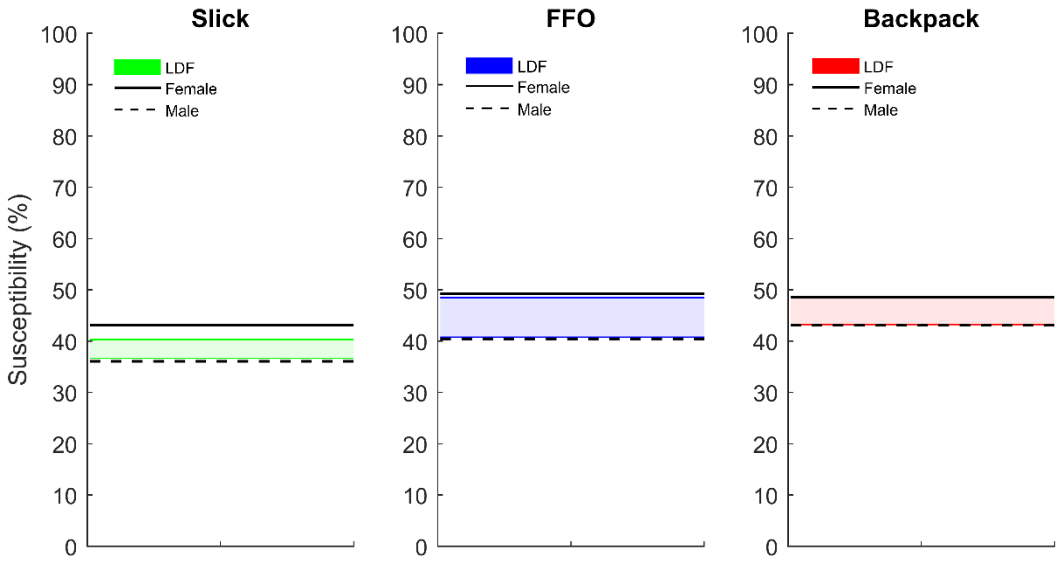

Figure C.3. Kneel-to-prone susceptibility as a factor of sex. Linear discriminant functions (LDFs) were scaled to best represent the average male and female movers. LDFs were created for the Slick (~5.5 kg), FFO (~22 kg), and Backpack (~38 kg) conditions. Solid black lines represent the average male mover and the dashed lines represent the average female mover. Each coloured band represents the upper and lower bounds of the scaled LDF model to the average mover. Scaling is based on the sum of root mean squared error of all movement trajectories compared to the mean movement.

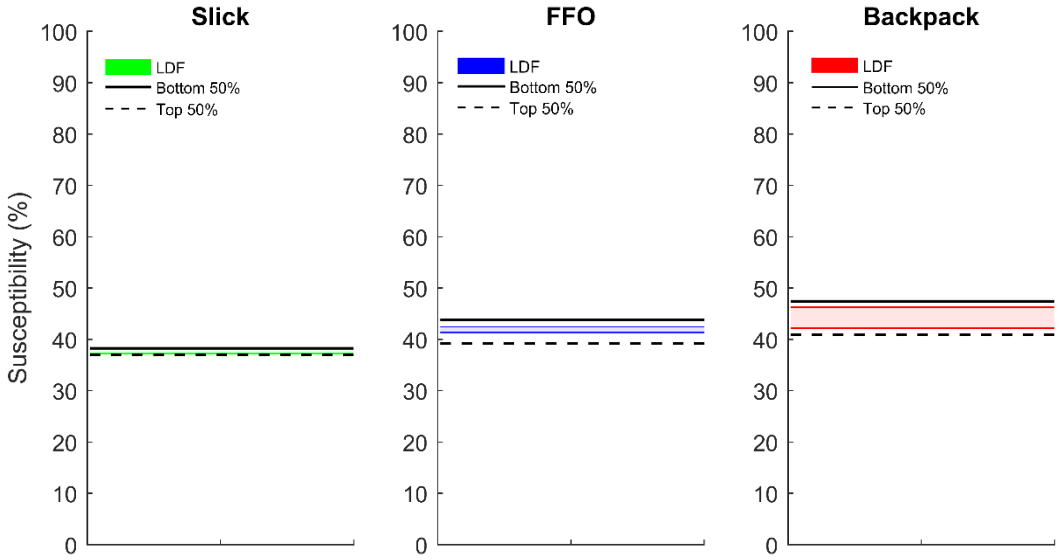

Figure C.4. Kneel-to-prone susceptibility as a factor of body mass. Linear discriminant functions (LDFs) were scaled to best represent the top 50% body mass (~89 kg) and bottom 50% body mass (~69 kg) from the participant pool. LDFs were created for the Slick (~5.5 kg), FFO (~22 kg), and Backpack (~38 kg) conditions. Solid black lines represent the average top 50% body mass mover and the dashed lines represent the average bottom 50% body mass mover. Each coloured band represents the upper and lower bounds of the scaled LDF model to the average mover. Scaling is based on the sum of root mean squared error of all movement trajectories compared to the mean movement.

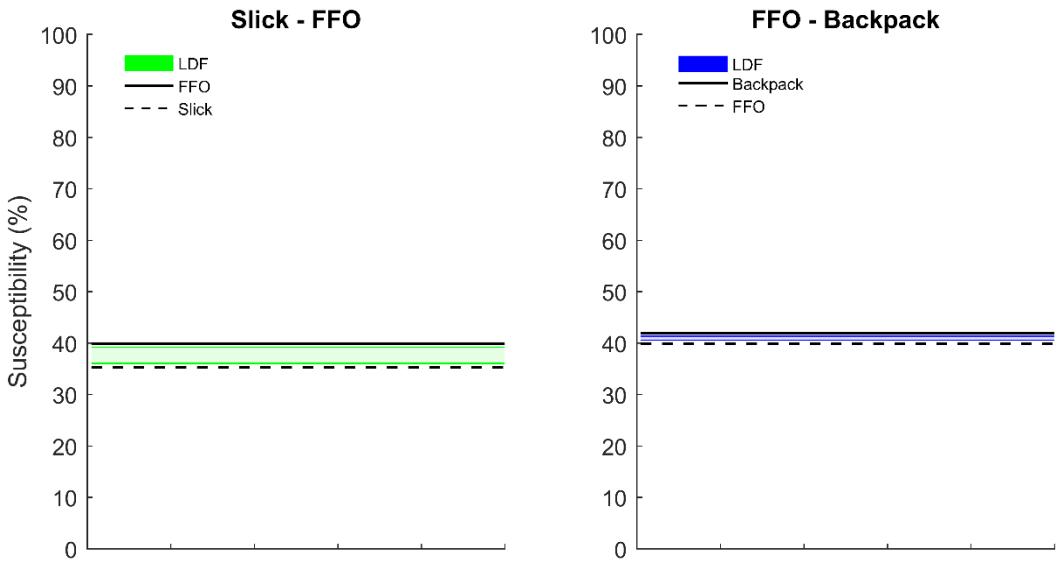

Figure C.5. Prone-to-kneel susceptibility as a factor of load. Linear discriminant functions (LDFs) were scaled to best represent the average Slick, FFO, and Backpack movers. LDFs were created for the Slick vs. FFO (~5.5 kg vs. ~22 kg), and FFO vs. Backpack (~22 kg vs. ~38 kg) conditions. Solid black lines in the Slick – FFO graph represent the average FFO mover and the dashed lines represent the average Slick mover. Solid black lines in the FFO – Backpack graph represent the average Backpack mover and the dashed lines represent the average FFO mover. Each coloured band represents the upper and lower bounds of the scaled LDF model to the average mover. Scaling is based on the sum of root mean squared error of all movement trajectories compared to the mean movement.

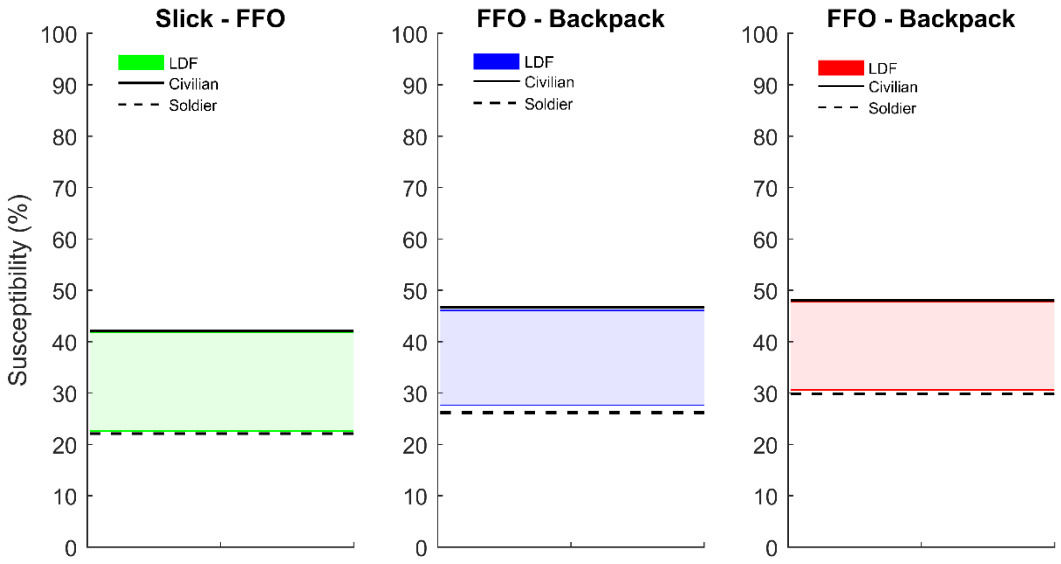

Figure C.6. Prone-to-kneel susceptibility as a factor of military experience. Linear discriminant functions (LDFs) were scaled to best represent the average civilian and soldier movers. LDFs were created for the Slick (~5.5 kg), FFO (~22 kg), and Backpack (~38 kg) conditions. Solid black lines represent the average civilian mover and the dashed lines represent the average soldier mover. Each coloured band represents the upper and lower bounds of the scaled LDF model to the average mover. Scaling is based on the sum of root mean squared error of all movement trajectories compared to the mean movement.

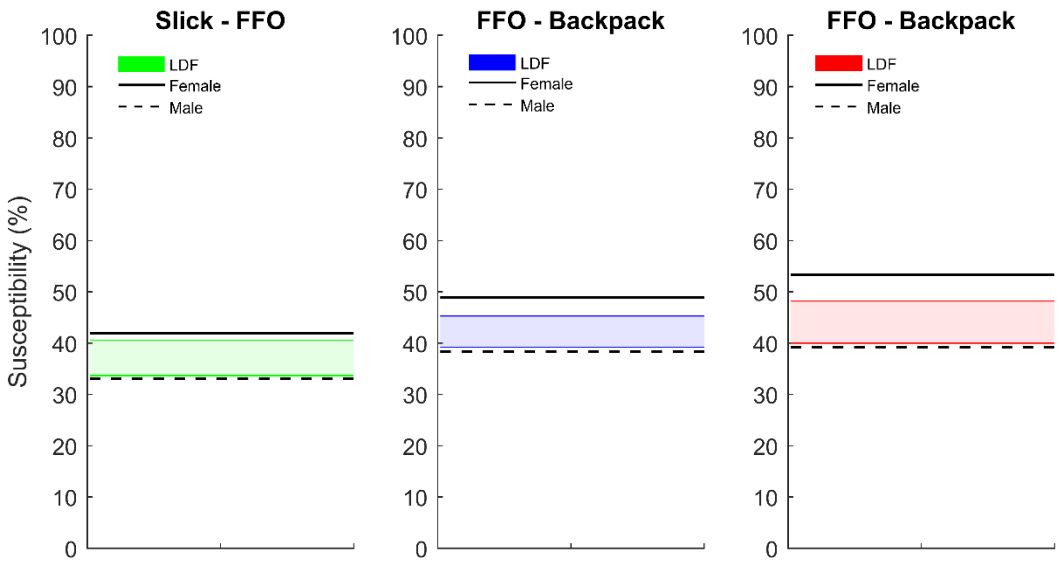

Figure C.7. Prone-to-kneel susceptibility as a factor of sex. Linear discriminant functions (LDFs) were scaled to best represent the average male and female movers. LDFs were created for the Slick (~5.5 kg), FFO (~22 kg), and Backpack (~38 kg) conditions. Solid black lines represent the average male mover and the dashed lines represent the average female mover. Each coloured band represents the upper and lower bounds of the scaled LDF model to the average mover. Scaling is based on the sum of root mean squared error of all movement trajectories compared to the mean movement.

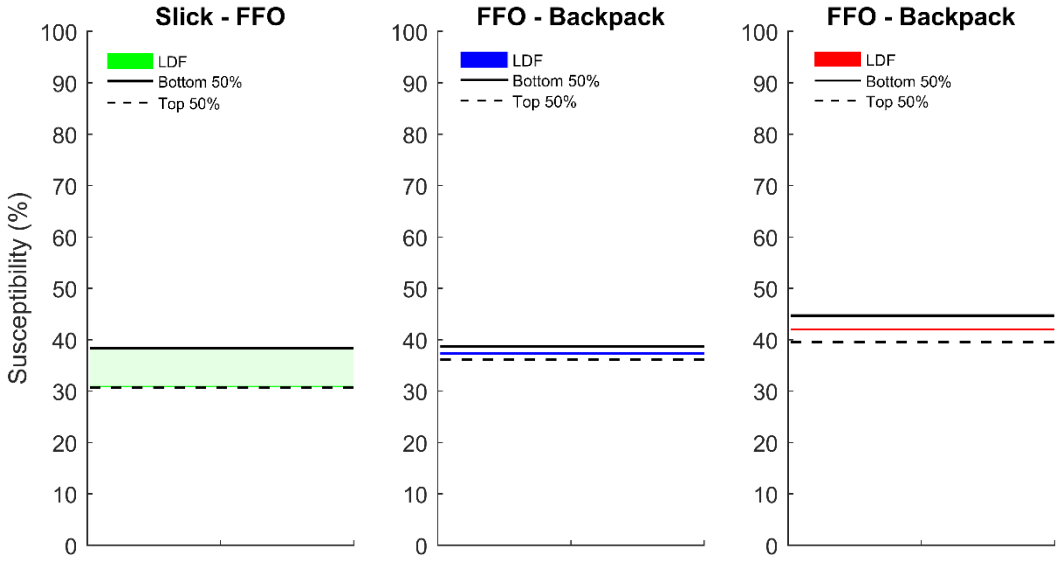

Figure C.8. Prone-to-kneel susceptibility as a factor of body mass. Linear discriminant functions (LDFs) were scaled to best represent the top 50% body mass (~89 kg) and bottom 50% body mass (~69 kg) from the participant pool. LDFs were created for the Slick (~5.5 kg), FFO (~22 kg), and Backpack (~38 kg) conditions. Solid black lines represent the average top 50% body mass mover and the dashed lines represent the average bottom 50% body mass mover. Each coloured band represents the upper and lower bounds of the scaled LDF model to the average mover. Scaling is based on the sum of root mean squared error of all movement trajectories compared to the mean movement.

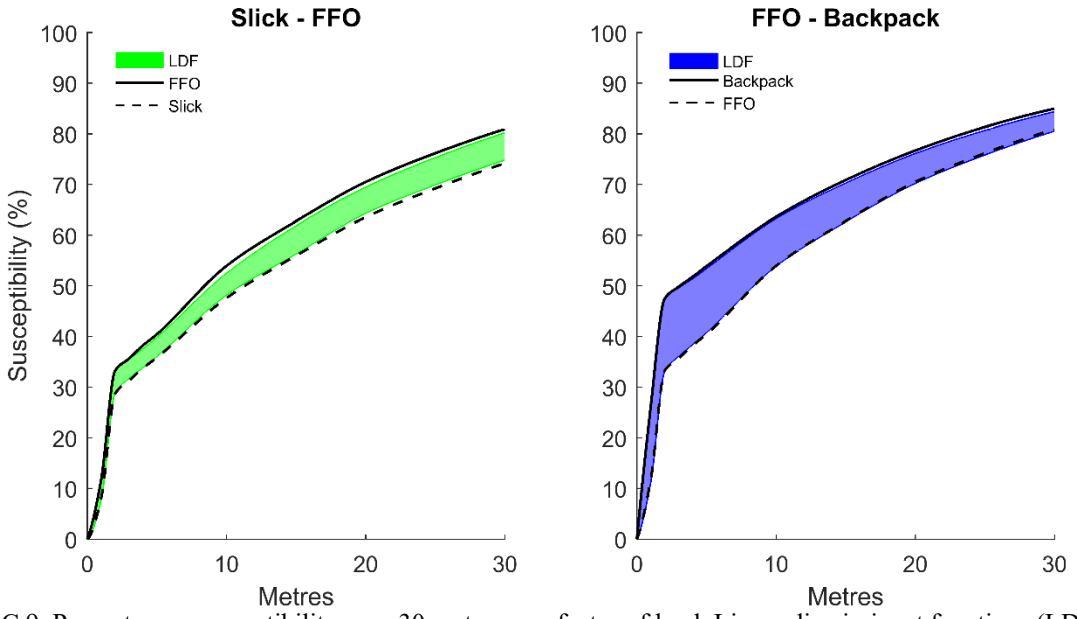

Figure C.9. Prone-to-run susceptibility over 30 metres as a factor of load. Linear discriminant functions (LDFs) were scaled to best represent the average Slick, FFO, and Backpack movers and combined together to make the mover run to each desired distance including a deceleration phase. LDFs were created for the Slick vs. FFO (~5.5 kg vs. ~22 kg), and FFO vs. Backpack (~22 kg vs. ~38 kg) conditions. Solid black lines in the Slick – FFO graph represent the average FFO mover and the dashed lines represent the average Slick mover. Solid black lines in the FFO – Backpack graph represent the average Backpack mover and the dashed lines represent the average FFO mover. Each coloured band represents the upper and lower bounds of the scaled LDF model to the average mover. Scaling is based on the sum of root mean squared error of all movement trajectories compared to the mean movement.

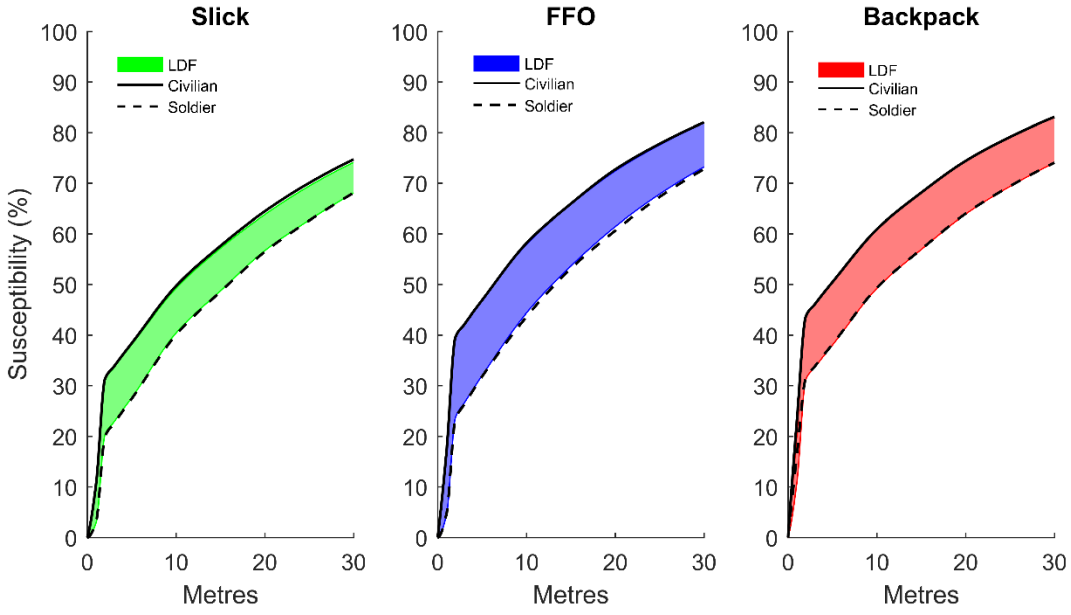

Figure C.10. Prone-to-run susceptibility over 30 metres as a factor of military experience. Linear discriminant functions (LDFs) were scaled to best represent the average civilian and soldier movers. LDFs were created for the Slick (~5.5 kg), FFO (~22 kg), and Backpack (~38 kg) conditions and combined together to make the mover run to each desired distance including a deceleration phase. Solid black lines represent the average civilian mover and the dashed lines represent the average soldier mover. Each coloured band represents the upper and lower bounds of the scaled LDF model to the average mover. Scaling is based on the sum of root mean squared error of all movement trajectories compared to the mean movement.

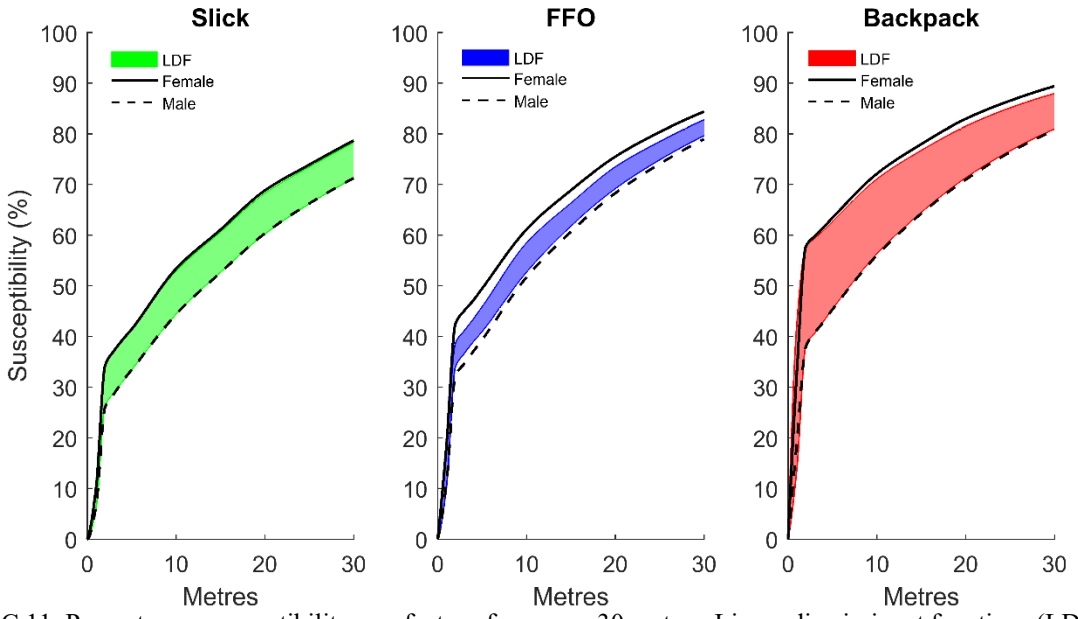

Figure C.11. Prone-to-run susceptibility as a factor of sex over 30 metres. Linear discriminant functions (LDFs) were scaled to best represent the average male and female movers. LDFs were created for the Slick (~5.5 kg), FFO (~22 kg), and Backpack (~38 kg) conditions and combined together to make the mover run to each desired distance including a deceleration phase. Solid black lines represent the average male mover and the dashed lines represent the average female mover. Each coloured band represents the upper and lower bounds of the scaled LDF model to the average mover. Scaling is based on the sum of root mean squared error of all movement trajectories compared to the mean movement.

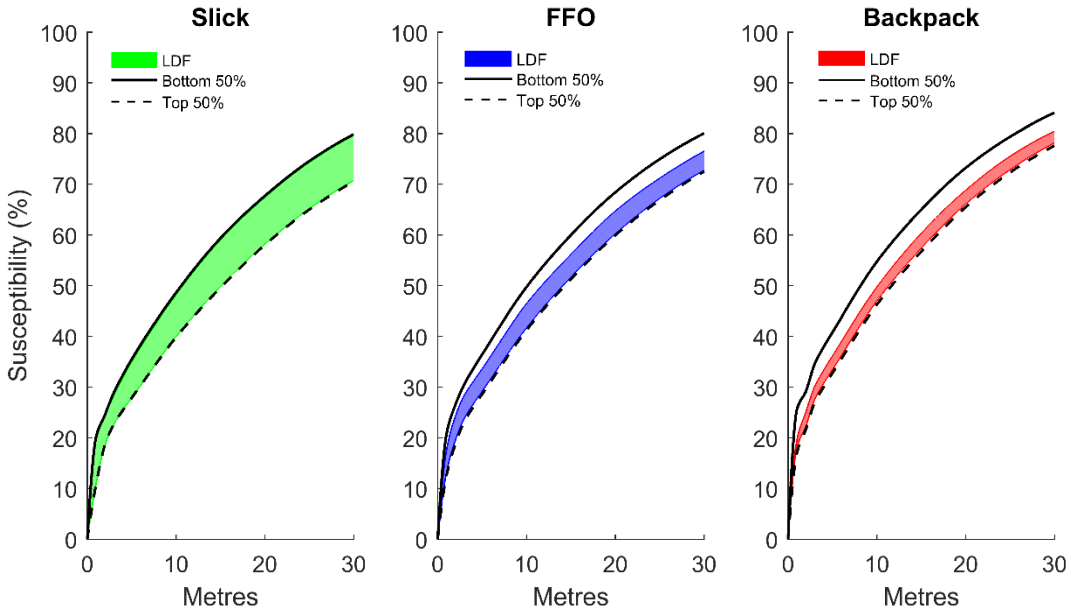

Figure C.12. Prone-to-run susceptibility as a factor of body mass. Linear discriminant functions (LDFs) were scaled to best represent the top 50% body mass (~89 kg) and bottom 50% body mass (~69 kg) from the participant pool. LDFs were created for the Slick (~5.5 kg), FFO (~22 kg), and Backpack (~38 kg) conditions. Solid black lines represent the average top 50% body mass mover and the dashed lines represent the average bottom 50% body mass mover. Each coloured band represents the upper and lower bounds of the scaled LDF model to the average mover. Scaling is based on the sum of root mean squared error of all movement trajectories compared to the mean movement.

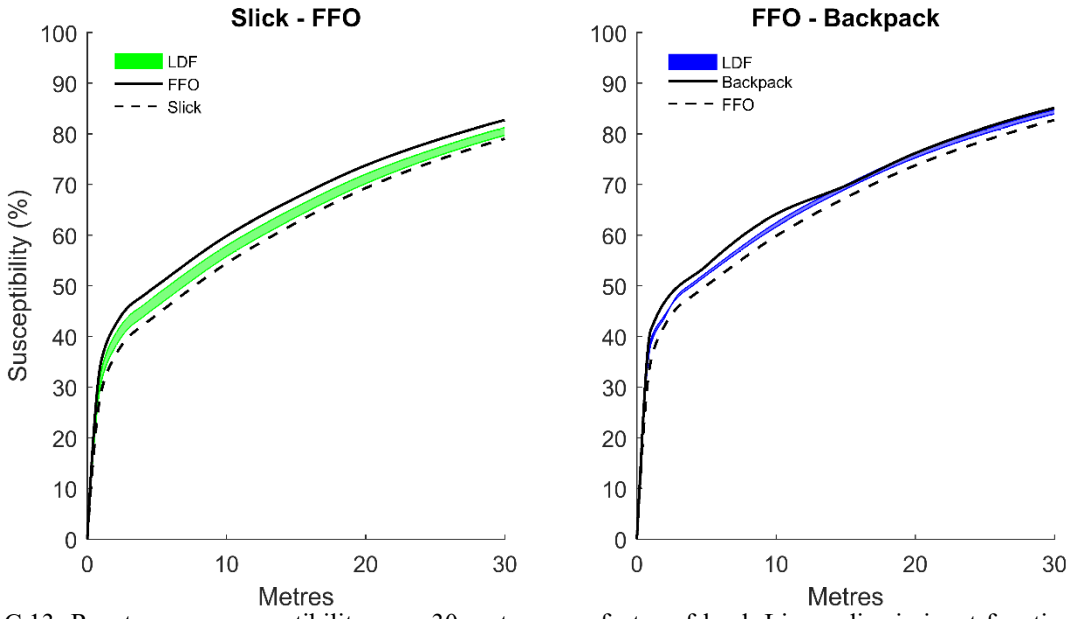

Figure C.13. Run-to-prone susceptibility over 30 metres as a factor of load. Linear discriminant functions (LDFs) were scaled to best represent the average Slick, FFO, and Backpack movers and combined together to make the mover run to each desired distance including a deceleration phase to prone. LDFs were created for the Slick vs. FFO (~5.5 kg vs. ~22 kg), and FFO vs. Backpack (~22 kg vs. ~38 kg) conditions. Solid black lines in the Slick – FFO graph represent the average FFO mover and the dashed lines represent the average Slick mover. Solid black lines in the FFO – Backpack graph represent the average Backpack mover and the dashed lines represent the average FFO mover. Each coloured band represents the upper and lower bounds of the scaled LDF model to the average mover. Scaling is based on the sum of root mean squared error of all movement trajectories compared to the mean movement.

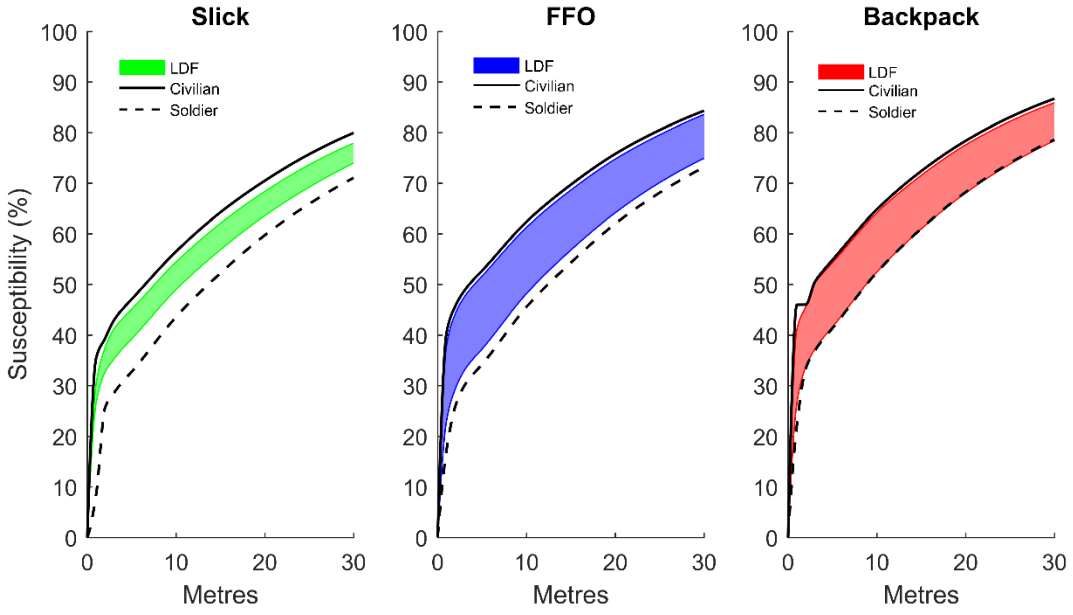

Figure C.14. Run-to-prone susceptibility over 30 metres as a factor of military experience. Linear discriminant functions (LDFs) were scaled to best represent the average civilian and soldier movers. LDFs were created for the Slick (~5.5 kg), FFO (~22 kg), and Backpack (~38 kg) conditions and combined together to make the mover run to each desired distance including a deceleration phase to prone. Solid black lines represent the average civilian mover and the dashed lines represent the average soldier mover. Each coloured band represents the upper and lower bounds of the scaled LDF model to the average mover. Scaling is based on the sum of root mean squared error of all movement trajectories compared to the mean movement.

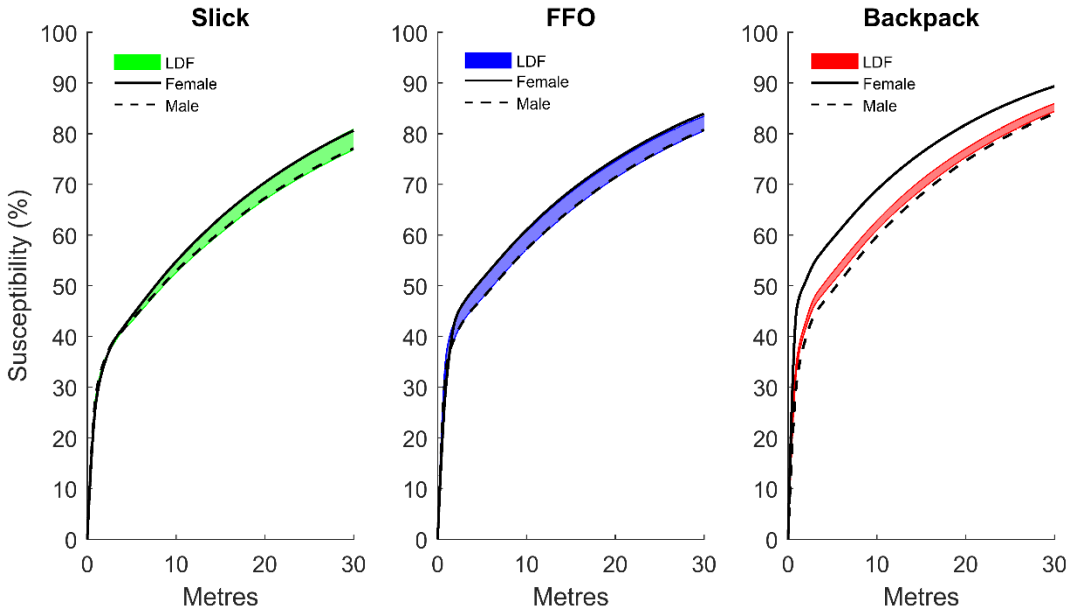

Figure C.15. Run-to-prone susceptibility over 30 metres as a factor of sex. Linear discriminant functions (LDFs) were scaled to best represent the average male and female movers. LDFs were created for the Slick (~5.5 kg), FFO (~22 kg), and Backpack (~38 kg) conditions and combined together to make the mover run to each desired distance including a deceleration phase to prone. Solid black lines represent the average male mover and the dashed lines represent the average female mover. Each coloured band represents the upper and lower bounds of the scaled LDF model to the average mover. Scaling is based on the sum of root mean squared error of all movement trajectories compared to the mean movement.

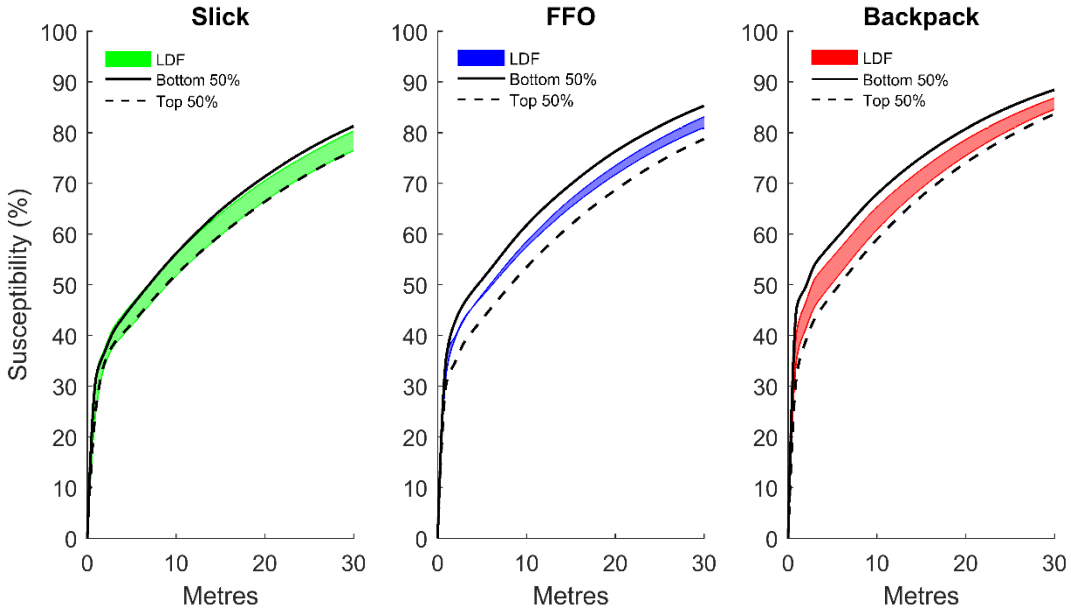

Figure C.16. Run-to-prone susceptibility over 30 metres as a factor of body mass. Linear discriminant functions (LDFs) were scaled to best represent the top 50% body mass (~89 kg) and bottom 50% body mass (~69 kg) from the participant pool. LDFs were created for the Slick (~5.5 kg), FFO (~22 kg), and Backpack (~38 kg) conditions and combined together to make the mover run to each desired distance including a deceleration phase to prone. Solid black lines represent the average top 50% body mass mover and the dashed lines represent the average bottom 50% body mass mover. Each coloured band represents the upper and lower bounds of the scaled LDF model to the average mover. Scaling is based on the sum of root mean squared error of all movement trajectories compared to the mean movement.

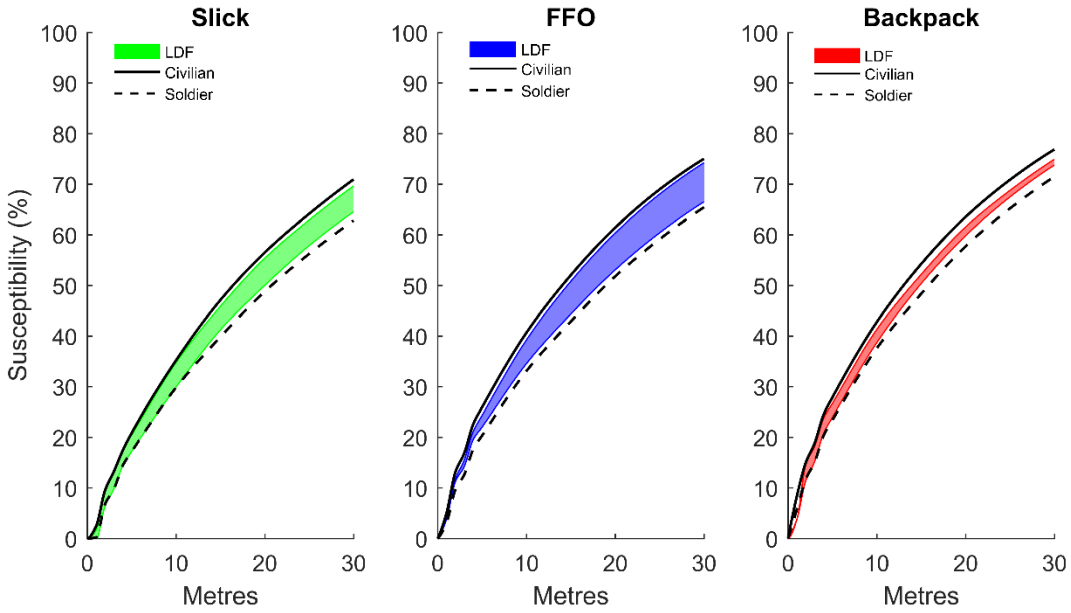

Figure C.17. Kneel-to-run susceptibility over 30 metres as a factor of load. Linear discriminant functions (LDFs) were scaled to best represent the average Slick, FFO, and Backpack movers and combined together to make the mover run to each desired distance including a deceleration phase. LDFs were created for the Slick vs. FFO (~5.5 kg vs. ~22 kg), and FFO vs. Backpack (~22 kg vs. ~38 kg) conditions. Solid black lines in the Slick – FFO graph represent the average FFO mover and the dashed lines represent the average Slick mover. Solid black lines in the FFO – Backpack graph represent the average Backpack mover and the dashed lines represent the average FFO mover. Each coloured band represents the upper and lower bounds of the scaled LDF model to the average mover. Scaling is based on the sum of root mean squared error of all movement trajectories compared to the mean movement.

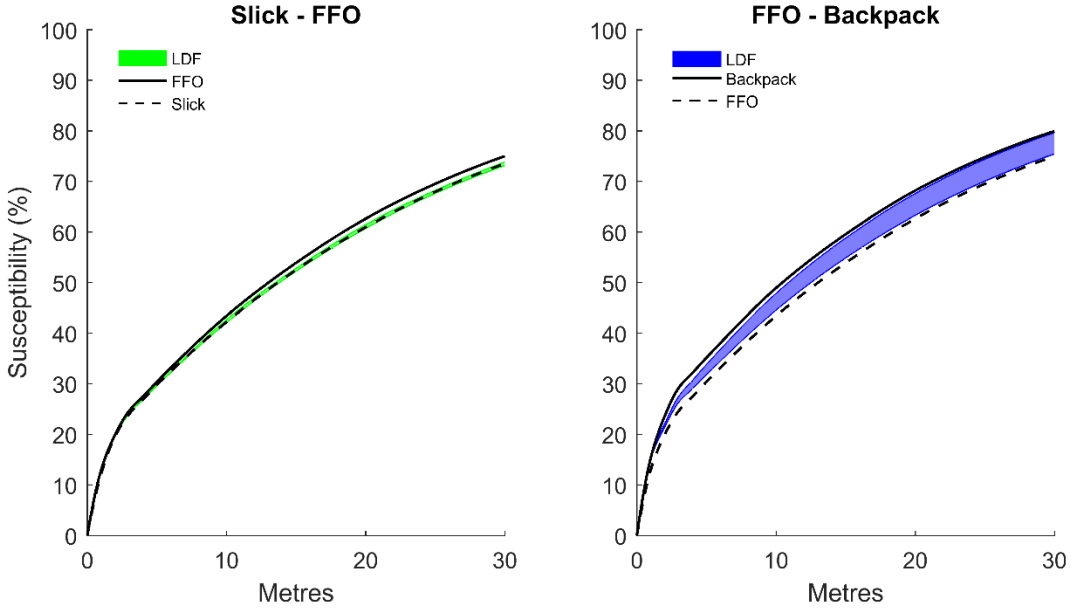

Figure C.18. Kneel-to-run susceptibility over 30 metres as a factor of military experience. Linear discriminant functions (LDFs) were scaled to best represent the average civilian and soldier movers. LDFs were created for the Slick (~5.5 kg), FFO (~22 kg), and Backpack (~38 kg) conditions and combined together to make the mover run to each desired distance including a deceleration phase. Solid black lines represent the average civilian mover and the dashed lines represent the average soldier mover. Each coloured band represents the upper and lower bounds of the scaled LDF model to the average mover. Scaling is based on the sum of root mean squared error of all movement trajectories compared to the mean movement.

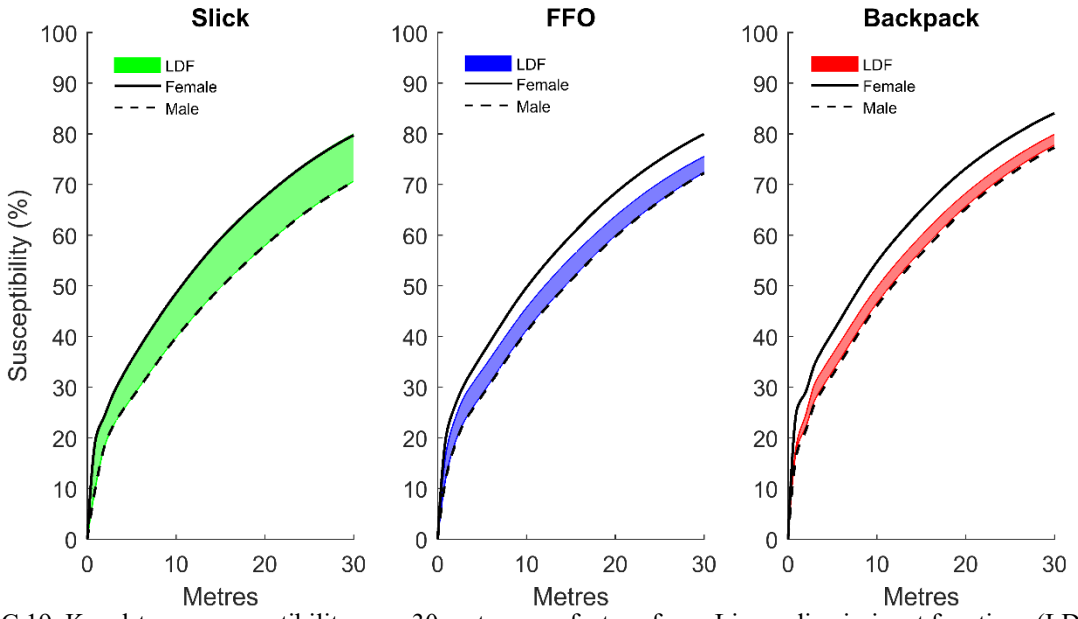

Figure C.19. Kneel-to-run susceptibility over 30 metres as a factor of sex. Linear discriminant functions (LDFs) were scaled to best represent the average male and female movers. LDFs were created for the Slick (~5.5 kg), FFO (~22 kg), and Backpack (~38 kg) conditions and combined together to make the mover run to each desired distance including a deceleration phase. Solid black lines represent the average male mover and the dashed lines represent the average female mover. Each coloured band represents the upper and lower bounds of the scaled LDF model to the average mover. Scaling is based on the sum of root mean squared error of all movement trajectories compared to the mean movement.

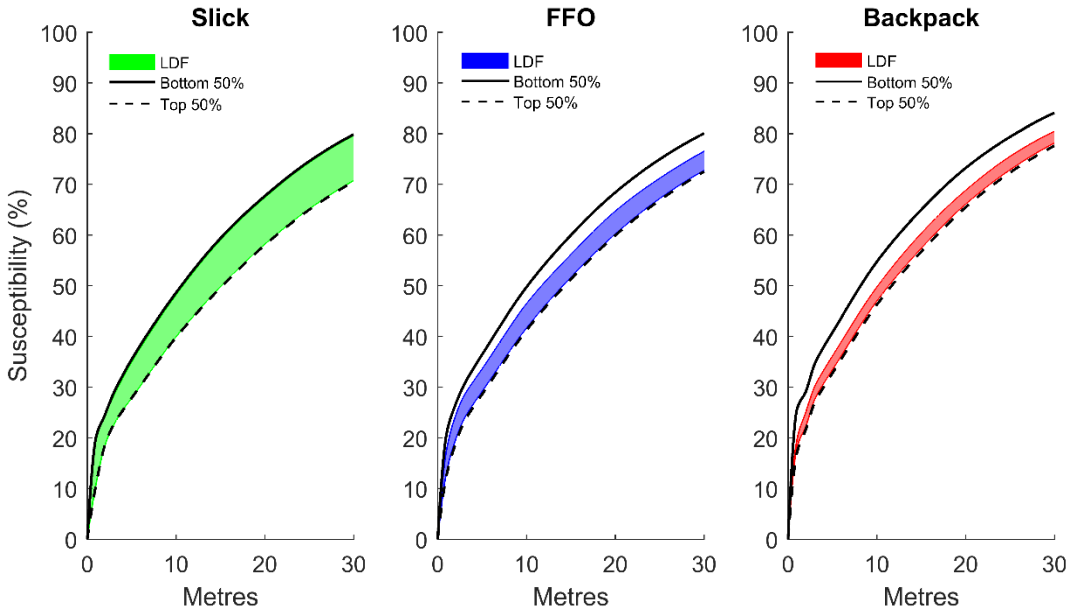

Figure C.20. Kneel-to-run susceptibility over 30 metres as a factor of body mass. Linear discriminant functions (LDFs) were scaled to best represent the top 50% body mass (~89 kg) and bottom 50% body mass (~69 kg) from the participant pool. LDFs were created for the Slick (~5.5 kg), FFO (~22 kg), and Backpack (~38 kg) conditions and combined together to make the mover run to each desired distance including a deceleration phase. Solid black lines represent the average top 50% body mass mover and the dashed lines represent the average bottom 50% body mass mover. Each coloured band represents the upper and lower bounds of the scaled LDF model to the average mover. Scaling is based on the sum of root mean squared error of all movement trajectories compared to the mean movement.

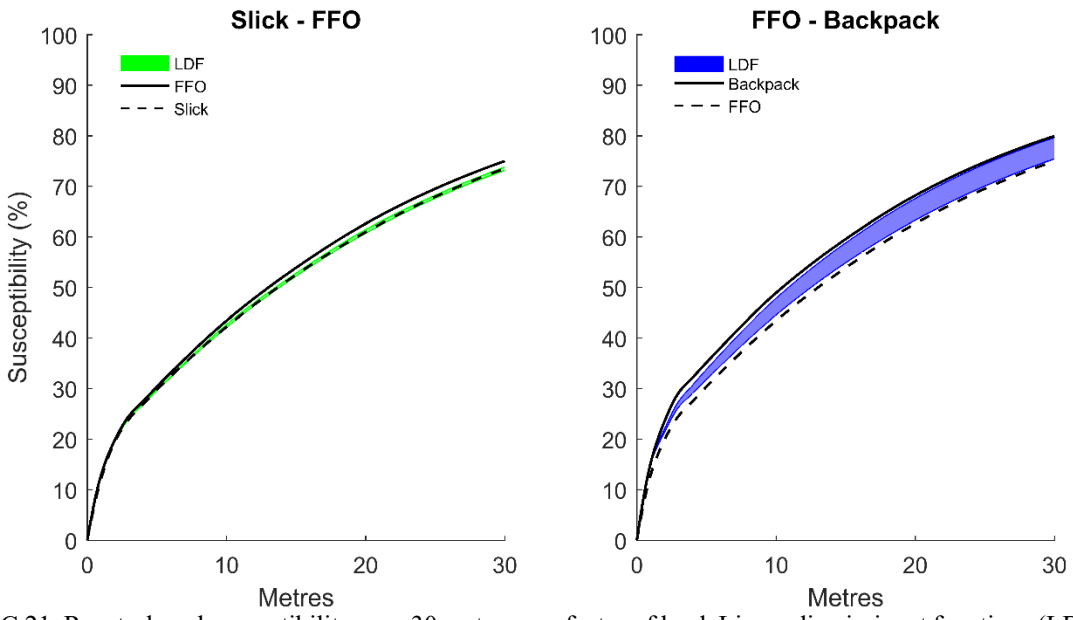

Figure C.21. Run-to-kneel susceptibility over 30 metres as a factor of load. Linear discriminant functions (LDFs) were scaled to best represent the average Slick, FFO, and Backpack movers and combined together to make the mover run to each desired distance including a deceleration phase to kneel. LDFs were created for the Slick vs. FFO (~5.5 kg vs. ~22 kg), and FFO vs. Backpack (~22 kg vs. ~38 kg) conditions. Solid black lines in the Slick – FFO graph represent the average FFO mover and the dashed lines represent the average Slick mover. Solid black lines in the FFO – Backpack graph represent the average Backpack mover and the dashed lines represent the average FFO mover. Each coloured band represents the upper and lower bounds of the scaled LDF model to the average mover. Scaling is based on the sum of root mean squared error of all movement trajectories compared to the mean movement.

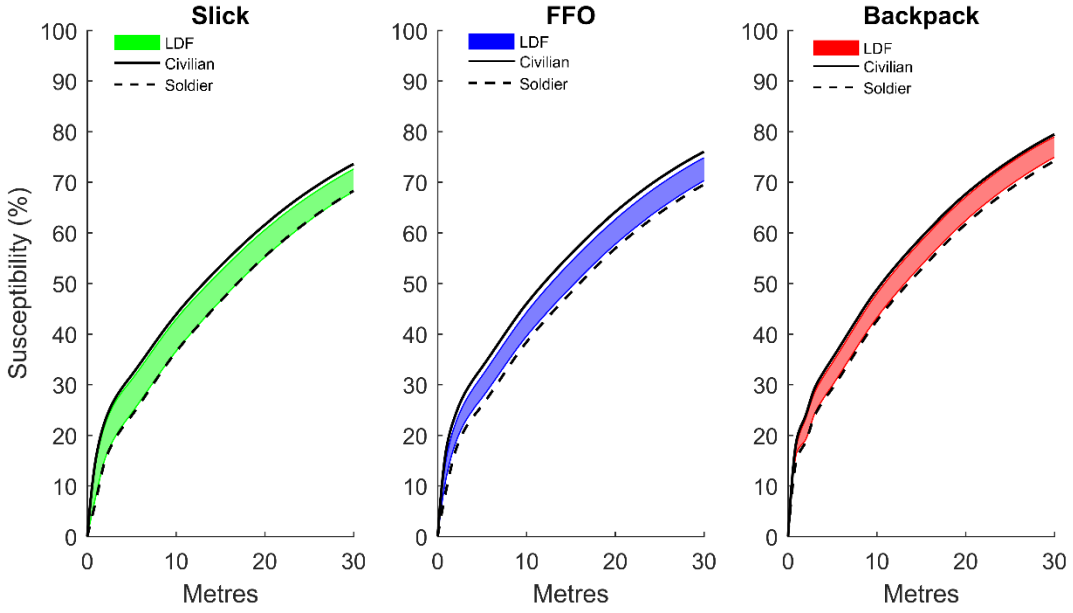

Figure C.22. Run-to-kneel susceptibility over 30 metres as a factor of military experience. Linear discriminant functions (LDFs) were scaled to best represent the average civilian and soldier movers. LDFs were created for the Slick (~5.5 kg), FFO (~22 kg), and Backpack (~38 kg) conditions and combined together to make the mover run to each desired distance including a deceleration phase to kneel. Solid black lines represent the average civilian mover and the dashed lines represent the average soldier mover. Each coloured band represents the upper and lower bounds of the scaled LDF model to the average mover. Scaling is based on the sum of root mean squared error of all movement trajectories compared to the mean movement.

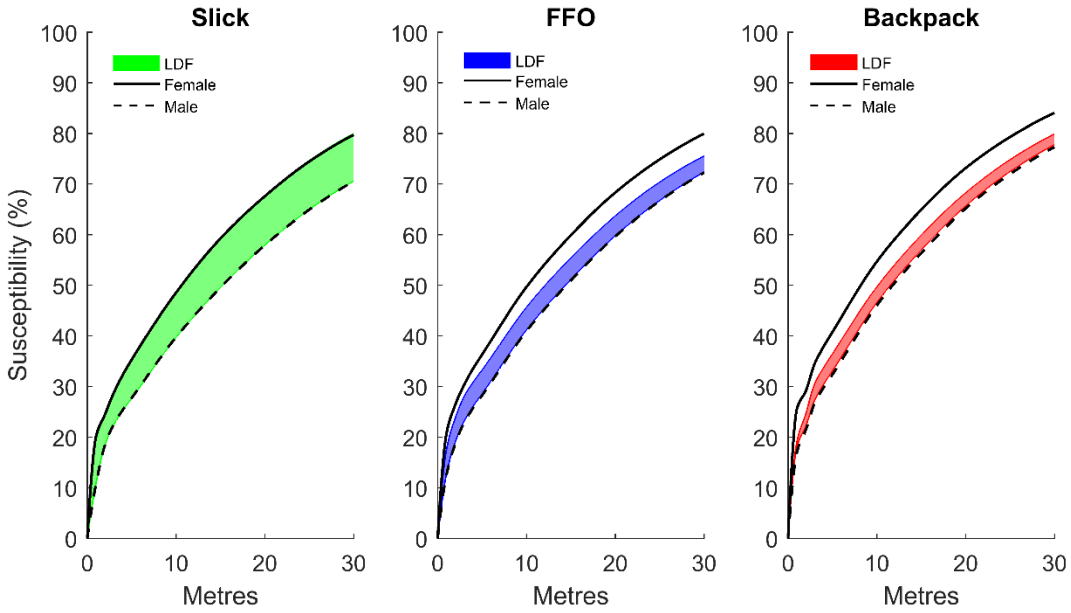

Figure C.23. Run-to-kneel susceptibility over 30 metres as a factor of sex. Linear discriminant functions (LDFs) were scaled to best represent the average male and female movers. LDFs were created for the Slick (~5.5 kg), FFO (~22 kg), and Backpack (~38 kg) conditions and combined together to make the mover run to each desired distance including a deceleration phase to kneel. Solid black lines represent the average male mover and the dashed lines represent the average female mover. Each coloured band represents the upper and lower bounds of the scaled LDF model to the average mover. Scaling is based on the sum of root mean squared error of all movement trajectories compared to the mean movement.

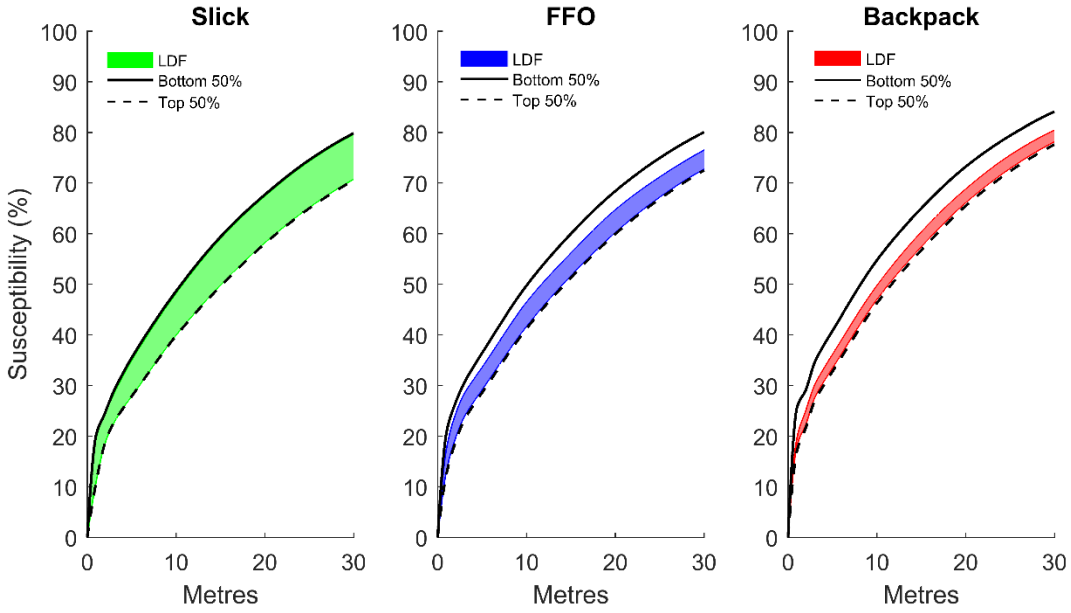

Figure C.24. Run-to-kneel susceptibility over 30 metres as a factor of body mass. Linear discriminant functions (LDFs) were scaled to best represent the top 50% body mass (~89 kg) and bottom 50% body mass (~69 kg) from the participant pool. LDFs were created for the Slick (~5.5 kg), FFO (~22 kg), and Backpack (~38 kg) conditions and combined together to make the mover run to each desired distance including a deceleration phase to kneel. Solid black lines represent the average top 50% body mass mover and the dashed lines represent the average bottom 50% body mass mover. Each coloured band represents the upper and lower bounds of the scaled LDF model to the average mover. Scaling is based on the sum of root mean squared error of all movement trajectories compared to the mean movement.

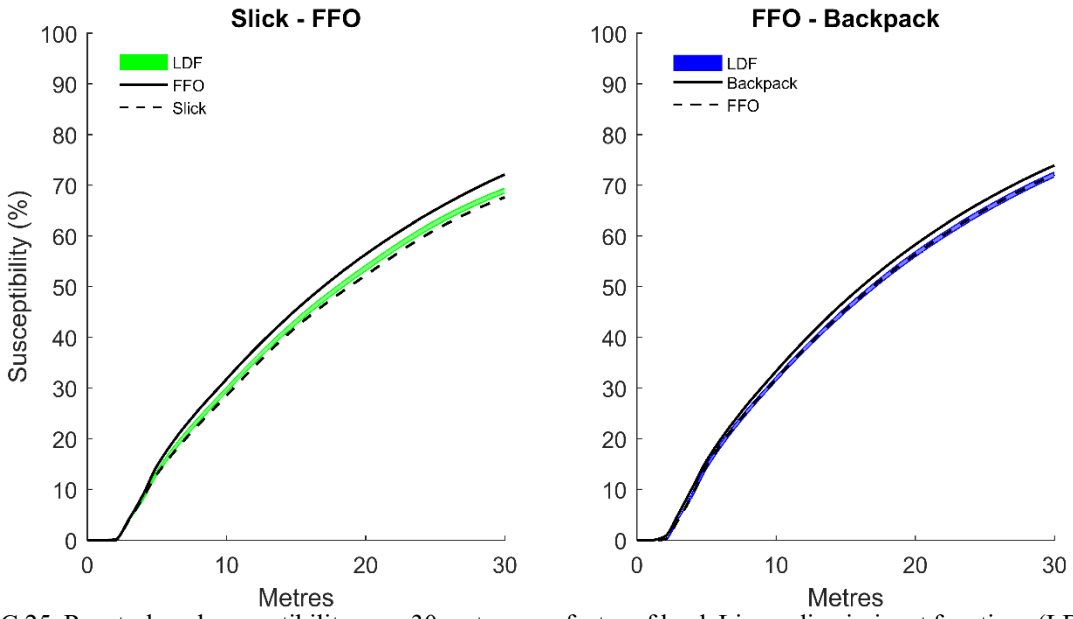

Figure C.25. Run-to-kneel susceptibility over 30 metres as a factor of load. Linear discriminant functions (LDFs) were scaled to best represent the average Slick, FFO, and Backpack movers and combined together to make the mover run to each desired distance including a deceleration phase to kneel. LDFs were created for the Slick vs. FFO (~5.5 kg vs. ~22 kg), and FFO vs. Backpack (~22 kg vs. ~38 kg) conditions. Solid black lines in the Slick – FFO graph represent the average FFO mover and the dashed lines represent the average Slick mover. Solid black lines in the FFO – Backpack graph represent the average Backpack mover and the dashed lines represent the average FFO mover. Each coloured band represents the upper and lower bounds of the scaled LDF model to the average mover. Scaling is based on the sum of root mean squared error of all movement trajectories compared to the mean movement.

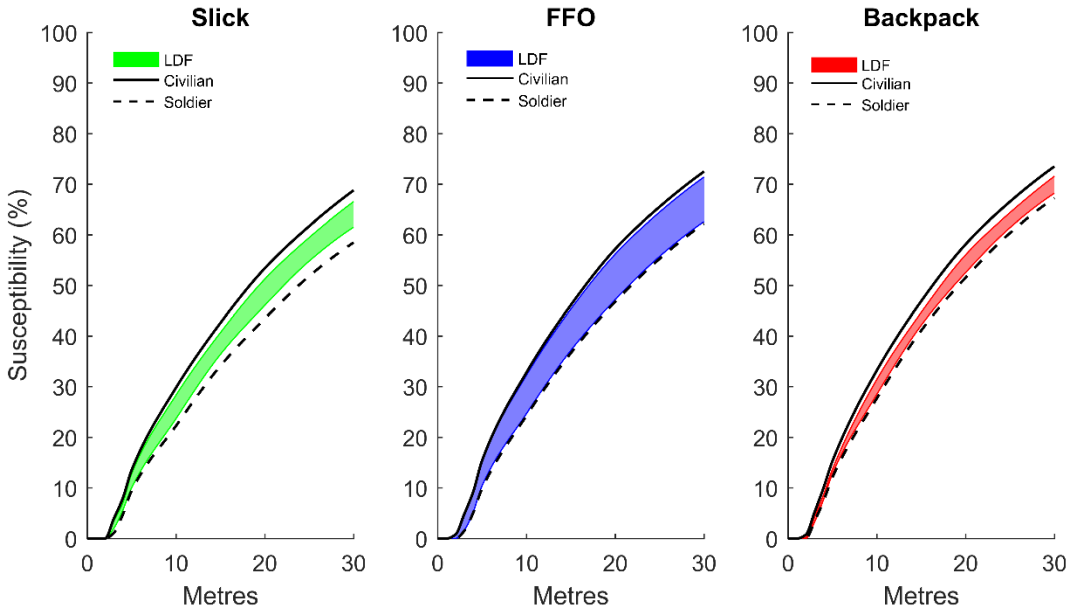

Figure C.26. Run susceptibility over 30 metres as a factor of military experience. Linear discriminant functions (LDFs) were scaled to best represent the average civilian and soldier movers. LDFs were created for the Slick (~5.5 kg), FFO (~22 kg), and Backpack (~38 kg) conditions and combined together to make the mover run to each desired distance including a deceleration phase. Solid black lines represent the average civilian mover and the dashed lines represent the average soldier mover. Each coloured band represents the upper and lower bounds of the scaled LDF model to the average mover. Scaling is based on the sum of root mean squared error of all movement trajectories compared to the mean movement.

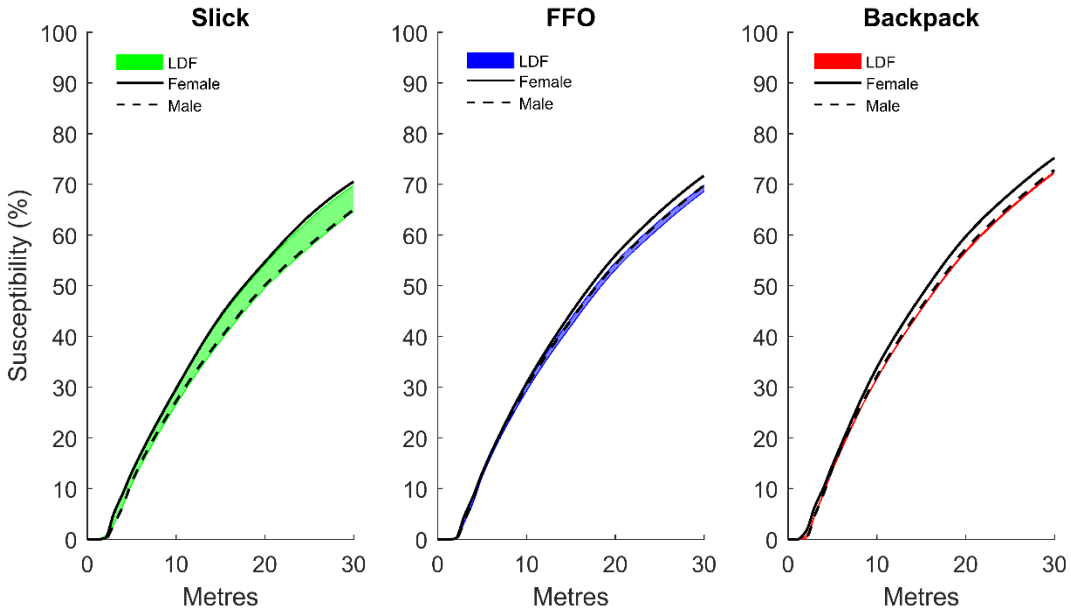

Figure C.27. Run susceptibility over 30 metres as a factor of sex. Linear discriminant functions (LDFs) were scaled to best represent the average male and female movers. LDFs were created for the Slick (~5.5 kg), FFO (~22 kg), and Backpack (~38 kg) conditions and combined together to make the mover run to each desired distance including a deceleration phase. Solid black lines represent the average male mover and the dashed lines represent the average female mover. Each coloured band represents the upper and lower bounds of the scaled LDF model to the average mover. Scaling is based on the sum of root mean squared error of all movement trajectories compared to the mean movement.

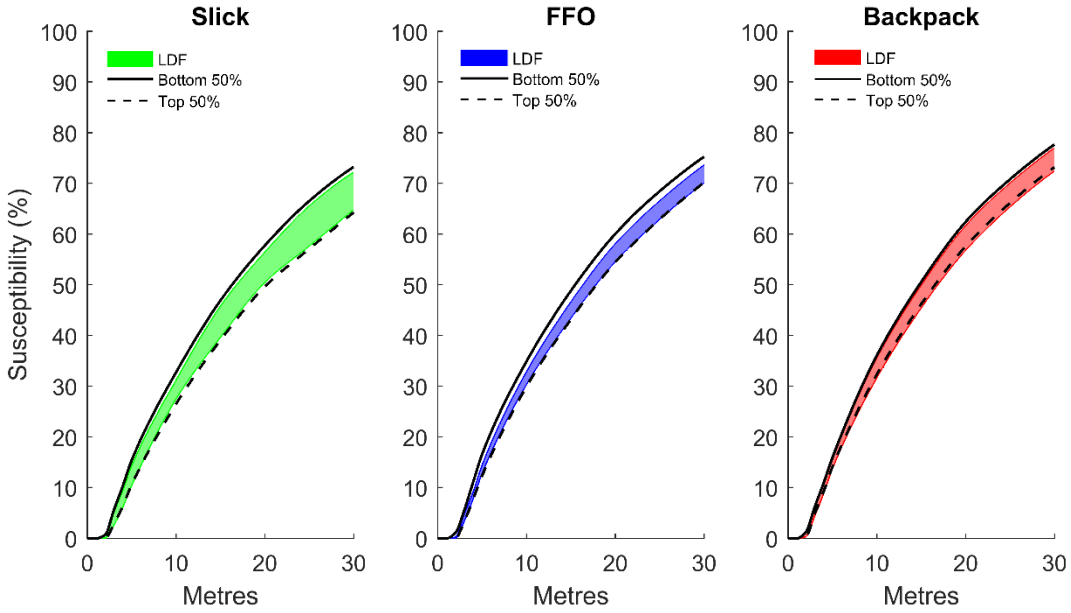

Figure C.28. Run susceptibility over 30 metres as a factor of body mass. Linear discriminant functions (LDFs) were scaled to best represent the top 50% body mass (~89 kg) and bottom 50% body mass (~69 kg) from the participant pool. LDFs were created for the Slick (~5.5 kg), FFO (~22 kg), and Backpack (~38 kg) conditions and combined together to make the mover run to each desired distance including a deceleration phase. Solid black lines represent the average top 50% body mass mover and the dashed lines represent the average bottom 50% body mass mover. Each coloured band represents the upper and lower bounds of the scaled LDF model to the average mover. Scaling is based on the sum of root mean squared error of all movement trajectories compared to the mean movement.

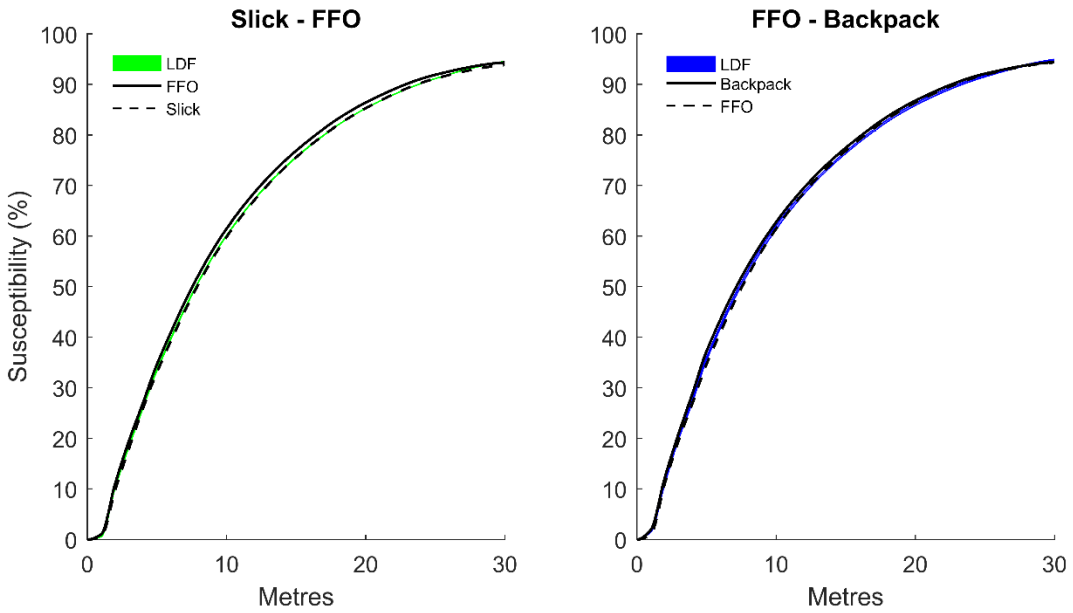

Figure C.29. Walk susceptibility over 30 metres as a factor of load. Linear discriminant functions (LDFs) were scaled to best represent the average Slick, FFO, and Backpack movers and combined together to make the mover run to each desired distance including a deceleration phase. LDFs were created for the Slick vs. FFO (~5.5 kg vs. ~22 kg), and FFO vs. Backpack (~22 kg vs. ~38 kg) conditions. Solid black lines in the Slick – FFO graph represent the average FFO mover and the dashed lines represent the average Slick mover. Solid black lines in the FFO – Backpack graph represent the average Backpack mover and the dashed lines represent the average FFO mover. Each coloured band represents the upper and lower bounds of the scaled LDF model to the average mover. Scaling is based on the sum of root mean squared error of all movement trajectories compared to the mean movement.

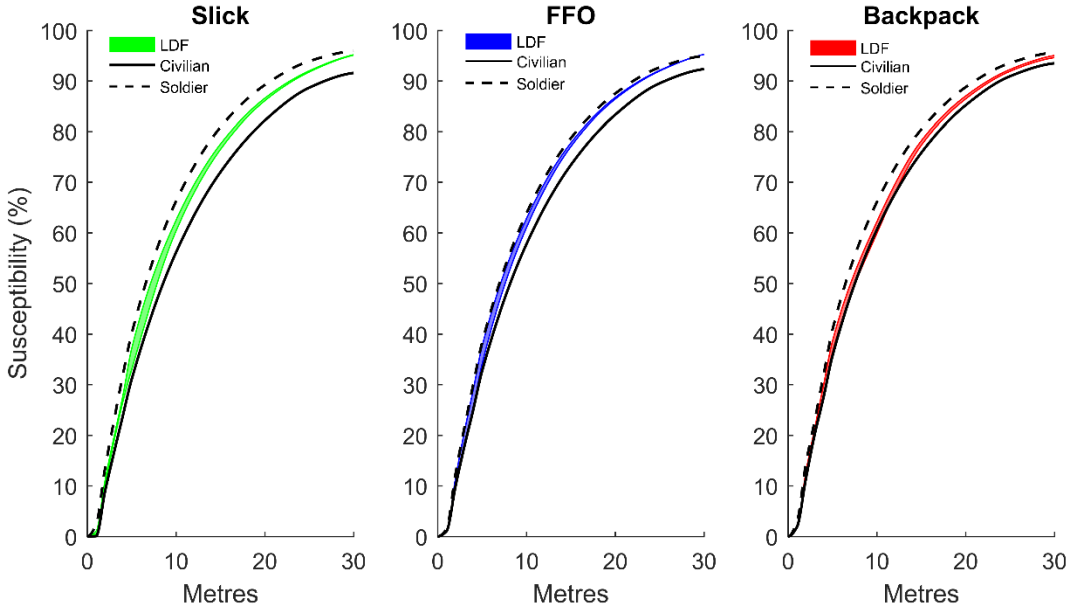

Figure C.30. Walk susceptibility over 30 metres as a factor of military experience. Linear discriminant functions (LDFs) were scaled to best represent the average civilian and soldier movers. LDFs were created for the Slick (~5.5 kg), FFO (~22 kg), and Backpack (~38 kg) conditions and combined together to make the mover run to each desired distance including a deceleration phase. Solid black lines represent the average civilian mover and the dashed lines represent the average soldier mover. Each coloured band represents the upper and lower bounds of the scaled LDF model to the average mover. Scaling is based on the sum of root mean squared error of all movement trajectories compared to the mean movement.

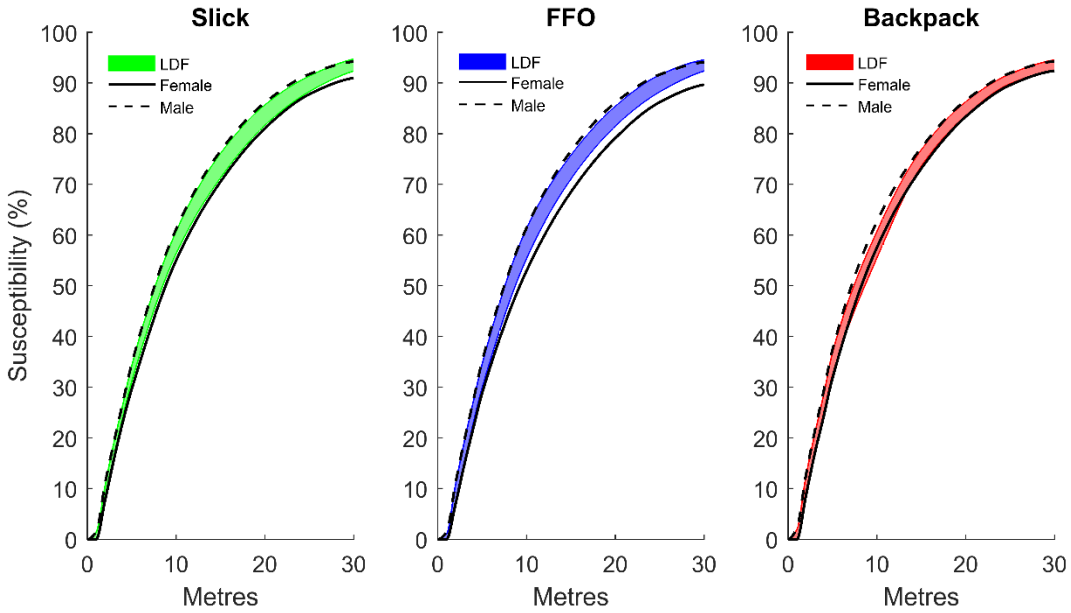

Figure C.31. Walk susceptibility over 30 metres as a factor of sex. Linear discriminant functions (LDFs) were scaled to best represent the average male and female movers. LDFs were created for the Slick (~5.5 kg), FFO (~22 kg), and Backpack (~38 kg) conditions and combined together to make the mover run to each desired distance including a deceleration phase. Solid black lines represent the average male mover and the dashed lines represent the average female mover. Each coloured band represents the upper and lower bounds of the scaled LDF model to the average mover. Scaling is based on the sum of root mean squared error of all movement trajectories compared to the mean movement.

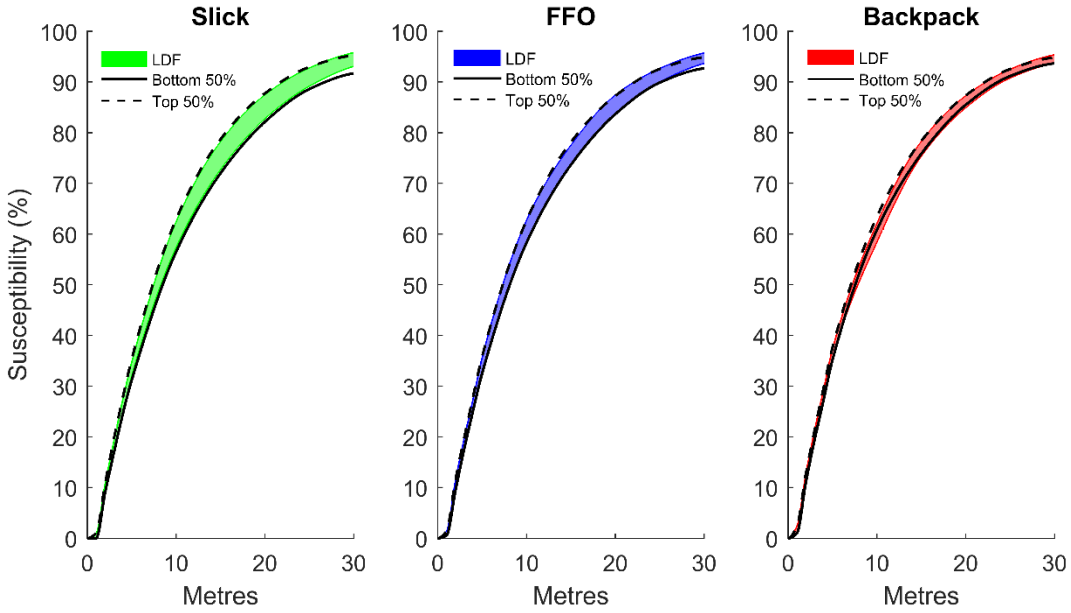

Figure C.32. Walk susceptibility over 30 metres as a factor of body mass. Linear discriminant functions (LDFs) were scaled to best represent the top 50% body mass (~89 kg) and bottom 50% body mass (~69 kg) from the participant pool. LDFs were created for the Slick (~5.5 kg), FFO (~22 kg), and Backpack (~38 kg) conditions and combined together to make the mover run to each desired distance including a deceleration phase. Solid black lines represent the average top 50% body mass mover and the dashed lines represent the average bottom 50% body mass mover. Each coloured band represents the upper and lower bounds of the scaled LDF model to the average mover. Scaling is based on the sum of root mean squared error of all movement trajectories compared to the mean movement.